Agent-Based Simulation of Nucleus Pulposus Cell Behavior in Alginate Hydrogels

Romi Bonomo

Master of Engineering

Department of Biological and Biomedical Engineering

McGill University
Montréal, Québec

August 2024

A thesis submitted to McGill University in partial fulfillment of the requirements of the degree of Master of Engineering in Biological & Biomedical Engineering.

Acknowledgments

I would like to express my deepest gratitude to everyone who has supported me throughout my graduate studies and contributed to the completion of this thesis. Firstly, I extend my heartfelt thanks to my supervisors, Dr. Nicole Li-Jessen and Dr. Jianyu Li, for their invaluable guidance, support, and advice throughout my research. Their expertise and insights have been instrumental in shaping this work. I am also grateful to Dr. Alireza Najafi Yazdi and Yvonna Li for their work in designing the initial software architecture that served as the cornerstone for this project. Additionally, I would like to thank Xuan Li for generously providing the cell culture and hydrogel data, which were integral for training and validating the model. My appreciation goes to the members of the Voice and Upper Airway Research team for their encouragement and constructive feedback throughout my studies.

Finally, I acknowledge the research operating grant from the Natural Sciences and Engineering Research Council of Canada (NSERC) under award number I252423C0G, the Canadian Institute of Health Research (CIHR) under award number I243217C0S (PI: Li-Jessen), and the Graduate Excellence Award in Biological & Biomedical Engineering under award number M159875C90. These grants made the work presented in this thesis possible. This thesis is dedicated to my mother for her unwavering encouragement and support.

Abstract

Introduction. Intervertebral disc (IVD) degeneration is a prevalent cause of back pain and disability, posing a significant socioeconomic burden. Current treatments often fail to stop the degenerative process or restore disc function. By varying calcium and alginate concentrations in hydrogels, biomaterial properties can be tuned to promote nucleus pulposus (NP) cell regeneration. Increased calcium crosslinking in hydrogels results in a stiffer matrix, directly affecting the synthesis of extracellular matrix (ECM) components such as aggrecan and collagen. Complementary to in vitro testing, computational modeling enables the optimization of biomaterial design and therapeutic strategies in a cost-effective and efficient manner. Agent-based modeling (ABM) proves particularly valuable in this context, where individual components interact with their environment according to programmed mathematical rules derived from literature. Governed by decision-making heuristics, ABM predicts emerging system properties from local interactions among autonomous entities. This structured approach facilitates detailed, high-throughput simulations of complex spatial-temporal systems, offering hypothesis-driven insights that are otherwise challenging to observe in traditional experimental settings.

Research Goal. This thesis aimed to develop an alginate hydrogel ABM to numerically simulate NP cellular activity related to IVD regeneration over 21 days.

Methods. In the intervertebral disc- hydrogel ABM (IVDH-ABM), NP cells were programmed to interact with each other and the environment through a set of

fundamental rules: migration, proliferation, apoptosis, and ECM and cytokine production, in response to the hydrogel physical properties, such as elasticity. The model was programmed using C++ and trained using regression analysis from literature data. Calibration was performed to iteratively adjust unknown model parameters to fit ABM outputs to in vitro experiments, using uncertainty quantification for days 3, 6, 9, and 12. The model was validated against an independent set of empirical data to assess predictive accuracy. Owing to the stochasticity of ABM, each simulation was run ten times to generate confidence intervals for the remaining 15, 18, and 21 days. The predicted outputs were considered accurate if they fell within the 95% confidence intervals of the experimental data points. After validation, the ABM was used for simulation experiments to determine the optimal hydrogel composition, such as alginate concentration and calcium crosslinking density for NP regeneration. Numerical results were visually represented using the Visualization Tool Kit (VTK) rendering in ParaView 5.7.0.

Results and Discussion. IVDH-ABM reproduced the relationship between hydrogel composition and elasticity. Higher calcium crosslinking density, alginate concentration and molecular weight, increased hydrogel stiffness, aligning with empirical data. The optimized hydrogel composition (200 kDa alginate, 1.95% w/v, 20 mM calcium) resulted in an elastic modulus of 3.66 kPa, supporting ECM production and cell proliferation. The IVDH-ABM provides insights into optimal hydrogel compositions for NP regeneration, advancing tissue engineering and regenerative medicine by offering a reliable platform for simulating NP cell behavior. Future work includes integrating heterogeneous biochemical

and mechanical stimuli, such as varying porosity and dynamic degradation rates, using Finite Element Method (FEM) techniques to capture spatial and temporal variations in tissue elasticity more realistically. Additionally, enhancing the model to encompass intricate biological signaling pathways, cell-to-cell interactions, and environmental factors such as nutrient availability will provide a more holistic understanding of NP cell behavior. Lastly, transitioning the model to in vivo conditions, including validation with real-time data and consideration of patient-specific variables such as genetic information and disc morphology, is essential for advancing towards clinical applications.

Abrégé

Introduction. La dégénérescence du disque intervertébral (DIV) est une cause fréquente de douleurs dorsales et de handicaps, posant un fardeau socio-économique significatif. Les traitements actuels échouent souvent à arrêter le processus dégénératif ou à restaurer la fonction du disque. En variant les concentrations de calcium et d'alginate dans les hydrogels, les propriétés des biomatériaux peuvent être ajustées pour promouvoir la régénération des cellules du nucleus pulposus (NP). Une augmentation de la réticulation au calcium dans les hydrogels entraîne une matrice plus rigide, affectant directement la synthèse des composants de la matrice extracellulaire (MEC) tels que l'aggrécan et le collagène. En complément des tests in vitro, la modélisation computationnelle permet d'optimiser la conception des biomatériaux et les stratégies thérapeutiques de manière rentable et efficace. La modélisation basée sur des agents (ABM) s'avère particulièrement précieuse dans ce contexte, où les composants individuels interagissent avec leur environnement selon des règles mathématiques programmées dérivées de la littérature. Régie par des heuristiques de prise de décision, l'ABM prédit les propriétés émergentes du système à partir des interactions locales entre des entités autonomes. Cette approche structurée facilite des simulations détaillées et à haut débit de systèmes complexes spatio-temporels, offrant des insights hypothétiques qui sont autrement difficiles à observer dans des contextes expérimentaux traditionnels.

Objectif de la recherche. Cette thèse visait à développer une ABM d'hydrogel d'alginate pour simuler numériquement l'activité cellulaire du NP liée à la régénération du DIV sur une période de 21 jours.

Méthodes. Dans l'ABM du disque intervertébral-hydrogel (IVDH-ABM), les cellules NP ont été programmées pour interagir entre elles et avec l'environnement par un ensemble de règles fondamentales : migration, prolifération, apoptose et production de MEC et de cytokines, en réponse aux propriétés physiques de l'hydrogel, telles que l'élasticité. Le modèle a été programmé en C++ et entraîné à l'aide d'analyses de régression basées sur des données de la littérature. La calibration a été réalisée pour ajuster itérativement les paramètres inconnus du modèle afin de faire correspondre les sorties de l'ABM aux expériences in vitro, en utilisant la quantification de l'incertitude pour les jours 3, 6, 9 et 12. Le modèle a été validé par rapport à un ensemble indépendant de données empiriques pour évaluer la précision prédictive. En raison de la stochasticité de l'ABM, chaque simulation a été réalisée dix fois pour générer des intervalles de confiance pour les jours restants (15, 18 et 21). Les sorties prévues étaient considérées comme précises si elles se situaient dans les intervalles de confiance à 95% des points de données expérimentaux. Après validation, l'ABM a été utilisé pour des expériences de simulation afin de déterminer la composition optimale de l'hydrogel, telle que la concentration d'alginate et la densité de réticulation au calcium pour la régénération du NP. Les résultats numériques ont été représentés visuellement à l'aide du Visualization Tool Kit (VTK) rendu dans ParaView 5.7.0.

Résultats et discussion. L'IVDH-ABM a reproduit la relation entre la composition de l'hydrogel et l'élasticité. Une densité plus élevée de réticulation au calcium, ainsi que le poids moléculaire et les concentrations d'alginate, ont augmenté la rigidité de l'hydrogel, en accord avec les données empiriques. La composition optimale de l'hydrogel (alginate de 200 kDa, 1,95% p/v, 20 mM de calcium) a résulté en un module élastique de 3,66 kPa, soutenant la production de MEC et la prolifération cellulaire. L'IVDH-ABM fournit des insights sur les compositions optimales d'hydrogel pour la régénération du NP, faisant progresser l'ingénierie tissulaire et la médecine régénérative en offrant une plateforme fiable pour simuler le comportement des cellules NP. Les travaux futurs incluent l'intégration de stimuli biochimiques et mécaniques hétérogènes, tels que la variation de la porosité et des taux de dégradation dynamique, en utilisant des techniques de la méthode des éléments finis (FEM) pour capturer plus réalistement les variations spatiales et temporelles de l'élasticité tissulaire. De plus, améliorer le modèle pour englober des voies de signalisation biologique complexes, les interactions cellule-à-cellule et les facteurs environnementaux tels que la disponibilité des nutriments, offrira une compréhension plus holistique du comportement des cellules NP. Enfin, le passage du modèle aux conditions in vivo, y compris la validation avec des données en temps réel et la prise en compte des variables spécifiques au patient telles que les informations génétiques et la morphologie des disques, est essentiel pour progresser vers des applications cliniques.

Contribution of Authors

Romi Bonomo: Conceptualization (equal), Investigation (lead), Development (lead), Software (lead), Methodology (equal), Formal Analysis (equal), Data Curation (equal), Writing – original draft (lead), Visualization (lead).

Nicole Li-Jessen: Supervision (lead), Conceptualization (equal), Funding Acquisition (lead), Resources (lead), Methodology (equal), Formal Analysis (equal), Data Curation (equal), Writing – review and editing (lead).

Jianyu Li: Supervision (equal), Conceptualization (equal), Funding Acquisition (equal), Writing – review and editing (equal).

Table of Contents

List of Figures

List of Tables

Nomenclature

Acronyms

2D	Two- dimensional
3D	Three- dimensional
ABM:	Agent-Based Modeling
ADAMTS	A Disintegrin and Metalloproteinase with Thrombospondin Motifs
AF	Annulus fibrosis
API	Application Programming Interface
CEP	Cartilage endplate
CUDA	Compute Unified Device Architecture
ECM	Extracellular Matrix
FEM	Finite element modeling
GAG	Glycosaminoglycan
GPU	Graphics Processing Unit
IL-1β	Interleukin-1 beta
IVD	Intervertebral disc
IVDH-ABM	Intervertebral disc hydrogel agent-based model
MMP	Matrix Metalloproteinase
NP	Nucleus pulposus
OAT	One-at-a-Time
OLS	Ordinary least squares
PDE	Partial differential equation
RMSE	Root Mean Square Error
SPOTPY	Statistical Parameter Optimization Tool for Python
TERM	Tissue engineering and regenerative medicine
TGF-β	Tumor Growth Factor- beta
TNF-α	Tumor Necrosis Factor- alpha

Chapter 1 Introduction

1.1 Research Motivation

Low back pain affects 632 million people worldwide[1] and is among the most prevalent, debilitating,[2] and costly[3] conditions. Approximately 84% of people will experience chronic lower back pain at some point during their lifetime,[4] leading to substantial healthcare expenditures. In the United States, direct and indirect medical costs related to spinal issues exceed $130 billion CAD annually.[5] Previous Canadian estimates indicated that healthcare costs for spinal disorders reached $2.44 billion CAD in 1994.[6] In less than ten years, healthcare expenditure for such disorders had escalated to $330 million CAD for Ontario alone in 2013.[7]

The prevalence of low back pain and its associated costs are expected to surge with the aging global population.[8] The onset and progression of low back pain are significantly influenced by intervertebral disc (IVD) degeneration, a leading cause of spinal instability,[3,9] that has a significant impact on quality of life worldwide.[10] Existing treatments often offer only temporary relief and fail to address the underlying disc degeneration. These shortcomings have led to a growing interest in regenerative medicine as a more sustainable and effective approach to treating IVD degeneration.

Tissue engineering leverages biomaterial development to combine scaffolds, cells, and bioactive molecules to create, maintain, or restore functional tissues. Regenerative

medicine replaces or regenerates tissues by stimulating the body's own repair mechanisms to restore normal function. In clinical practice, regenerative medicine uses materials that facilitate healing by releasing growth factors and cytokines into injured tissues. Tissue Engineering in Regenerative Medicine (TERM) presents a promising approach for treating disc degeneration by leveraging biomaterials, such as hydrogels, to support cell growth and tissue regeneration. However, a comprehensive understanding of how cells interact with biomaterial physical properties remains elusive, limiting the full potential in therapeutic outcomes. Computational modelling has become more prevalent in medical research, particularly in TERM.[11] Mathematical and machine learning algorithms are used to simulate complex biological processes and predict therapeutic outcomes, aiding experimental design and biomaterial property optimization. These in silico simulations allow researchers to rapidly test hypotheses,[12] explore various scenarios, and make predictions that inform and complement traditional laboratory testing in a more cost- and time- efficient manner,[13] as shown in **Figure 1.1**.

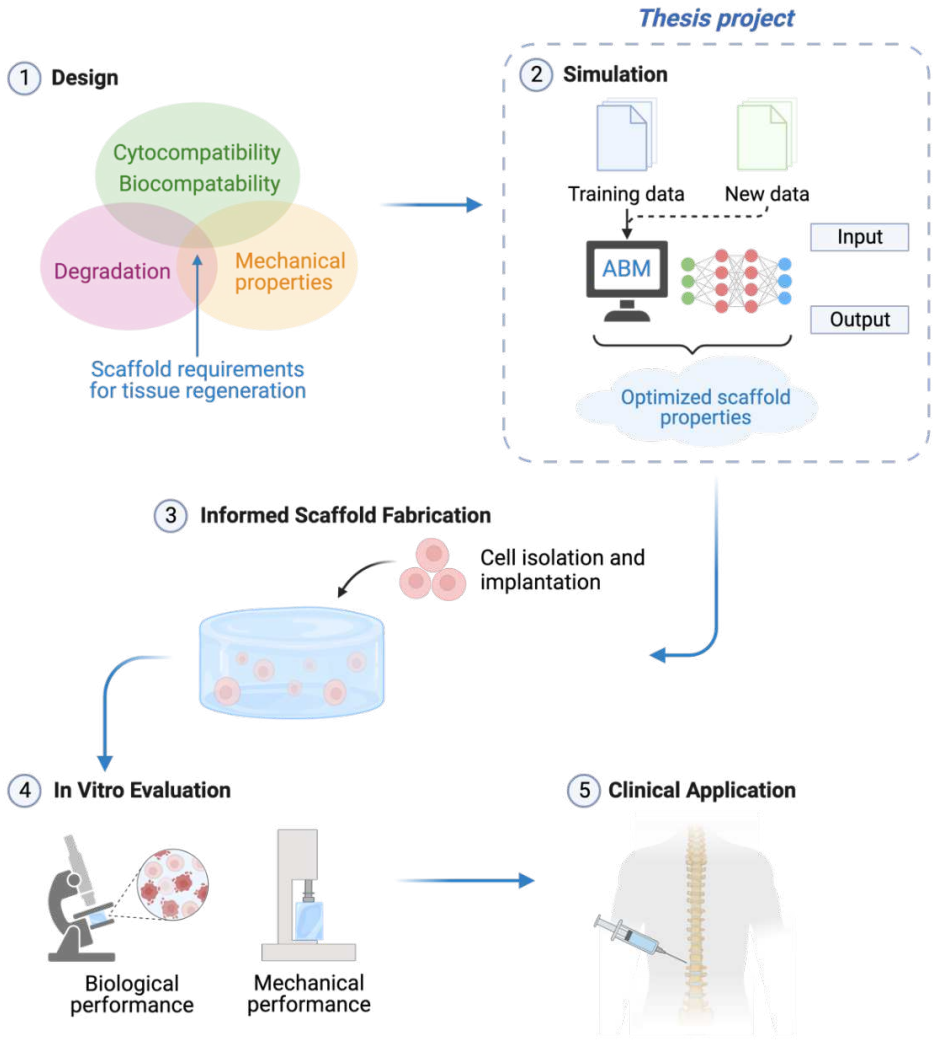

Figure 1.1 Overview of the Tissue Engineering Process. The integration of computational simulations to determine the optimal hydrogel mechanical properties for IVD-tissue regeneration, informing the scaffold fabrication, guiding in vitro testing, and clinical implantation. Created with Biorender.com.

This study leverages computational modelling to predict the regenerative ability of the IVD. More specifically, an agent-based model (ABM) is used to understand the behavior of these cells within a biomaterial environment, ultimately contributing to

advancements in tissue repair and regeneration strategies. In the ABM, autonomous entities known as *agents* are each governed by distinct sets of rules and behaviors.[14] The fundamental principle of ABM is that simple rules at the individual level lead to emergent behavior at the system level.[15] Each agent in ABMs evaluates their situation and makes decisions based on predetermined rules, such as moving, interacting with other agents, or changing its state, over a sequence of time steps.

Existing IVD-specific models have primarily focused on the effects of biochemical stimuli and basic mechanotransduction processes, such as local tensile and compressive mechanical loads, and the impact of nutrition levels on cell activity and viability.[16] These models, however, fall short in simulating and optimizing the parameters of biomaterials, critical for tissue engineering applications. This thesis research integrates mechanotransduction to simulate nucleus pulposus (NP) cells within a hydrogel environment. Furthermore, this thesis work introduces an in silico framework for experimental testing and optimization of biomaterial designs, mimicking the interactions between NP cells and the varied physical properties of hydrogel compositions (**Figure 1.1**).

1.2 Research Objectives

The overall goal of this thesis was to develop an agent-based computational model for the investigation of the regenerative capabilities of the IVD-specific cells; namely the NP cells, within alginate-based hydrogels. **Figure 1.2** depicts a workflow overview of the ABM development process. This study has two specific aims:

Specific Aim 1. Developed, Calibrated, and Validated the IVD Hydrogel ABM for Regeneration.

An IVD-hydrogel ABM (IVDH-ABM) was developed to numerically simulate the biological response of NP cells within an alginate hydrogel over a period of 21 days. The NP cells, represented as model agents, interacted with each other and the hydrogel environment through a set of key rules; cell migration, proliferation, apoptosis, cytokine synthesis, and extracellular matrix (ECM) production, in response to the mechanical properties of the hydrogel; elasticity, porosity, and degradation of the scaffold matrix. The biological model outputs included the cell viability, ECM deposition, cytokine levels, and the mechanical properties of the hydrogel. The model was calibrated using literature data, and the output was subsequently validated against in vitro experiments. The IVDH-ABM was expected to achieve a strong correlation between the simulated predictions and empirical in vitro results.

Specific Aim 2. Performed In Silico Evaluation of the NP Regenerative Responses to a Physiologically Relevant Hydrogel Elasticity.

The validated ABM was utilized to investigate NP cell regeneration in response to an alginate hydrogel designed to match the elasticity of a healthy middle-aged human lumbar NP tissue. Employing an exhaustive combinatorial optimization algorithm, the validated model systematically explored every permutation of hydrogel composition within physically acceptable defined ranges. Hydrogel conditions were identified by recording the datapoint sets that yielded outputs within the targeted physiological range. Subsequently, an in silico experiment was conducted, wherein the optimized alginate concentration and calcium crosslinking density were inputted into the model to simulate NP cell behavior. The model predicted cell viability, cytokine expression levels, and ECM production profiles within the hydrogel over a 21-day period. Statistical analysis was then performed to evaluate the predicted regenerative dynamics of the cells, comparing the optimized output to the other hydrogel conditions previously used to validate the model. This aim leverages the understanding that mechanical properties, particularly elasticity, are crucial for IVD functionality and regenerative capacity. Focusing on physiologically relevant conditions enhances the translation of computational modeling into effective clinical treatments in regenerative medicine.

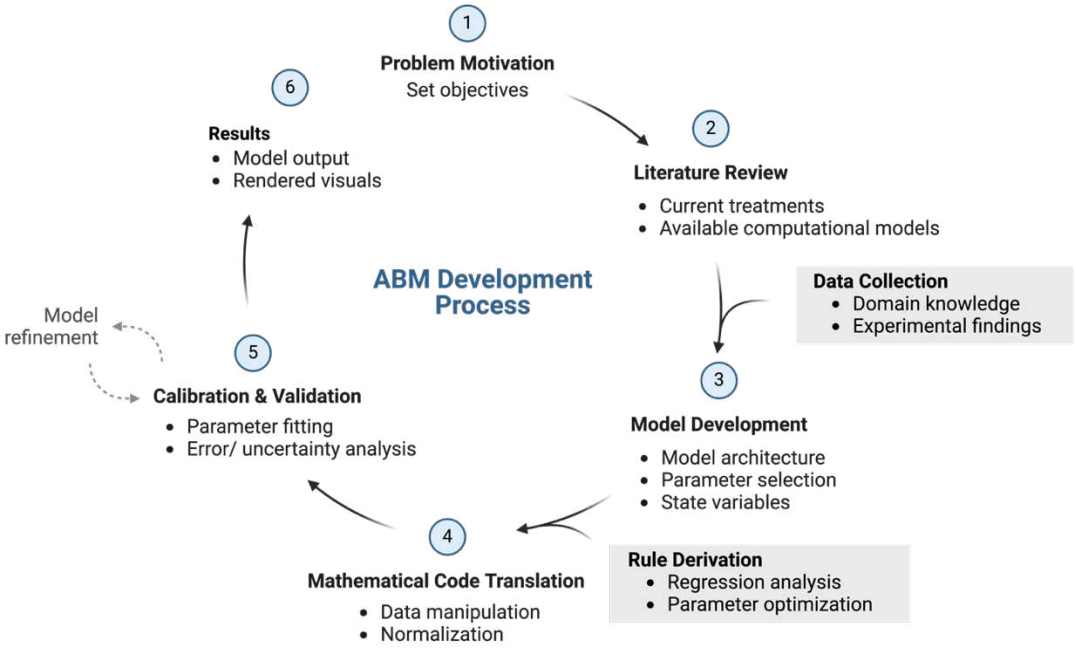

Figure 1.2 Workflow of Agent-Based Model in this Thesis Research. Created with Biorender.com.

1.2.1 Research Significance

The thesis research holds significance across different aspects of biomedical engineering and healthcare. First, the model presented in this thesis provides predictive insights on the regenerative potential of NP cells, guiding experimental designs and reducing the number of trials needed for optimization. A computational approach saves both time and resources, which is particularly important given the high cost of research infrastructure for in vitro studies. Second, the algorithms used in this model can be readily adapted for broader applicability in regenerative medicine, with strong translational potential in clinical settings.

1.3 Thesis Organization

This thesis is organized into five chapters. **Chapter 1** introduces the project, establishing the motivation and clearly defines the research goals. **Chapter 2** comprises a comprehensive literature review and identifies the research gap in current IVD regeneration treatments. **Chapter 3** outlines the ABM development methodology, detailing data extraction from relevant scientific literature and its translation into mathematical code for subsequent numerical simulation and parameter calibration. **Chapter 4** presents the results of the model simulations, where the prediction outcomes and their effectiveness in optimizing scaffold designs are quantitatively evaluated. Finally, **Chapter 5** offers a discussion of the simulation outcomes, assessing its implications in the broader context of tissue engineering and regenerative medicine. This chapter also serves to draw conclusions, summarizing the research contributions and proposing directions for future work in the development of the model.

Chapter 2 Literature Review

This chapter is organized as followed: the anatomy and physiology of the IVD (**section 2.1**), the mechanobiology of the IVD and existing treatments and limitations for IVD degeneration (**section 2.3**), an overview of tissue engineering approaches (**section 2.4**) and the utility of computational modelling in biomedical research (**section 2.5**).

2.1 Intervertebral Disc Anatomy and Physiology

The IVD is a complex, multi-component structure that serves as a cushion between each vertebra and forms a flexible spinal column. It is composed of three components, namely, the cartilage endplate (CEP), the annulus fibrosus (AF), and the nucleus pulposus (NP) (**Figure 2.1**). The combination of mechanical properties provided by each component allows for efficient shock absorption while transferring loads between vertebrae during daily mobility activities such as walking, running, and lifting.[17]

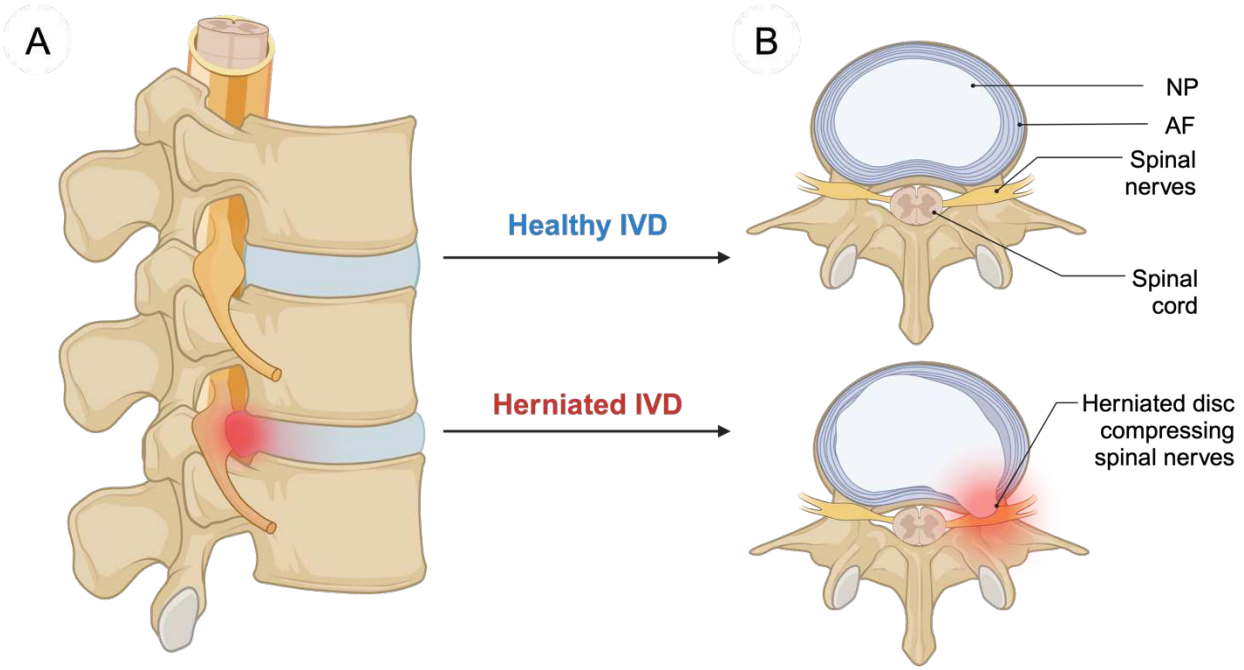

Figure 2.1. Lumbar Spine Anatomy. A lumbar spinal segment consisting of a diagram of the sagittal section of the vertebral body and IVD (A), and the superior view of a healthy (top) and herniated (bottom) IVD, during disc degeneration (B). Created with BioRender.com.

The CEPs measure less than 1 mm in height and are composed of hyaline cartilage layers that separate the disc from the adjacent vertebrae.[18] The endplates serve as a protection barrier to prevent wear and tear while also being responsible for nutrient transport. The AF is made up of concentric layers of fibrocartilage that form the outermost ring of the disc. When the IVD is subject to torsional and shear stresses caused by bending and twisting of the spine, the rigid AF will provide rotational stability.[19] Confined within the AF, the gel-like NP acts as a hydraulic cushion that deforms and adapts to the various loading conditions.

When the spine undergoes physiological compression forces, the NP bares most of the load and redistributes it radially outward towards the AF, which will expand and contract in accommodation, minimizing the impact on the vertebrae.[20] The NP tissue is composed of various proteins and cells. These cells and their secreted extracellular matrix (ECM) form a scaffold that allows for the tissue-level load-distributing capability of the disc.[21]

2.2 Mechanobiology of the Extracellular Matrix

The physiological function of the IVD is highly dependent on its ECM remodelling kinetics. Serving as a biochemical and biomechanical scaffold, key ECM components like collagen and proteoglycans are synthesized and secreted by chondrocyte cells. These components facilitate critical cell-ECM interactions that govern cell adhesion, migration, growth, differentiation, death, chemokine secretion, and protein synthesis.[22]

Aggrecan is a key proteoglycan in the NP, accounting for 65-85% of its dry weight.[23] It plays a multifaceted role in cellular and mechanical functions within the NP. By interacting with cell surface receptors, aggrecan activates signaling pathways that are crucial for cell survival, proliferation,[24] and differentiation.[25] It also modulates the activity of growth factors and cytokines by binding to them, thereby creating localized gradients that guide cell migration.[26] Structurally, aggrecan contains negatively charged glycosaminoglycans (GAGs) that attract and retain water. This water-binding capability leads to elevated hydration levels,[27] contributing to the development of hydrostatic pressure that enables the NP to absorb and disperse compressive forces, rendering the NP

with a gelatinous consistency and unique elastic properties.[20] This is particularly vital in load-bearing tissues, where mechanical support is essential.[28] The hydrated, gel-like environment also facilitates the efficient exchange of nutrients, signaling molecules, and waste products between cells and their surroundings.[29]

Alternatively, collagen plays a pivotal role in the mechanical and cellular functions of the IVD, exhibiting tissue-specific variations in both the NP and AF. The mechanical properties of the tissue, including stiffness and elasticity, are significantly influenced by fiber orientation and density. In the AF, type-I collagen fibers are densely organized, providing tensile strength and structural integrity, which prevents excessive deformation during spinal activities.[30] Conversely, the NP primarily contains type-II collagen, making up 15-20% of its dry weight.[23] This type of collagen provides a flexible matrix that allows for resistance against multi-directional forces common during spinal movement, such as torsion and shear.[31] Collagen influences cell behavior through mechanotransduction, a process in which cells translate mechanical signals into biochemical responses such as cell proliferation and matrix synthesis or degradation.[32]

The ECM serves as a substrate for cell adhesion, allowing cells to communicate via transmembrane receptors,[33] which triggers intracellular signaling pathways that regulate cell proliferation and differentiation.[34] Additionally, collagen provides a structural lattice for cell migration, essential for tissue regeneration, and regulates cell motility through interactions with cell surface receptors.[35]

Aggrecan and collagen work together to regulate the mechanical properties and cellular behavior of the ECM (**Table 2.1**). The water-binding ability of aggrecan complements tensile strength supplied by the collagen, resulting in a composite material that resists both compressive and tensile forces.[35] This mechanical synergy is critical for the proper function and adaptability of load-bearing cartilage tissues like IVD.

Table 2.1 Summary of Major ECM Components in the Adult IVD.

ECM component	Biomechanical function	Concentration (NP dry weight)	
		Healthy	Degenerated
Collagen II [a]	• Structural integrity (stiffness) • Promotes cell proliferation	15-20%	~90% decrease [36]
Aggrecan	• Elasticity • Promotes cell viability and proliferation • Facilitates nutrient diffusion	65-85%	~50% decrease [37]

[a] Collagen-II decreases ~90% and collagen-I increases ~210% during degeneration compared to healthy discs.

2.3 Biomechanics of Matrix Degradation and Disc Degeneration

In a healthy IVD, the ECM is in constant dynamic equilibrium, undergoing physiological remodelling to maintain its structure and function. This homeostasis requires a delicate balance in anabolic and catabolic processes (**Figure 2.2**). Anabolic processes maintain ECM replacement and repair. ECM anabolic activities are primarily driven by growth factors like transforming growth factor (TGF-β), which promote ECM component

synthesis. TGF-β binds to the NP cell surface receptors and triggers a signalling cascade that promotes collagen and aggrecan synthesis.[38] Proinflammatory cytokines, such as interleukin-1 beta (IL-1β) and tumour necrosis factor alpha (TNF-α), increase catabolic activity[39] by stimulating the secretion of ECM degradation enzymes, e.g., Matrix Metalloproteinases (MMPs), A Disintegrin and Metalloproteinase with Thrombospondin Motifs (ADAMTS) etc.[40] Tissue Inhibitors of Metalloproteinases (TIMPs) regulate these enzymes, ensuring that degradation does not exceed synthesis and thus maintaining homeostasis.[41]

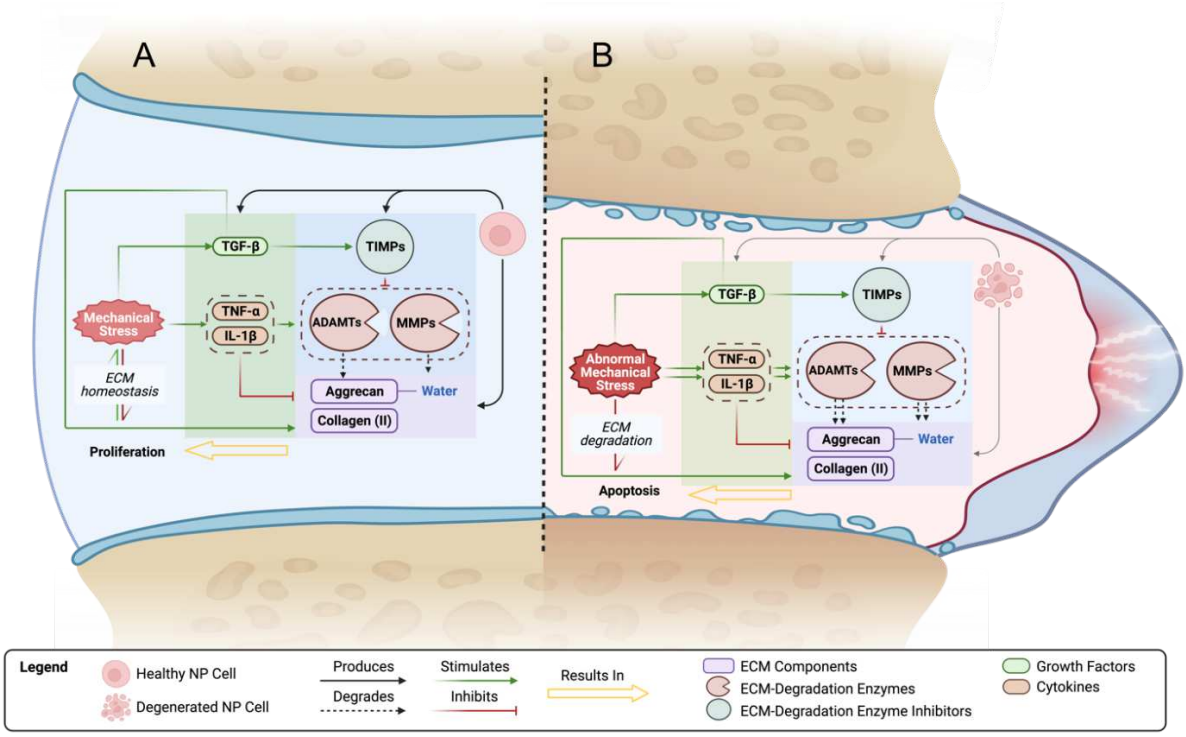

Figure 2.2. Anterior Coronal View of the IVD Microenvironment. A schematic comparison between the physiological microenvironment of the healthy IVD (A), and the pathological microenvironment of the degenerated IVD (B). Created with BioRender.com.

Degradation of the ECM occurs when catabolic processes exceed anabolic processes. The upregulation of cytokines in the ECM leads to a net loss of essential matrix components (**Figure 2.2**).[42] Aggrecan and collagen abundance peaks in early adulthood and then gradually decline due to a decrease in matrix-synthesizing cells[43] and an increase in enzymatic degradation.[44] This imbalance is caused by etiological factors such as aging, mechanical overload, or inflammation.[44] The inflammatory microenvironment influences MMP expression and correlates positively with the extent of IVD degeneration. Under normal physiological conditions, MMPs are expressed in low levels and increased in an

inflammatory environment.[45] Furtwangler et al., (2013) found that ADAMTS expression levels accumulated and contributed to ECM changes during disc degeneration.[46] Results showed reduced cell activity and collagen content after the intradiscal injection of ADAMTS.

The mechanical properties of the IVD are compromised as the ECM deteriorates. The ECM composition is altered due to a decrease in proteoglycans and collagen type-II and an increase in collagen type-I.[34] The fragmented water-retaining GAG chains from the aggrecan results in a decrease in hydration levels[47] and impair the hydrostatic properties of the disc,[48] and the decreased collagen type-II levels cause structural weaknesses,[49] while the increased collagen type-I levels stiffen the NP. Available evidence suggests that a stiff substrate causes NP cell phenotypic changes such as apoptosis and is associated with disc degeneration.[50] Mechanical failures can accelerate the degenerative process by triggering an inflammatory response, resulting in a feedback loop of mechanical and biochemical failures.[36] For instance, increased compressive stresses ranging from 1-3 MPa[51] above the 0.1-0.5 MPa norm (120% of the body weight)[52] can cause microtears in the collagen network,[53] triggering an inflammatory response and increasing the activity of catabolic enzymes. These biochemical changes cause additional mechanical failures and worsen the current state.[54]

The collective changes in the mechanobiology of the NP limit the disc's flexibility and range of motion.[55] This makes the disc more prone to mechanical failures such as tears and ruptures, which can lead to degenerative conditions such as disc herniation, in

which the NP leaks out, causing nerve impingement and severe pain,[56] affecting daily activities and overall quality of life. Due to avascularity, the IVD is limited in self-healing capacities[57] and rely on external regenerative intervention. Understanding the mechanisms by which the ECM degrades is critical for developing effective treatment strategies for disc degeneration.

2.4 Tissue Engineering Approaches for IVD Regeneration

IVD degeneration treatment is expensive and often unsuccessful.[58] The annual outpatient physician visits for spinal conditions in Ontario result in direct healthcare costs of approximately $330 million CAD.[7] In cases where conservative treatments, such as physical therapy and pain medication, fail to alleviate symptoms, surgical intervention is frequently sought.[59] The most common surgical procedure to treat lumbar hernias is a discectomy, in which the affected area is removed to alleviate pressure on the spinal nerves.[60] While these treatments may succeed in providing pain relief, they do not halt the degeneration process nor restore the disc to its original function[61] and are associated with significant postoperative complications, such as such as prosthesis failure, infection, and pain in 10-13% of patients.[38]

Moreover, despite surgical advancements, between 25% to 30% of patients continue to experience persistent back pain post-surgery.[62] This limitation has sparked increased interest in regenerative medicine and tissue engineering to develop therapeutic strategies to restore the structure and function of the degenerated IVD.[63] This growing demand for

effective IVD regeneration treatments has directly contributed to the rapid expansion of the global tissue engineering market (**Figure 2.3**). The global tissue engineering market is valued at $13.58 billion CAD in 2019 and is projected to grow at an annual growth rate of 14.28% from 2020 to 2027. [64] Moreover, as evidenced by 21 tissue engineering companies in the United States, the annual research and development investment is estimated at $6.45 billion CAD in 2017 alone.[65] Within this market, the orthopedics, musculoskeletal, and spine segment holds the highest market share of 31% in 2022.[66]

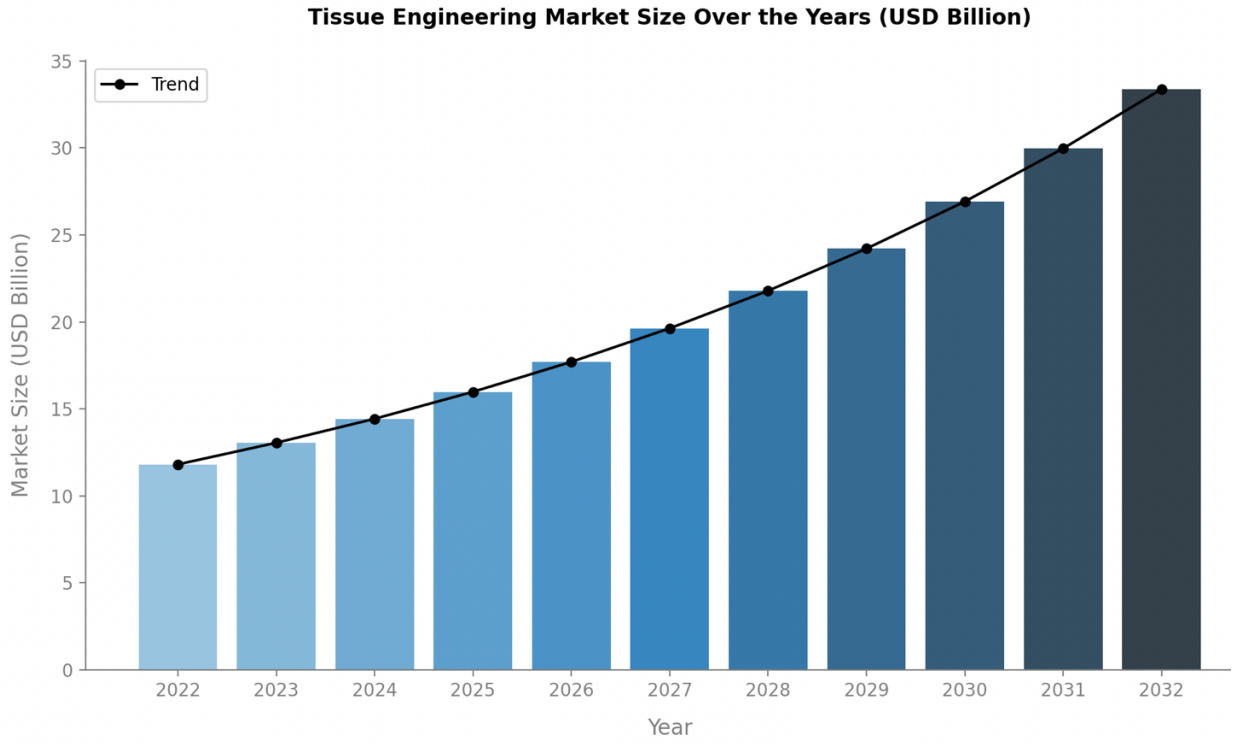

Figure 2.3 Tissue Engineering Market Size. Bar graph depicting the global tissue engineering market size accounted at $11.8 billion USD in 2022 and is expected to reach $33.38 billion USD

by 2032, growing at a rate of 11%. This graph was created based on the published data from Precedence Research.[66]

Tissue engineering approaches, such as cell-based therapy, growth factor delivery, and biomaterial scaffolds, present a promising treatment option for the degenerating IVD.[38] Cell-based therapy for IVD regeneration involves autologous or allogenic IVD cells or differentiating mesenchymal stem cells (MSCs).[67] Though cell retrieval is relatively simple, challenges arise with in vivo transplantation, including immunological responses and cell expansion deficiencies.[68] Another form of a tissue engineering approach is the delivery of biologically active substances to the degenerated site.[69] Growth factors, such as TGF-β, stimulate cell proliferation and ECM synthesis. However, their application is limited by rapid diffusion and degradation.[70] To circumvent this challenge, growth factors can be loaded into biomaterials to control their delivery and degradation rate.[71]

2.4.1 Biomaterial-Based Tissue Engineering Approaches

Biomaterial tissue engineering aims to develop functionalized tissue replacements that can facilitate tissue regeneration and restore the function of damaged tissues in parallel. The choice of biomaterial largely depends on the implantation site, although the ideal biomaterial offers biocompatibility, mechanical durability, and the capacity for integration with the host tissue.[72] Hydrogels are common in regenerative biomaterials due to their biocompatible, tunable, and biomimetic properties.[38] These three-dimensional networks of hydrophilic polymers are excellent in replicating the natural tissue

environment, given that they can absorb large amounts of water while retaining their structural integrity.[73]

Both natural and synthetic derived biomaterials have been explored for NP tissue engineering. Natural polymer-based biomaterials, include chitosan, gelatin, hyaluronic acid (HA), fibrin, and alginate. These natural materials are derived from animal or plant sources and are attractive due to their availability, biocompatibility, non-toxicity, and biodegradability properties.[74] However, disadvantages include rapid in vivo degradation after implantation and difficulty in maintaining integrity of mechanical properties.[75] Synthetic hydrogel materials mainly comprise poly-(D,L-lactide) (PLA), polyethylene glycol (PEG), poly-(lactic-co-glycolic acid) (PLGA), polyethylene glycol diacrylate (PEGDA), and poly-(vinyl alcohol). Such materials are advantageous for their improved mechanical strength and durability due to their strong covalent bonds.[76] In contrast, synthetic biomaterials require additional chemical modifications for in vivo compatibility and cell adhesion.[77] An overview of the properties of each material is provided in **Table 2.2**.

Table 2.2 Overview of Main Biomaterials Used in IVD Tissue Engineering.

Material	Main Characteristics	Ref.
	Natural Materials	
Chitosan	• Excellent biocompatibility, biodegradability, and cell adhesion. • Controllable degradation rate and pore size.	78
Collagen/ gelatin	• Excellent mechanical and biochemical properties, biocompatibility, and cell viability. • Low cost and biodegradable. • Reduced immune response.	79
Hyaluronic acid	• Good biocompatibility, proliferation, and cell adhesion. • Superior mechanical properties.	80
Alginate	• Tunable mechanical properties (similar to native cartilage). • Excellent regeneration, proliferation, cell adhesion, biocompatibility, flexibility, and degradation.	81
Fibrin	• Good biocompatibility and high elasticity. • High degradation.	82
	Synthetic Materials	
PEGDA/ PEG	• High cytocompatibility (minimized inflammatory responses). • Controllable mechanical strength. • Tuneable properties.	83
PVA	• Similar to natural cartilage • High water content (good diffusion and permeability) • Chemically resistant	84
PLGA/ PLA	• Biodegradable • Good mechanical strength.	85

To survey the current application of NP tissue engineering, a search for research papers published was performed on The National Center for Biotechnology Information (NCBI) PubMed between 2019 and 2023 using the following combined terms; *"alginate," "gelatin," "hyaluronic acid," "chitosan," "fibrin," "PEG," "PVA," "PLGA," "PLA,"* and *"intervertebral disc"* (**Figure 2.4**). The search generated 76 research studies. Alginate

(22%; N= 17) and PVA (8%; N= 6) were respectively the most common natural and synthetic materials used in hydrogels.

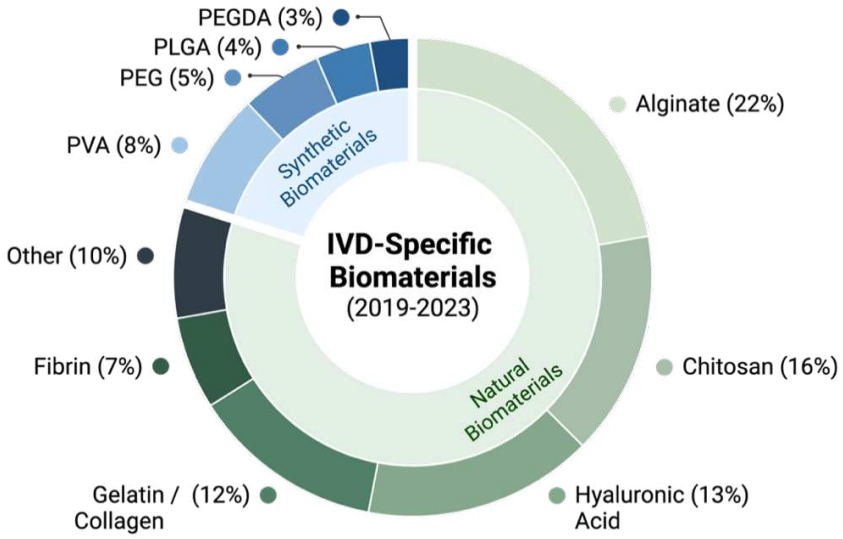

Figure 2.4 Biomaterials Used in IVD Tissue Engineering. Nested pie chart was generated by surveying published articles between 2019-2023 using NCBI PubMed, wherein alginate is the most abundant biomaterial. Created with BioRender.com.

Alginate-based hydrogels have been the focus for NP tissue engineering due to their biocompatibility and versatile physiochemical properties.[86] Alginate is a water-soluble, natural, linear polysaccharide, derived from the cell walls of bacteria and brown algae and can be transformed into a hydrogel upon hydration. Being a natural polymer, it is not considered as a foreign body by the immune system and can be effectively integrated into the surrounding tissue.[81] The physical and mechanical properties of alginate hydrogels,

including stiffness, viscoelasticity, stress relaxation, and degradation,[87] can be finely tuned via chemical modification, allowing for successful replication of the NP ECM.[88]

The concentration of crosslinking ions used can significantly influence the mechanical properties of alginate hydrogels.[81] Higher concentrations of crosslinking ions, like calcium, lead to an increased crosslinking density, resulting in stiffer hydrogels. Leone et al. (2008) developed an amidic derivative of alginate (AAA hydrogel) to increase viscosity while maintaining the rigidity of the hydrogel.[89] The chemical modification showed increased water uptake over the degenerated NP, potentially restoring the disc height. In addition, the authors also noted an increase in chondrocyte proliferation, collagen (II), and proteoglycan production, fundamental aspects of NP regeneration. The concentration of alginate in the precursor solution is directly related to the mechanical properties of the resulting hydrogel. Higher concentrations result in stiffer hydrogels due to the increased density of the polymer network and chain entanglement.[81] Moreover, Bron et al., (2011) evaluated the relationship of alginate concentration on scaffold stiffness and subsequent assessment of the ECM expression during NP regeneration.[90] The alginate scaffolds successfully replicated the viscoelastic properties of NP, wherein the outcomes showed prolonged NP cell viability.

Stress relaxation also affects NP cell behaviors and ECM remodelling. The stress relaxation of the alginate hydrogel can also be controlled by manipulating the alginate molecular weight,[91] whereby decreasing the molecular weight enhances stress relaxation. In addition, the viscoelasticity and degradation rate of alginate hydrogels can be adjusted

to match the NP regeneration rate via the material's crosslinking density.[91] For instance, the higher the linking density, the slower the degradation rate. Finally, the porosity of the hydrogel may be controlled through the alginate concentration,[92] wherein higher concentrations result in lower porosity. The lower porosity restricts sufficient nutrient diffusion and waste exchange and limits cell migration and proliferation.[93]

In addition, the swelling ratio of a hydrogel significantly influences cytokine diffusion, establishing a crucial relationship that impacts the efficacy in tissue regeneration. As the hydrogel swells from water uptake, its network polymer expands, increasing the pore size and thus facilitating cytokine mobility.[94] This increased mobility allows cytokines to diffuse more freely and rapidly through the hydrogel, creating concentration gradients essential for directing cellular activities such as migration. Alginate hydrogels can be precisely tailored to alter critical characteristics associated with the ideal environment for ECM production, cell proliferation and regeneration.

The modification of IVD hydrogel properties remains challenging since in vitro studies do not offer reproducibility due to various factors such as biological variability and experimental design. Laboratory experiments are performed under highly controlled and simplified conditions. They often fail to capture the complex interactions within a living system, leading to inconsistencies when replicating results.[95] In vitro modulation of the immune response to the hydrogel is a concern due to the inability to accurately recreate the complex spectrum of immune interactions in the in vivo environment, leading to an overly simplified and inadequate representation.[96] Finally, data integration is

difficult for in vitro studies. These studies generate extensive data, but a lack of reliable methods to integrate and analyze it can make it difficult to draw conclusions and predict in vivo behavior. Computational models could thus be leveraged to complement preclinical models for characterizing biological phenomena that are non-intuitive, unexpected, or difficult to explore experimentally.

2.5 Computational Modelling for Biomaterial Design

Computational modelling in tissue engineering and regenerative medicine (TERM) has become increasingly popular in recent years as researchers seek to understand complex biological systems through mathematical simulations (**Figure 2.5**). Mathematical models are foundational tools in many scientific disciplines, providing a structured framework for describing, analyzing, and predicting complex systems, offering insights into behavior that are difficult to study through experimental means alone. In biology, mathematical models are used to represent biological processes and phenomena using equations and computational algorithms.

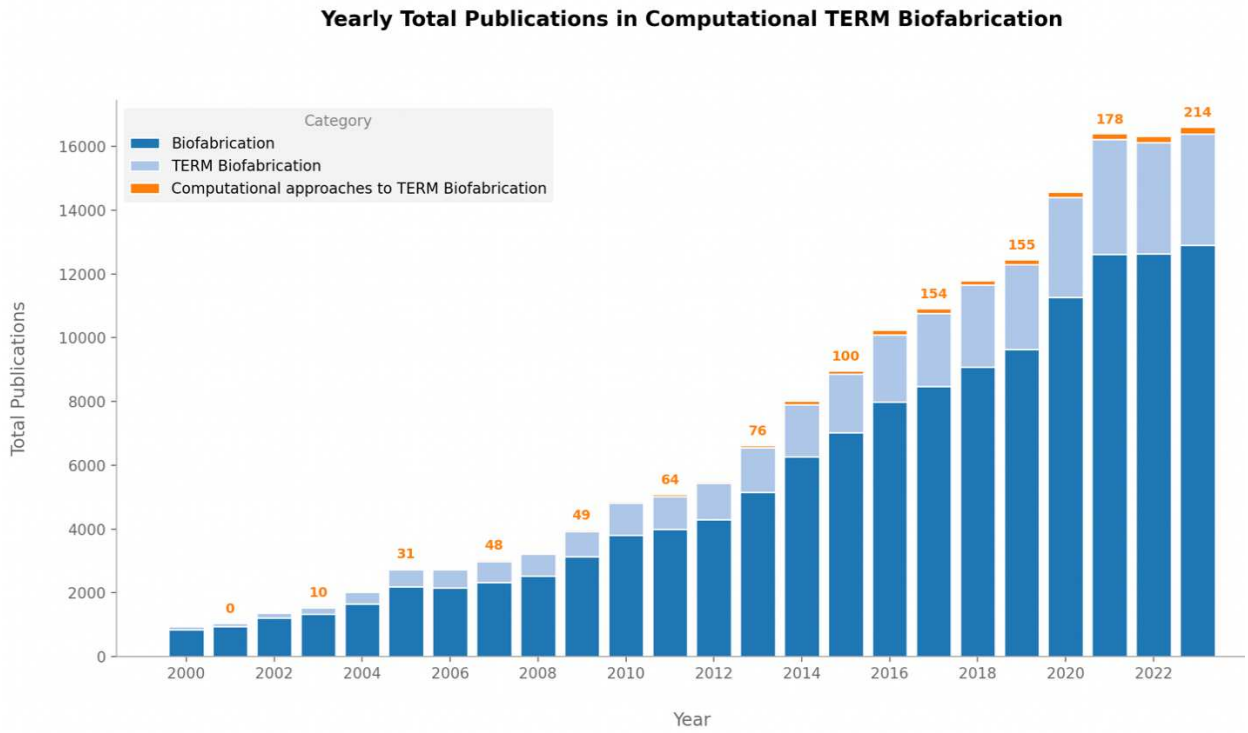

Figure 2.5. Annual Distribution of Scientific Publications Related to Tissue Engineering and Regenerative Medicine (TERM). The annual distribution of scientific publications in biofabrication, TERM biofabrication, and computational approaches for TERM research domains from years 2000 to 2023. This stacked bar chart is categorically divided to highlight the respective contributions of each research domain. The rising trend in publications utilizing computational methods for biomaterial design reflects a shift in interest towards data-driven strategies. This shift underlines the increasing relevance of predictive modeling in advancing regenerative medicine. The data from this graph was collected from Bardini et al.[13]

In regenerative tissue engineering, computational modelling can be used to predict how various biomaterial properties—such as stiffness and biochemical composition impact cellular behavior. Simulated testing conditions allow for standardizing parameters, including initial conditions, biomaterial composition, and cell species, which reduces variability when comparing outcomes between repeated experimental procedures.[97] This

enables researchers to optimize biomaterial design while eliminating the need for time-consuming, costly, and invasive experimentation.[98] There are several types of computational modelling used for tissue engineering, each with their own strengths and limitations. Such models can be categorized based on the scale at which they operate, ranging from the molecular level to the cellular level and up to the tissue or organ level.

At the molecular scale, Molecular Dynamics Simulations (MDS) focus on the atomic and molecular interactions. These simulations provide detailed insights into the molecular structure, dynamics, and interactions under various physical and chemical conditions. In tissue engineering, MDS can be particularly useful for designing biomaterials at the molecular level, ensuring compatibility and optimizing interactions with biological molecules. For example, MDS can be used to investigate the structural characteristics of aggrecan in the degenerated IVD.[99] The strength of MDS lies in its detailed resolution and predictive capability for molecular interactions. However, it is computationally intensive and generally limited to small systems or short time scales, which can be a significant limitation when trying to scale up to larger tissues or longer durations.[100]

At the tissue or organ scale, Finite Element Analysis (FEA) breaks down complex structures into smaller, manageable parts and analyzes the stresses and strains under various conditions. In tissue engineering, FEA is valuable for designing and evaluating scaffolds and implants under physiological loads, ensuring that the engineered tissues can withstand actual bodily stresses.[101] FEA allows for detailed simulation of stresses and strains, providing crucial data for optimizing the mechanical properties and structural

integrity of engineered tissues. However, there is a need for defined input data regarding material properties and geometries, and it can be computationally demanding for large or highly detailed models.[102]

Lastly, cellular automata models, including agent-based modelling (ABM), effectively integrate multiple biological scales from molecular to tissue levels to offer a comprehensive perspective on cell-cell and cell-ECM interactions.[103] This computational modeling technique offers an exploration of how interactions at the cellular level govern the emergent behavior at the tissue level over an extended time period. **Section 2.5.1** delves into the specific components and details how ABM is employed in an IVD tissue engineering context.

2.5.1 Agent-Based Modelling

ABM is a computer modeling technique that simulate complex dynamic interactions between autonomous *agents.* The individual agents follow predefined rules in a system to predict emergent behaviors otherwise difficult to achieve through traditional experimental methods alone.[104] At each time increment, each agent evaluates its surroundings and current state variables to determine its next action.[105] The versatility of ABM is seen by their applications across various disciplines such as economics[106] and sociology,[107] to those as intricate as the biological simulations of inflammation and wound healing,[108] tumour growth,[109] and spinal cord injuries.[110]

In tissue engineering, ABM provides a means to simulate the interaction of individual cells with their microenvironment, including biomaterials and other cells. Individual cells are modelled as software agents with independent states (position, cycle status) and activities (motility, proliferation, matrix secretion). Each cell agent reacts to stimuli from their microenvironment, which causes changes in their behavior (**Figure 2.6**).[111] A variety of empirical data can be standardized into a set of simpler biological interactions that can be translated into mathematical expressions, referred to as *rules*, using regression analysis and subsequently encoded into an executable model for virtual world exploration.[112] This approach allows for the prediction of tissue growth, organization, and response to various stimuli, which guides the design and optimization of engineered tissues.[113]

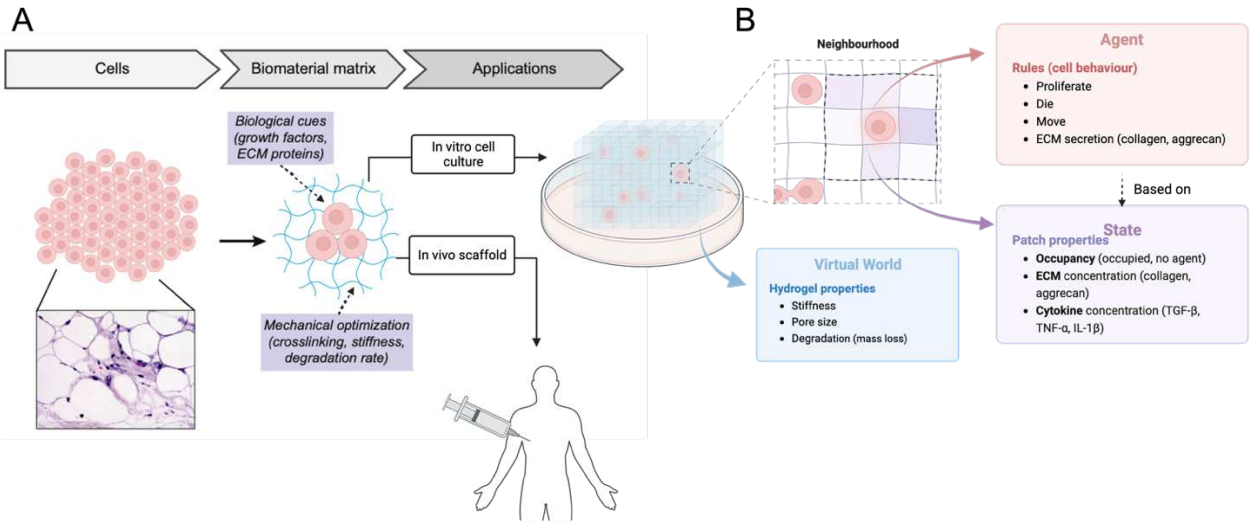

Figure 2.6 Agent-Based Modelling in Tissue Engineering. the principles of biomaterial regenerative tissue engineering. Adapted from Raia et al., 2020 [114] (B) the design principles of the ABM model; biomaterial world; state variables; and agent behavior. Created with BioRender.com.

ABM is particularly useful when examining the dynamics of cellular biology, such as the slow process of NP degeneration and regeneration in an efficient time frame, which traditionally requires extended periods of cell culture time.[115,116] For instance, the viability of NP cells over time can be transposed into a model as a set of probability values. These probabilities are derived from empirical in vitro data and can be incorporated into the model's mathematical framework to simulate the dynamic behaviors of NP cells in various scenarios.[16] When selecting optimal biomaterial properties, researchers can efficiently examine NP cell behavior and viability within different biomaterial compositions by simply modifying the parameters of the model and re-running the simulation. This approach allows for the rapid iteration of simulations under diverse conditions, thus

facilitating the exploration of NP cell behavior in relation to the biomechanical and biochemical properties of different biomaterial compositions.

2.6 Existing ABM in IVD Research

At present, very few IVD-ABM simulate the effect of external stimuli on cellular behavior. **Table 2.3** presents a summary of the two published models, including their inputs, outputs, and limitations, particularly their exploration of proinflammatory cytokines and ECM turnover — important factors in NP cell regeneration, highlighting their relevance to this research.

Table 2.3 Review of current IVD-ABM.

Authors	Input	Output	Limitations
(Baumgartner, Reagh et al., 2021)[117]	• Nutritional stimuli: 0 - 5 mM Glucose, 0 - 10 mM Lactate, • 6.5 - 7.4 pH, • IL-1β mRNA expression.	• Cell viability, • Immunopositive cells for IL-1β, • Aggrecan, collagen, MMP-3, and ADAMTS mRNA expressions.	• Should contain a more complex feedback looping network for dynamic IL-1β regulation, • Only considered additive biochemical factor contributions.
(Baumgartner, Sadowska et al., 2021)[16]	• Nutritional stimuli: 0 - 5 mM Glucose, • 6.5 - 7.4 pH, • TNF-α and IL-1β mRNA expressions.	Aggrecan and collagen mRNA expressions for: • Non-inflamed, • IL-1β immunopositive, • TNF-α immunopositive, • Both IL-1β and TNF-α immunopositive.	Relationship between mRNA expression and protein synthesis not always linearly proportional.

A commonality among these models is their focus on the biochemical response of NP cells to variations in nutrient concentrations and cytokine levels. However, treating each biochemical factor in isolation, without considering their synergistic and inhibiting interactions with the mechanical environment led to a reduced level of confidence in simulation results. Disregarding the influence of the physiological mechanical environmental forces resulted in an over-prediction of simulated inflamed cells. A refined model should also incorporate additional cell behavioral regulators, such as the influence of direct mechanotransduction. Hydrogel stiffness has been shown to play an important role in influencing the cell behavior and mediating remodelling. Generally, softer hydrogels tend to result in an increased cell proliferation[118] while stiffer substrates promote ECM synthesis and cell morphology.[119]

2.7 Research Gaps and Hypothesis

Both TERM and computational modeling are rapidly evolving fields where bridging these gaps could lead to significant advancements in medical science and patient care. While there have been advances in biomaterial development, challenges remain in fully integrating these materials with native tissue while considering biocompatibility, bio-functionality, and the mechanical integration. Existing computational models were available for simulating NP cell behavior under rudimentary cytokine and nutrition variations. However, these models did not adequately incorporate mechanotransduction — the process by which cells convert local physical stimuli into biochemical signals.

Therefore, this thesis proposes a computational ABM that integrated mechanical, chemical, and biological stimuli to inform biomaterial design in tissue engineering. By simulating the relationship between the chemical makeup of the hydrogel and its physical properties, this model would provide insights into the influence of hydrogel formulations in supporting NP cell regeneration. It was hypothesized that the validated ABM would accurately model the NP cell dynamics, such as cell viability and ECM matrix regeneration as well as captured the material properties of the hydrogel under the tuned chemical composition.

Chapter 3 Methodology

3.1 Agent-Based Model Overview

An IVD-hydrogel ABM (IVDH-ABM) was developed to simulate the response of NP cells to calcium-crosslinked alginate hydrogels for IVD regeneration. In vitro experimental conditions and results previously collected from alginate hydrogel formulations[88] were used to set up, calibrate, and validate the proposed IVDH-ABM. The model's inputs included the hydrogel formulation, such as the calcium crosslinking density and alginate concentration, along with the NP cell seeding density. The outputs of the model consisted of hydrogel physical properties (specifically elasticity), time-series viable cell counts, concentrations of cytokines (TNF-α, IL-1β, and TGF-β) and ECM components (collagen-II and aggrecan).

3.2 Computational Framework and Execution Environment

The IVDH-ABM was a lattice-based stochastic model to numerically simulate NP cell responses to alginate hydrogels designed for IVD regeneration. Developed in C++ programming language, the IVDH-ABM used parallel computing to increase performance and reduce the computational time, Open Multi-Processing (OpenMP) version 4.0.3 application programming interface (API) for multi computer processing unit (multi- CPU) execution and Compute Unified Device Architecture (CUDA) version 11.0 for graphics

processing units (GPU) acceleration. The GNU compiler (gcc version 8.4.0) was used to compile the model and execute on Digital Research Alliance supercomputer nodes with 32 Intel CPUs, 2 NVIDIA GPUs, and 64 GB of memory for efficient processing. In addition, ParaView 5.11.0 was used to visualize the numerical value of model outputs.

The IVDH-ABM has three major components: the *environment*, *agents*, and *state variables*. The *environment* consists of the spatial-temporal setup and initialization of the simulation (**section 3.3**). The *agents* consist of motile discrete entities that obey specified rules whereas the *state variables* consist of the hydrogel physical properties, the ECM and cytokine levels (**section 3.4**).

3.3 Model Initialization

3.3.1 The Environment

The IVDH-ABM *world* is represented as a three-dimensional alginate hydrogel and is mapped onto the x- y- z- cartesian coordinate system. To initiate the IVDH-ABM, the *world* was seeded with the most abundant type of cells found in the NP region of the IVD, namely, chondrocyte-like NP cells. These motile cells are represented as *agents* within the model. To emulate in vitro conditions (**section 3.3**), the *world* size was set to 3 mm x 3 mm x 3 mm and was spatially segmented into lattice *patches* at 10 µm x 10 µm x 10 µm. The patch size was designed to match the average size of an NP cell[120] and ensure that each *patch* could accommodate no more than one cell at a time. 27 000 NP cell agents were randomly initialized throughout the world.

3.3.2 Spatial-Temporal Organization

The IVDH-ABM adopted a lattice-based spatial architecture to optimize computational efficiency when simulating the spatial dynamics of cellular environments. This choice contrasts with a lattice-free method, allowing for more precise computational modeling of cells within a structured environment.[121] The environment of the model was segmented into a grid-like pattern of discrete *patches*, with each *patch* functioning as a discrete node. These nodes serve dual purposes: they provide a single housing for individual cells, preventing any cell-cell overlap, and they maintain a record of local information about the state of agents and their environment at any given time.[122] This lattice arrangement confined cell migration to discrete positions in the 3D cartesian coordinate system, enabling an orderly update and tracking of cell movements and interactions within the model. The use of discrete nodes simplifies the computational process, as each cell's position is unambiguously defined, streamlining the simulation of complex cellular behaviors and interactions.[123]

Each *patch* stores *state variables*, such as the cartesian coordinates, numerical values of ECM, cytokine concentrations and mechanical properties (floating point) as well as cell occupancy (Boolean). Each simulation step, referred to as *ticks*, corresponds to 30 minutes in the real-world. **Table 3.1** summarises the IVDH-ABM initial conditions.

Table 3.1. Initial Conditions of the IVDH-ABM.

Entity	Component	Value
Agents [a]	NP cells	27 000
World Size [c]	Alginate hydrogel [L x W x H]	3 × 3 × 3 [mm^3]
Patches [c]	Patch size [L x W x H]	10 × 10 × 10 [μm^3]
	Number of patches	27×10^6
ECM [b]	Collagen (II)	0 [µg]
	Aggrecan	0 [µg]
Cytokines [b]	TNF-α	0 [pg]
	IL-1β	0 [pg]
	TGF-β	0 [pg]
Time [c]	Simulation duration	21 [days] [a]
	Time step (tick)	30 [minutes]

[a] value taken from Li et al.'s *in vitro* study of alginate hydrogel for IVD repair.[88]
[b] values taken from various studies in literature.
[c] constant values throughout the simulation.

3.4 IVDH- ABM Components and Rule Derivation

3.4.1 Overview of Simulation Routines

During each simulation time *tick*, NP cell agents executed a series of programmed decisions, or *rules*, which included behaviors such as proliferation, apoptosis, secretion, and migration (**Figure 3.1**). In the simulation, an agent can be in one of three states: inactive, active, or dead. The cell can migrate and proliferate but cannot perform any secretion functions when in the inactive state. In the active state, the cell can perform all the functions as in the inactive state with the additional capacity to synthesize ECM components, including collagen-II and aggrecan, as well as cytokines, including TNF-α,

IL-1β, and TGF-β. In the dead state, the NP cell is no longer able to perform any function and is removed from the simulation at the end of the time step. Agent activation was determined by probability and the local concentration of TGF-β. An agent can become activated if the concentration of TGF-β exceeds the activation level. However, the agent can return to its inactive state if the concentration ever falls below the threshold.

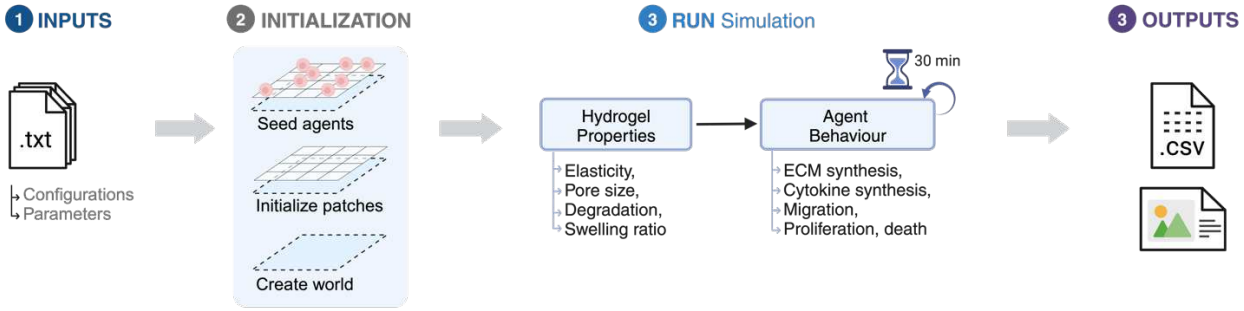

Figure 3.1 IVDH-ABM Procedural Overview. The procedure begins with inputs from a configuration text file, leading to the initialization of patches to create the simulated world, and randomized agent seeding. The agent behaviors (migration, proliferation, ECM, and cytokine synthesis) are executed and influenced by the alginate hydrogel properties. Agent states are updated, and the process repeats until the input simulation time is reached. Outputs are generated in **.csv* and **.vtk* files, representing data on cell count, ECM and cytokine concentrations, and hydrogel properties. Created with BioRender.com

The set of decisions were made after the *agents* evaluated both their current internal state and surrounding environment conditions *state variables*. These variables included characteristics of the hydrogel material, such as elasticity, porosity, and degradation over time (mass loss), as well as the occupation of space by other nearby

cells, concentrations gradients of cytokines (TNF-α, IL-1β, and TGF-β), and ECM components (collagen-II and aggrecan). The interactions between the NP cell *agents* and these *patches*, through the *state variables* they hold, drive the emergent behaviors observed in the model, such as tissue regeneration.

In this model, *agent behavior* defined the actions or responses of NP cell agents to their internal states and the stimuli present in their environment (**Figure 3.2**). These behaviors encompass the agents' programmed decisions to proliferate, undergo apoptosis, migrate, and synthesize ECM components and cytokines. Conditional "*if-then*" logic statements link such behaviors to external stimuli, based on existing literature regarding the response of NP cells to properties of calcium crosslinked alginate hydrogels. Each agent-rule represents a specific agent behavior as a function of external stimuli, and can be understood with a general mathematical expression below:

$$Agent\ Behaviour(\boldsymbol{U}, \boldsymbol{D}) = \boldsymbol{b} + \left(\sum_{i=1}^{n} \boldsymbol{U}_i^{Stimulus_i} + \sum_{i=1}^{n} (-\boldsymbol{D})_i^{Stimulus_i} \right) \qquad \text{Equation 1}$$

Where **b** is base value, in the absence of a stimuli (baseline rate), **U** represents the effect of the set of stimuli upregulating the behavior, and **D** represents the effect of the set of stimuli downregulating the agent behavior. Specific agent-rules (e.g., proliferation rates, apoptosis, migration patterns, responses to biophysical stimuli), state variables (e.g., cytokine and ECM concentration) and simulation routines are detailed in **sections 3.4.2 - 3.4.5**

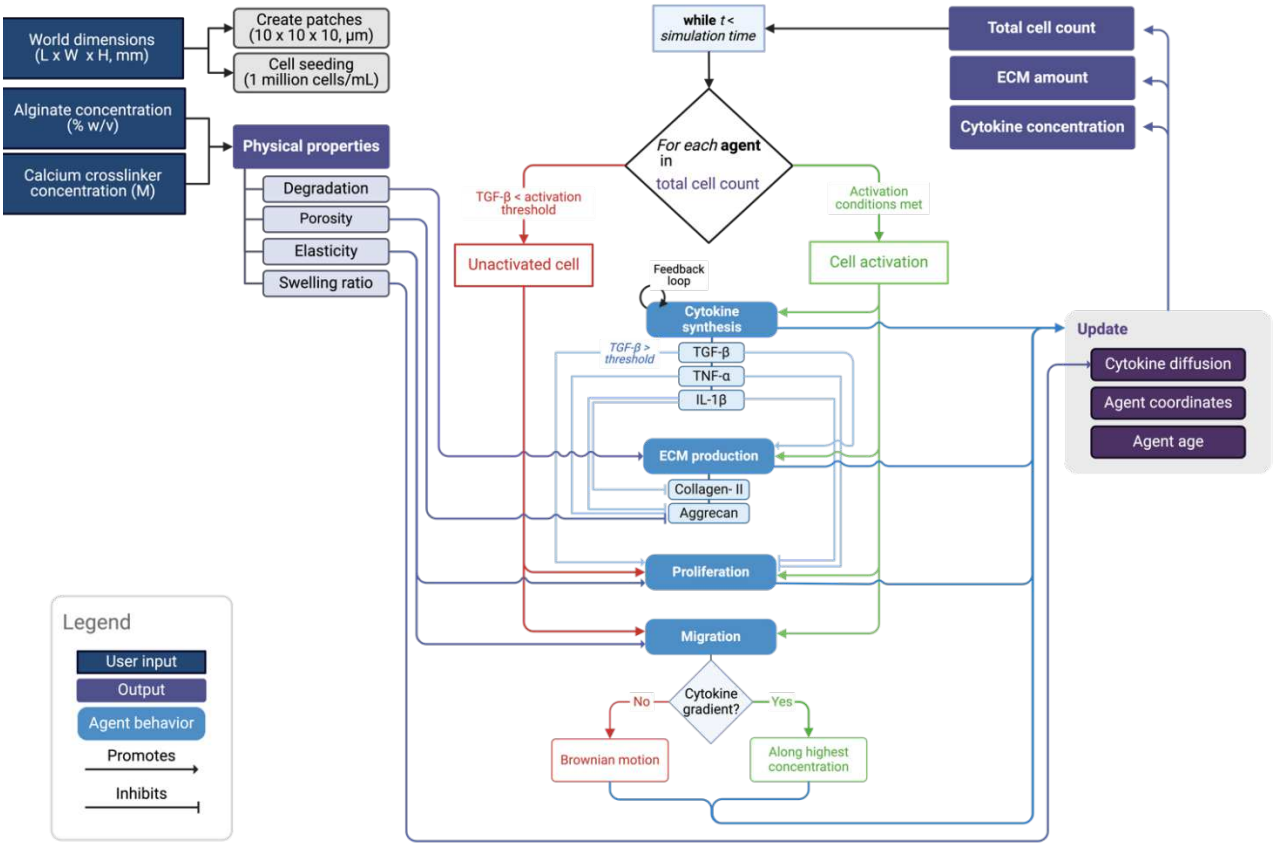

Figure 3.2 Flowchart of the IVDH-ABM Rules. Overview of simulation parameters and processes, including the world dimensions, hydrogel properties, and the cascade of cell behaviors. Dashed and solid-lined arrows indicate inhibitory and promotional influences, respectively. Created with BioRender.com.

3.4.2 NP Cell Agent Behaviors

NP cell agents had the capacity to perceive and respond to their surroundings, including neighboring cells, ECM and cytokine concentrations, and environmental physical properties, thereby simulating cell-cell and cell-hydrogel interactions. Agents sensed environmental cues through conditional checks, mimicking cellular perception in

biological reality. Depending on the cue, cells could decide to either proliferate, die, migrate, or activate and secrete cytokines and ECM components (**Table 3.2**).

Table 3.2 Summary of Agent Rules in IVDH-ABM.

Behavior	Rule	Controlling Variables
	Agents	
Cell migration speed $[\mu m/min]$	$v = k_1 \ln(E) + k_2$	
Cell viability rate $[\%]$	$v_r = k_3 \ln(Day) + k_4$	Cell lifespan ~14 $[days]$. [124]
Proliferation rate $[\%]$	$x = \begin{cases} -1, & TGF > k_5 \\ 1, & TGF \leq k_5 \end{cases}$ Every k_6 hours, *evaluate*: $Proliferation\ Probability = \ln(1 + TNF + IL1\beta + \boldsymbol{x}TGF)$ $Proliferation\ rate = k_{10} + k_{13}(Day) + k_9(Alg_{wv}) + k_8(Day)(Ca_{XL}) + k_{11}(Alg_{wv})(Ca_{XL})$	
TGF-β synthesis $[pg/mL]$	$TGF = k_{15} + k_{16}(TGF) + k_{17}(IL1\beta) + k_{18}(TNF)$	
TNF-α synthesis $[pg/mL]$	$\mathrm{TNF} = \mathrm{k_{19}} + \mathrm{k_{20}}\left(\frac{\mathrm{IL1\beta}}{1 + \mathrm{k_{21}(TGF)}}\right)$	
IL-1β synthesis $[pg/mL]$	$\mathrm{IL1\beta} = \mathrm{k_{22}} + \mathrm{k_{23}}\left(\frac{\mathrm{TNF}}{1 + \mathrm{k_{24}(TGF)}}\right)$	
Effective cytokine diffusion coefficient $[mm^2/min]$	$D = 0.0018 * 0.1(Q)$	• Effect of cytokine molecular weight on diffusivity coefficient: 0.0018.[125] • Effect of swelling ratio on diffusivity constant: 0.1.[126]

Cell activation probability	$\text{Collagen Stimulation} = \frac{\ln(1 + k_{31}\text{TGF})}{1 + k_{32}\text{IL1}\beta}$ $\text{Aggrecan Stimulation} = \frac{\ln(1 + k_{36}\text{TGF})}{1 + k_{37}\text{TNF}}$	
Collagen synthesis rate (ug/mL)	$Collagen = k_{33}(Day) + k_{34}$	Collagen increases over time.[127]
Aggrecan synthesis rate (ug/mL)	$Aggrecan = k_{38}(Day) + k_{39}$	Aggrecan increases over time.[128]
Hydrogel		
Elastic Modulus [kPa]	$E = c_1 + c_2(Alg_{wv}) + c_3(Ca_{XL}) + c_4(Alg_{Mw}) + c_5(Alg_{wv})(Ca_{XL}) + c_6(Alg_{wv})(Alg_{Mw}) + c_7(Ca_{XL})(Alg_{Mw})$	
Pore size [μm]	$Pore\ size = c_8(Ca_{XL}) + c_9$	
Mass loss [%]	$Degradation = c_{10} + c_{11}(Ca_{XL}) + c_{12}(Day) + c_{13}(Ca_{XL})(Day)$	
Swelling ratio [%]	$Q = c_{14} + c_{15}(Day) + c_{16}(Alg_{wv}) + c_{17}(Day)(Ca_{XL}) + c_{18}(Alg_{wv})(Ca_{XL})$	

3.4.2.1 Proliferation and Apoptosis

Each agent had an internal *clock* that advanced with each computational iteration since the cell was initialized, akin to cellular aging in a biological system. The progression of the *clock* triggered changes in the internal state and decision-making logic, affecting its ability to proliferate and produce ECM components.

Proliferation. The proliferation of NP cells was contingent upon meeting the following criteria: proliferation rate, probability of proliferation, cytokine levels, availability of space, and hydrogel biophysical stimuli.

First, the *proliferation rate*, was determined by the change in the cell population and the initial number of cells. The probability of proliferation was modeled using a simulated dice roll to represent random chance. If the generated chance was greater than the predetermined proliferation probability, then the cell division function was carried out and the other criteria was checked. The opportunity for an NP cell to undergo division was evaluated every 24 hours, aligning with typical biological checkpoints for cell cycle lifecycles.[129]

Secondly, the proliferation of a cell was further modulated by the cytokines present in the local environment through a logarithmic function (**Table 3.2**). In particular, this probability was modulated by TGF-β cytokine levels, where lower concentrations up to 10 [ng/mL] had a positive effect, and higher concentrations negatively influenced proliferation.[130] This binary response was encoded into the model as a factor of either +1 or -1, which ultimately adjusted the cytokine influence on the proliferation rate (**Table 3.2**).

Lastly, the proliferation rate was dependent on both the simulation time and the elasticity of the matrix (**Table 3.2**). Stiffer substrates promote cell growth and enhance the proliferation rate.[131] The presence of surrounding cells also influenced cell proliferation. The spatial component of proliferation was handled by ensuring that division could only

occur into adjacent, unoccupied patches. Once the criteria for proliferation were satisfied, the NP cell agent would first search for an unoccupied patch using a trial- and- error method and attempt to divide into one of the possible 27 adjacent patches in the Moore's neighbourhood.[132] This attempt was repeated up to eight times to account for the spatial constraints on proliferation imposed by cell density. If the agent was unable to locate an unoccupied patch before exhausting the maximum trials, cell division was abandoned until the next eligible cycle.

Apoptosis. Apoptosis is the process of programmed cell death, as part of the cell lifecycle. One of two factors influenced NP cell death. First, the concentration of TNF-α induced the apoptosis rate by roughly 3.5 folds, as reported in literature.[36] Second, the age of the cell influenced its probability of death (**Table 3.2**). Upon cell initialization, each cell was assigned a randomized lifespan variable, varying between 7 and 14 days to emulate the stochastic nature of cellular mortality.[124] This internal age was continually assessed against the predetermined death age of the agent; when the simulation time matched the agent's end-of-life threshold, the model enacted a programmed cell death. Consequently, the agent was flagged for removal from the simulation.

3.4.2.2 Migration

Driven by the gradients of cytokines, all NP cell agents could move through the hydrogel matrix. The Moore's neighborhood method[132] was adopted to examine the three-dimensional space surrounding the agents for available space before any migration or proliferation decision was made. If an unoccupied patch was found, the agents had the

opportunity to migrate towards it, either along cytokine gradients[133] or in random Brownian directions,[134] or to proliferate towards this space. This mechanism ensured that cell proliferation or movement occurred only if sufficient space was available, reflecting real-world spatial limitations.

Further, agents would compare the local concentrations of cytokines in each Moore's neighbouring patch when deciding to migrate along their gradient, a behavior simulated by adjusting the agent's directional probability. The migration speed was also modulated by the stiffness of the hydrogel. Softer matrices encourage faster movement, whereas stiffer ones restrict cell displacement, reflecting how cells navigate the extracellular environment in real tissue.[135,136]

3.4.2.3 Cytokine and ECM Secretion

Upon activation, NP cell agents had the opportunity to secrete TGF-β, TNF-α, and IL-1β cytokines, as well as ECM components including collagen-II and aggrecan. The cytokines released by the NP cells engaged in autocrine and paracrine loops, regulating the behavior of both the secreting and adjacent NP cells. Depending on the cytokine profile, this can lead to either stimulatory or inhibitive effects on the proliferation rate and ECM production.

Cytokine diffusion was modeled to simulate the spread of signaling molecules within the hydrogel. The secretion of TGF-β initiated a positive feedback mechanism, establishing an autocrine loop, directly promoting its own synthesis, as well as a paracrine loop, enhancing the ECM production.[130] TNF-α, and IL-1β cytokines also operated in

similar manner, wherein their diffusion through the environment modulated cellular activities such as proliferation and ECM production as well as further cytokine synthesis. For example, higher levels of TGF-β ($> 10\ ng/mL$) increases the proliferation rate by roughly 3.5 folds and the aggrecan production rate by 1.5 folds,[130] whereas TNF-α and IL-1β inhibit the stimulation of aggrecan and collagen production by roughly 0.5 folds.[137] Given that the half-lives of collagen and aggrecan are 215 years[31] and 12 years[29] respectively, this slow degradation would have minimal effects on the model dynamics. As such, aggrecan and collagen were modeled with having "infinite life" in this IVDH-ABM.

3.4.3 Biophysical Stimuli

The mechanical environment within the hydrogel matrix plays a critical role in influencing cellular behaviors. Physical properties such as elasticity, porosity,[138] degradation rate,[139] and swelling ratio[140] each can modulate cell behavior in the hydrogel. For example, higher alginate and calcium concentrations resulted in increased hydrogel stiffness, a factor known to influence cell migration[135]. Similarly, the rate of hydrogel degradation was modulated by the calcium crosslinking density.[141] However, despite the abundance of quantitative data on hydrogel-cell interactions, the specific data pertaining to NP cell behaviors in relation to these factors are relatively scarce. Consequently, they have not been explicitly modeled in the current ABM framework.

In this IVDH-ABM, studies that examined the effects of alginate concentration and calcium crosslinking density on hydrogel elasticity,[142] porosity,[92] and degradation[143] were

used to develop the relation between cell behavior and the hydrogel physical properties. (**Table 3.2**) Specifically, elasticity was employed as the primary biophysical influence on the proliferation[127] and migration[52,144]. For instance, cell movement was non-linearly dependent on matrix stiffness. The model encoded the stiffness of the hydrogel into a parameter that influenced the likelihood of migration or proliferation. The agents referenced this parameter to adjust their behaviors and decision-making. This mechanistic sensing allows agents to make informed decisions about migration, proliferation, or activation. For instance, cell movement was modulated to be non-linearly dependent on the matrix stiffness,[144] reflecting the varying motility in different hydrogel conditions.

3.4.4 State Variables

Within the IVDH-ABM framework, *state variables* are essential components that include the occupation status of each *patch* by agents, concentrations of key ECM components such as collagen and aggrecan, and the levels of cytokines including TNF-α, IL-1β, and TGF-β. Additionally, the physical properties of the hydrogel matrix, such as elasticity, porosity, and swelling ratio are accounted for as state variables, linking the chemical and mechanical microenvironment to cellular activities (**Figure 3.3**).

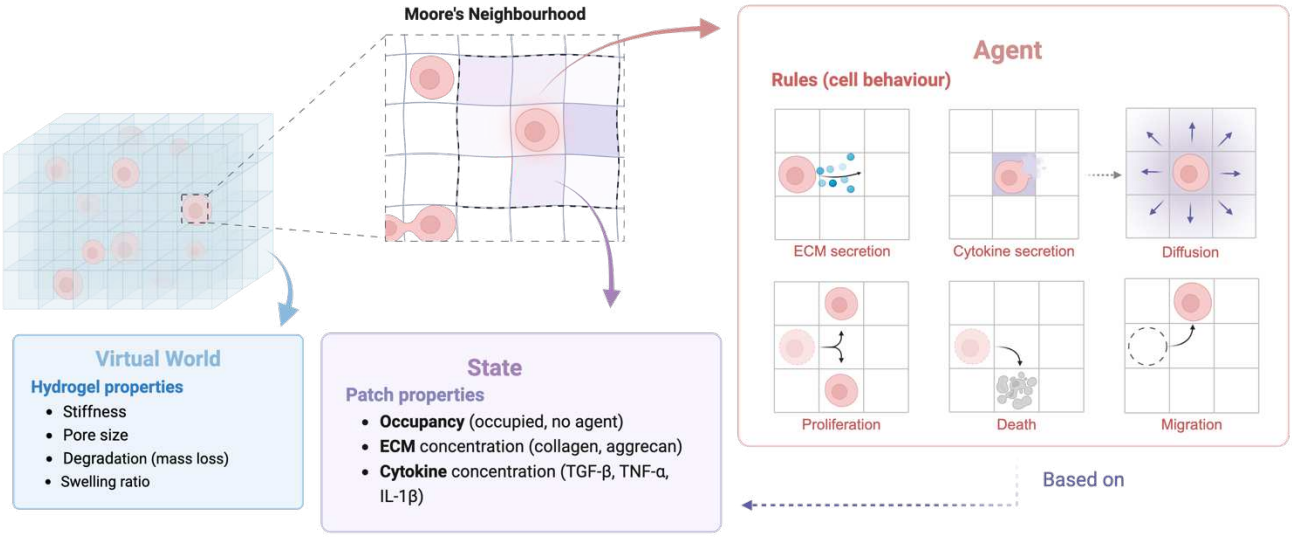

Figure 3.3 Agent Behaviors in Lattice- Based IVDH-ABM. Illustration of the virtual world defined by the hydrogel properties and state variables within each lattice patch. The agents interact with their environment and with each other through predefined behaviors such as proliferation, death, and migration, driven by local conditions like ECM and cytokine concentrations and physical properties of the hydrogel. Created with Biorender.com.

3.4.4.1 Cytokine Diffusion

Building upon the published vocal fold (VF)-ABM,[145] the model incorporated a diffusion algorithm, designed to capture cytokine kinetics within the virtual world. Parallel processing with GPUs were used to handle the convolution-based diffusion calculations. By performing multiple convolution operations simultaneously, the model would update concentrations on numerous patches at once, significantly reducing simulation time. Specifically, partial differential equations (PDEs) were used to compute the spatial distribution of cytokine levels over time, based on molecule diffusivity coefficients and their individual decay rates (**Table 3.3**). Once secreted by their NP cell sources, the

cytokines diffused outwards, creating concentration gradients crucial for the directed migration of agents. For each patch, indexed by "*ix*", "*iy*", "*iz*", the cytokine concentrations at *tick* "*t+1*" was updated based on its previous concentration as well as the concentrations in the neighbouring patches, at *tick* "*t*". This calculation reflected the continuous movement and interaction of cytokines within the *world*.

The diffusion coefficient **D** and time step **dt** was used to update the concentration of cytokines on each patch, using the three-dimensional diffusion Equation 2. The diffusion coefficient, **D**, (0.0018 mm^2/min)[146] was calculated by the inverse of the cube root of the cytokine molecular weight and quantified how rapidly the cytokines spread through the hydrogel, where the patch length is $\mathbf{dx} = \mathbf{dy} = \mathbf{dz} = 0.01\ mm$.

$$dt < \frac{dx^2}{6D} \quad \text{Equation 2}$$

Biologically, as hydrogels swell, the increased water content causes the polymer network to expand and results in larger pore sizes. The larger pores facilitate the diffusion of the entrapped molecules. As such, this IVDH-ABM also accounted for the effect of the swelling ratio of the hydrogel, "Q", on cytokine diffusion with an inclusion of an effective diffusivity equation into the diffusion algorithm. An adjustment coefficient of 0.1 (**Table 3.2**)[126] was incorporated to modify the diffusivity of cytokines within the hydrogel matrix, accounting for changes in the physical properties of the hydrogel as it swells.

3.4.5 Model Stochasticity and Synchronous Updates

The IVDH-ABM was structured to capture the inherent variability and unpredictability of biological systems through the introduction of stochastic elements. In biological systems, the complexity and number of influences on each cell make it computationally infeasible to account for every action or response individually. ABM addresses this challenge by generating populations of agents, where the behavior of the entire group informs the probability functions for individual behaviors.[105] These probabilities can then be integrated into the rules governing each agent, allowing for efficient simulation of various cellular actions and interactions.

Natural randomness was embedded within the decision-making process of the agents via a random number generator. This generator produced a number which was then assessed against predefined probability thresholds to decide if an agent could proceed with a specific action. This mechanism mirrored the unpredictability present in natural biological environments, allowing for a realistic representation of cellular behavior.

Integrating stochasticity to the operational logic introduced a layer of complexity to the simulation. The actions performed by the agents were contingent upon both its local surroundings and internal state. Meanwhile, within each simulation tick, a dynamic sequencing approach was adopted, where agents were called in sequence, but the order of their actions was randomized. This method was designed to prevent biases and ensure that outcomes were not influenced by any fixed sequence, maintaining the integrity of the simulation results.

Following the executed actions of agents, any modifications in location, activation status, age, or local concentrations of secreted components were recorded but not immediately updated. Instead, modifications across all agents were simultaneously applied at the end of each simulation tick (**Algorithm 1**). This method of synchronous updating allowed for all agents to operate under consistent environmental conditions and ensured that simulation outcomes were not influenced by the sequential order in which agents were addressed. By decoupling the decision-making process from modification updates, the model avoids biases that could skew the simulation results and preserve the consistency of the model outputs across all simulation runs.

Algorithm 1. Pseudocode of IVDH-ABM Operations.

```
IVDH-ABM Procedure:
Initialize patches
Initialize cells → (migration speed, ECM and cytokine production rates,
proliferation rate, and viability rate)
While time ≤ 21 days do
        For each patch
                Add cells function
                ECM function
        For each cell
                Cell function
        For each cytokine
                Diffuse cytokine function

        Update attributes → (Cell, ECM, Patch, Cytokine)
return
```

3.5 Model Calibration

Given the computational impracticality of creating a simulation model that captures every detail and behavior of the actual system, it is necessary to make some assumptions about the system for model construction. Essentially, a simulation model serves as an abstract representation of a physical system.[147] These necessary abstractions and assumptions can introduce inaccuracies into the simulation. Model calibration is therefore a crucial process that aims to minimize these uncertainties by adjusting the model parameters and event occurrence probabilities, using machine learning techniques, to align more closely with real-world observations.[148]

3.5.1 Data Sources for Model Calibration

The *in vitro* study by Li et al., (2023) provided the primary empirical data source for calibrating IVDH-ABM. Li et al. had evaluated the performance of alginate hydrogels in terms of their regenerative potential and effectiveness in restoring disc biomechanics.[88] The hydrogel formulations were synthesized from a mixture of sodium alginate and calcium sulfate solutions. Four alginate hydrogel formulations were investigated: 1 kPa-high MW (1 kPa-H), 1 kPa-low MW (1 kPa-L), 3 kPa-high MW (3 kPa-H), and 3 kPa-low MW (3 kPa-L), where the concentrations of calcium were 14, 15, 20, and 23 mM, respectively. High and low molecular weights (MW) refer to the respective alginate molecular weights of 1500 and 92 kDa. NP cells were sourced from healthy human IVD tissues (from McGill Spinal Tissue Biobank) and were seeded into a 28 mm^3 alginate

hydrogel at a final density of 1 million cells/mL.[88] Sulfated glycosaminoglycan (sGAG) was quantified using the DMMB assay and the cell viability was evaluated using confocal imaging of Live/Dead assay.

In computational modeling, data is typically partitioned into separate sets for calibration and validation, typically adhering to an 80:20 ratio where 80% of the data is used to fine-tune the model parameters, and the remaining 20% is reserved to evaluate the model's predictive power.[149] This distribution is a common practice as it provides a balance data for establishing robust model parameters and assessing model performance on new data. However, a 75:25 split can sometimes be advantageous.[150] In this project, a 75:25 data partition was chosen for model calibration and validation. Allocating 25% of the data for validation enhances the diversity and the number of data points used to test the model, thus increasing the reliability of validation. As such, aggrecan accumulation on days 3, 6, 9, and 12 and on days 15, 18, and 21 from Li et al., were used for IVDH-ABM calibration and validation, respectively.[88] NP cell viability data points on days 1, 3, and 7 were used for calibration and those on days 14 and 21 were used for model validation.

Li et al., (2023) reported the viscoelastic properties and gelation kinetics of the hydrogel using rheological measurements.[88] However, literature typically relates cellular behavior to the elastic modulus of hydrogels.[135,144,151] To align with this standard and calibrate the model based on hydrogel stiffness, sGAG content, and cell viability, the

shear modulus reported by Li et al., (2023) was therefore converted into the Young's Elastic Modulus using Equation 3.[152]

$$\mathbf{E = 2G'(1 + \upsilon)} \quad \text{Equation 3}$$

Where **E** is the Young's Elastic Modulus (in kPa), **G'** is the Shear Modulus (in kPa), and **υ** is Poisson's ratio, assumed to be 0.5 for alginate hydrogels.[153] Hydrogel elasticity was calibrated against calcium concentrations of 14 mM and 20 mM, and the elasticity for calcium concentrations of 15 mM and 23 mM were reserved for validation.[152] The initial elasticity model was developed based on a comprehensive literature review on alginate hydrogel compositions and related mechanical properties (**Figure 3.4**). Regression coefficients were computed based on preliminary analyses and adjusted as necessary to reflect the impact of each variable; alginate concentration, calcium crosslinker concentration, and molecular weight on the resulting elasticity (**section 4.2**). These coefficients included specific interaction terms to account for the complex relationships between components.

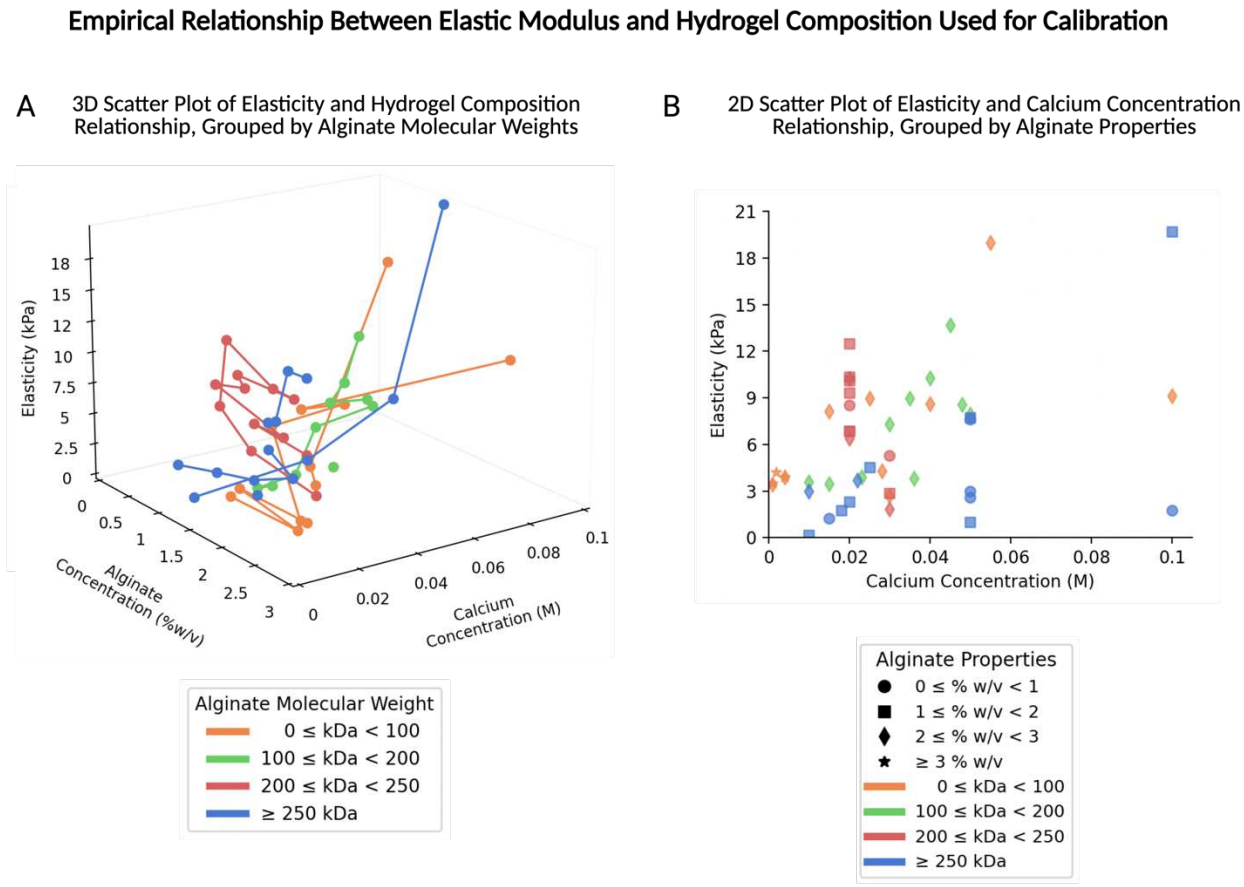

Figure 3.4 Empirical Elasticities of Varying Hydrogel Compositions. Panel A shows a 3D view of the empirical relationship between hydrogel elasticity and calcium concentration, grouped by alginate molecular weights. Panel B shows a 2D view of the empirical relationship between hydrogel elasticity and calcium concentration, grouped by different alginate concentrations and molecular weights. Data points were taken from different empirical studies.[135,154]

3.5.2 Calibration Protocol

The IVDH-ABM has 50 known parameters and 8 latent parameters. Known parameters refer to those whose values were directly measurable or obtainable from experimental data or existing literature (**Table 3.3**). In contrast, latent parameters

represent those whose values were not directly measurable or readily available in literature specifically related to NP cells.[155] These latent parameters included activation probabilities, apoptosis rates, and ECM stimulation probabilities. Among them, eight latent parameters were selected for calibration in this study because of their significant impact on key model outcomes such as cell viability, ECM production, and elasticity of the hydrogel (**Table 3.4**).

Although not readily available in literature, the effect of the intermediate threshold of TGF-β levels parameter on cell activation was not calibrated. The One-at-a-Time (OAT) Sensitivity Analysis was employed to determine the sensitivity of model outcomes to the intermediate threshold of TGF-β levels parameter. This approach involved systematically varying the TGF-β levels while holding all other parameters constant to assess the impact on simulation results.[156] It was found that the simulation outcomes were not sensitive to variations in this parameter, which justified its exclusion from further calibration. Similarly, an OAT Sensitivity Analysis was conducted for the effect of activating factors on cell proliferation stimulation, and it also showed negligible impact on the model outcomes, leading to its exclusion from the calibration process.

Table 3.3 Known IVDH-ABM Parameter Values from Literature.

Parameter	Description	Value	Ref.
	Agent- Related Parameters		
k_1	Effect of elastic modulus on cell migration speed	0.11	[136]
k_2	Baseline cell migration speed $[\mu m/min]$.	0.233	[52]
k_4	Baseline cell viability rate	97.45	[157]
k_5	Threshold of TGF stimulating/ inhibiting cell proliferation $[ng]$	10	[130]
k_6	Hours between cell proliferation	24	[129]
k_8	Combined effect of calcium crosslinker density and time on cell proliferation	(-) 0.043	[158]
k_9	Effect of alginate concentration on cell proliferation	(-) 8.828	[158]
k_{10}	Baseline cell proliferation rate	14.64	[159]
k_{11}	Combined effect of alginate concentration and calcium crosslinker density on cell proliferation	(-) 2.65	[158]
k_{13}	Effect of time on cell proliferation rate	0.288	[159]
k_{14}	Effect of cytokines on cell proliferation stimulation	1	[160]
k_{15}	Baseline TGF synthesis rate	9.98	[161]
k_{16}	Effect of feedback TGF on TGF synthesis rate	2.25	[162]
k_{17}	Effect of IL1b on TGF synthesis rate	1.3	[162]
k_{18}	Effect of TNF on TGF synthesis rate	5.11	[163]
k_{19}	Baseline TNF synthesis rate	5.16	[164]
k_{20}	Effect of IL1b on TNF synthesis rate	2.42	[165]
k_{21}	Effect of TGF on TNF synthesis rate	4.22	[166]
k_{22}	Baseline IL1b synthesis rate	2.11	[164]
k_{23}	Effect of TNF on IL1b synthesis rate	5.43	[167]
k_{24}	Effect of TGF on IL1b synthesis rate	3.26	[166]
k_{25}	Intermediate threshold of patch TGF on cell activation	10	[130]
k_{27}	High threshold of TGF on cell activation	25	[130]
k_{29}	Probability of cell deactivation	25	
k_{30}	Hours between collagen synthesis	12	[36]
k_{31}	Effect of stimulation factors on collagen synthesis	1	[168]
k_{33}	Effect of time on collagen synthesis rate	6.45	[127]

k_{34}	Baseline collagen synthesis rate	3.6	[127]
k_{35}	Hours between aggrecan synthesis	12	[29]
k_{36}	Effect of stimulation factors on aggrecan synthesis	1	[130]
k_{38}	Effect of time on aggrecan synthesis rate	38	[128]
k_{39}	Baseline aggrecan synthesis rate	16.6	[128]
k_{40}	TGF-β half-life [minutes]	2.5	[169]
k_{41}	IL-1β half-life [minutes]	150	[170]
k_{42}	TNF-α half-life [minute]	30	[171]
	Hydrogel- Related Parameters		
c_1	Error variable for elastic modulus	(-) 125	[135,154]
c_2	Effect of alginate concentration on elastic modulus	58	[135,154]
c_3	Effect of calcium crosslinker density on elastic modulus	(-) 971	[135,154]
c_4	Effect of alginate molecular weight on elastic modulus	1.037	[135,154]
c_8	Effect of calcium crosslinker density on pore size	(-)1769.8	[172]
c_9	Baseline pore size	258.5	[172]
c_{10}	Baseline mass loss	0.234	[172]
c_{11}	Effect of calcium crosslinker density on mass loss	7.785	[172]
c_{12}	Effect of time on mass loss	0.15	[172]
c_{13}	Combined effect of calcium crosslinker density and time on mass loss	(-) 1.36	[172]
c_{14}	Baseline swelling ratio	72.478	[140]
c_{15}	Effect of time on swelling ratio	(-) 0.131	[140]
c_{16}	Effect of alginate concentration on swelling ratio	(-) 22.034	[140]
c_{17}	Combined effect of time and calcium crosslinker density on swelling ratio	(-) 3.284	[140]
c_{18}	Combined effect of calcium crosslinker density and alginate concentration on swelling ratio	35.752	[140]

Table 3.4 The Eight Latent IVDH-ABM Parameters Subjected to Calibration. These parameters represent those whose NP cell- specific values were not directly measurable, nor readily available in literature.

Parameter	Description	Value	Ref.
	Agent- Related Parameters		
k_3	Effect of time on cell viability rate	0.73	[124]
k_7	Effect of time on cell proliferation	0.28	[129]
k_{28}	Independent probability of cell activation	2	-
k_{32}	Effect of inhibitory factors on collagen synthesis	1	[173]
k_{37}	Effect of inhibitory factors on aggrecan synthesis	1	[173]
	Hydrogel- Related Parameters		
c_5	Combined effect of alginate concentration and calcium crosslinker density on elastic modulus	756	[135,154]
c_6	Combined effect of alginate concentration and alginate molecular weight on elastic modulus	(-) 0.516	[135,154]
c_7	Combined effect of alginate molecular weight and calcium crosslinker density on elastic modulus	(-) 0.165	[135,154]

The *world* dimensions of the IVDH-ABM were scaled down from 3 mm x 3 mm x 3 mm to a more computationally manageable size of 0.3 mm x 0.3 mm x 0.3 mm for calibration. This decision was supported by preliminary tests, which showed that the proposed down-scaling did not affect the essential model dynamics with respect to cell number and ECM concentrations (**Figure 3.5**). Consequently, the simulation duration for a 21-day period was reduced from an average of 3.5 hours to a mere 2.5 minutes, resulting in a time-saving factor of approximately 60 to 80-fold.

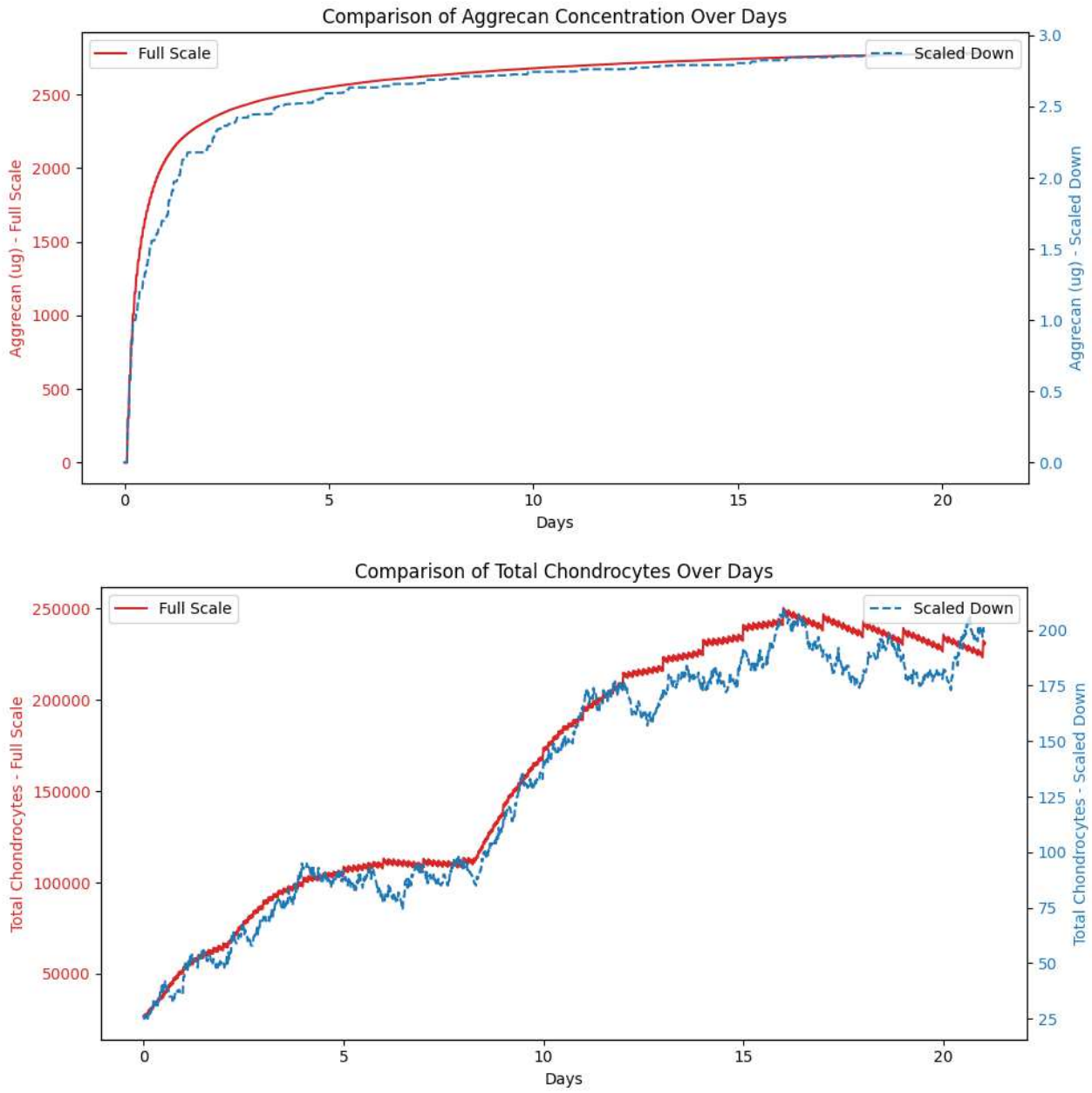

Figure 3.5 Full Scale and Scaled Down Simulation Comparison. Comparison of predicted aggrecan accumulation (top) and cell counts (bottom) between full-scale (red) and scaled down (blue) model.

Drawing upon established practices from the previous VF-ABM work,[174] iterative adjustments of these parameters were conducted using the Statistical Parameter

Optimization Tool for Python (SPOTPY).[175] The Nelder-Mead protocol was adopted for the calibration of latent parameters within the IVDH-ABM. This iterative approach refines parameters using outcomes from prior simulations to guide subsequent ones. This protocol's efficiency comes from its ability to use smaller sets of high-performing parameter vectors, significantly accelerating the calibration process.[175] In addition, the Nelder-Mead algorithm evaluates the model's performance for each set of parameters by computing a fitness score, which reflects the agreement between the model's predictions and the empirical data. The protocol then applies robust optimization techniques to refine the parameter values, focusing on those that consistently improve model fidelity across multiple simulations.[176] On average, roughly 30 simulation runs were needed for each of the latent parameters during calibration. This estimation leads to a total of 30×8 (for each latent parameter) calibration runs, translating to an initial calibration phase of approximately 4-6 hours of computational time - a drastic reduction from the 21-28 days that would have been required with the full-scale model which was beyond the timeframe of this thesis project.

The objective function chosen for this calibration was the root mean square error (RMSE), as it emphasised the importance of minimizing absolute errors in early-stage predictions. The RMSE was calculated as the average difference between the predicted and empirical data points, with the aim to reduce this value as close to zero as possible, using Equation 4.

$$\mathbf{RMSE} = \sqrt{\frac{1}{\mathrm{n}}\sum_{\mathrm{i}=1}^{n}\left(\boldsymbol{Y}_i^{empirical} - \boldsymbol{Y}_i^{predicted}\right)^2} \qquad \text{Equation 4}$$

Where $Y_i^{predicted}$ represented the predicted value, $Y_i^{empirical}$ denoted the corresponding empirical value for data point "i", and "n" was the number of observations. Low RMSE values, closer to 0, indicated that the model produced more accurate predictions. This method allowed for the iterative adjustment of parameter values until the simulated outputs closely matched the observed data, ensuring the model parameters were as accurate and reliable as possible.

By squaring the errors before averaging and taking the square root, RMSE effectively gave more weight to larger errors, ensuring that the calibration process was particularly sensitive to significant deviations from the observed data. This approach was deemed crucial for accurately simulating the initial responses of the tissue to the biomaterial, as large errors in these early predictions could significantly impact the model's overall predictive reliability and validity.

3.6 Model Validation

Following calibration, the IVDH-ABM underwent validation to ensure its predictive accuracy. Model predictions were compared against experimental data that were not used for calibration as briefly described in **Section 3.5.1** This section details the data sources and protocol that were used for model validation.

3.6.1 Data Sources for Model Validation

Quantitative model verification was performed with data from Li et al., (2023) on aggrecan accumulation (days 15, 18, and 21) and NP cell viability (days 14 and 21).[88] Aggrecan production and NP cell viability were assessed within four distinct alginate hydrogel formulations, differentiated by their calcium concentrations.

While collagen is another critical ECM component for IVD regeneration,[30] Li et al.'s work did not include such measurements. Additional sources were thus sought to qualitatively validate the trend of collagen production within the model. Collagen production patterns were compared with empirical data from two key studies. First, Chiba et al., (1997) reported collagen production in an alginate hydrogel that closely matches the chemical composition modeled in this simulation.[127] They monitored collagen synthesis at multiple time points, specifically on days 4, 7, 11 and 14, providing a direct comparison for assessing temporal patterns of collagen accumulation. Second, Wan et al., (2008) explored collagen production of chondrocytes within similar hydrogel compositions.[142] Although the primary focus was on chondrocytes, the comparability to NP cells is significant due to the similarity in both their transcriptional profiles, ECM production,[177] and proliferative capacity.[178] The collagen synthesis was measured in 2% alginate gels with calcium crosslinker densities; 1.8, 4, and 8 mM. Cross-validating the IVDH-ABM with temporal data (Chiba et al., 1997)[127] and hydrogel composition (Wan et al., 2008)[142] from these two extra sources would be essential for generalizing the model's applicability.[179]

Besides cell and ECM validation, the elasticity of the hydrogel was also verified in this model. Elasticity was incorporated into the model based on the constitutive relation derived from the physical properties that arise from different hydrogel formulations, such as component concentrations and molecular weights (**Table 3.2**). Although hydrogel elasticity was a static parameter in the ABM, i.e., not subject to change over the simulated period, it was imperative to validate elasticity outputs based on its chemical composition due to its influence on NP cell behavior and matrix production within the ABM framework. The elasticity of the hydrogel formulations was thus validated against experimental findings from Li et al.'s paper.[88]

3.6.2 Validation Protocol

A non-parametric statistical method was adopted to evaluate the model's predictive performance, similar to the previous protocol implemented in VF-ABM.[174] Validation was performed for the four alginate hydrogel formulations as reported in Li et al.'s work.[88]

Quantitative Evaluation of Time-Series Data. The time-dependent predicted aggrecan synthesis levels and NP cell viability were quantitatively validated against empirical data. Given the stochastic nature of the IVDH-ABM, the full- scale model was executed 10 times up to day 21 for all four hydrogel conditions.[180] From these runs, means ($\bar{\boldsymbol{X}}$) and standard deviations ($\boldsymbol{\sigma}$) of the predicted aggrecan accumulation and NP cell viability biomarkers were to be calculated. A two-sided 95% confidence interval (**CI**) was computed for each biomarker at the designated time points; 15, 18, and 21 for aggrecan

accumulation, 14 and 21 for NP cell viability, and 4, 7, 11, and 14 for collagen using Equation 5.

$$\boldsymbol{CI = \bar{X} \pm Z \times \frac{\sigma}{\sqrt{n}}} \qquad \text{Equation 5}$$

Where $\mathbf{Z}$ is the Z-score corresponding to the chosen confidence level and $\boldsymbol{n}$ is the number of simulations runs (in this case, 95% and 10 respectively). The predicted outputs were deemed accurate if the empirical datapoints fell within the 95% confidence interval. As each full-scale simulation took approximately 2-4 hours, the total time needed to run 10 simulations for all 4 conditions was ~120 hours or 5 days. The chosen number of simulations was deemed sufficient and realistic to validate the accuracy of the IVDH-ABM within the confines of available computational resources.

Qualitative Evaluation of Time-Series Data. Drawing from the concept of pattern-oriented analysis used in previous VF-ABM work,[181] the same principle was applied to the validation process of collagen production in the current model. The validity of the IVDH-ABM was demonstrated by confirming that the predicted profiles of collagen synthesis closely match those observed in real-world settings. This approach is useful where calibrating every parameter is impractical or impossible due to the complexity of the biological systems involved direct parameter calibration is not always feasible or available.[182]

Quantitative Evaluation of Static Data. For validating the prediction of hydrogel elasticity, tests were conducted at calcium concentrations of 15 mM and 23 mM,

in which were not used during model calibration. The validation of the elasticity equation was considered successful if the predicted values fell within the standard deviation range of the empirical elasticity measurements. This criterion ensured that the model predictions were not only statistically accurate but also practically significant, mirroring the variability observed in real-world experimental data. For example; the elastic modulus of a hydrogel with alginate molecular weight of 1500 kDa, an alginate concentration of 2% w/v, and a calcium concentration of 14 mM, should fall within the range of 2.91 ± 0.33 kPa.[88] Additionally, the elastic modulus of a hydrogel with an alginate molecular weight of 90 kDa, an alginate concentration of 2% w/v, and a calcium concentration of 22 mM, the predicted elasticity should be within 2.89 ± 0.364 kPa.[88] These validation outcomes enhance confidence in the model's ability to simulate NP cell behavior accurately, ensuring its utility for in silico experimentation.

3.7 In Silico Experiment Under Physiological Elasticity

Specific Aim 2 involved using the validated IVDH-ABM to perform the in silico experimentation and evaluation of NP cell regenerative responses to a hydrogel with physiologically relevant elasticity. The alginate hydrogel was first reverse engineered to match the elastic modulus of healthy middle-aged human lumbar NP tissue. Second, the model was executed, wherein the NP cell viability, ECM deposition, and cytokine levels were output (**Figure 3.6**).

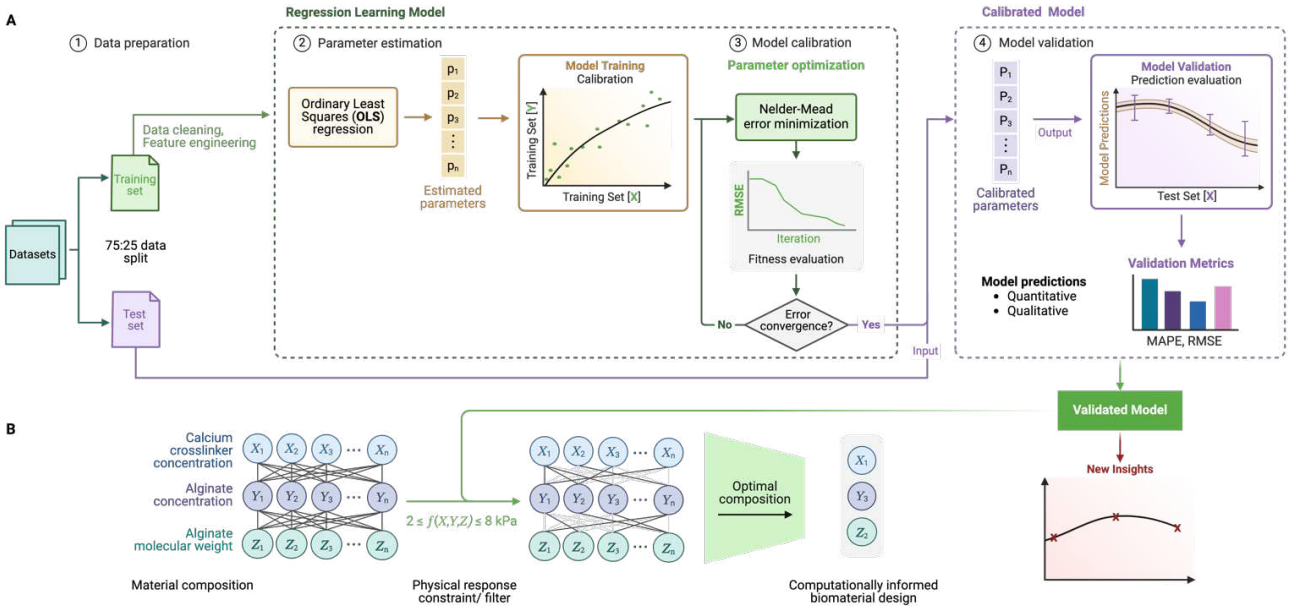

Figure 3.6 Reverse-Engineering Approach for Optimal Hydrogel Composition. Panel A depicts an overview of the IVDH-ABM model calibration and validation process. Parameters are estimated using the Ordinary Least Squares (OLS) regression method. The parameter optimization is then performed using the Nelder-Mead error minimization technique, which stops when convergence is reached. Prediction evaluation is conducted by comparison against empirical data, using validation metrics such as root mean square error (RMSE), to ensure accuracy. The validated model is utilized to determine the optimal hydrogel composition for achieving a target elasticity. Panel B shows the exhaustive combinatorial optimization algorithm used to iterate through alginate and calcium conditions (depicted as X1, X2, ..., Xn for calcium crosslinker concentrations, Y1, Y2, ..., Yn for alginate concentrations, and Z1, Z2, ..., Zn for alginate molecular weights) to identify the combination that best matches the elastic modulus of native NP tissue. Created with Biorender.com.

3.7.1 Hydrogel Composition Optimization

The key parameters included alginate concentration and calcium crosslinking density, chosen for their critical roles in determining the elastic modulus of the hydrogel.

To achieve a hydrogel composition that closely mimics the elasticity of the natural NP tissue, an extensive selection of alginate molecular weights was employed, ranging from 35 to 1500 kDa. These were categorized into three distinct groups for analysis: low molecular weights ($0 \leq$ kDa < 200), medium molecular weights ($200 \leq$ kDa < 500), and high molecular weights (kDa ≥ 500). Alginate concentration was systematically varied from 0.5% to 3% by weight, alongside calcium crosslinker concentrations spanning from 0.001 M to 0.2 M. This range was selected to allow for a targeted experimentation across a wide spectrum of hydrogel compositions.

Through a systematic reverse engineering approach, the computational analysis proceeded by systematically testing all possible combinations of molecular weight, alginate concentration, and calcium crosslinking density using the calibrated elasticity equation (**Table 3.2**). Each combination was evaluated to determine if its predicted elasticity fell within the physiologically relevant range of in vivo NP tissue in the human lumbar region, typically ranging between 5.39 ± 2.56 kPa.[183] Compositions meeting the criteria were visualized using a scatter plot to display the distribution of viable options, with color coding to differentiate among molecular weight categories.

3.8 IVDH-ABM Visualizations

Visualization is the process of converting raw data from experiments or simulations into a form that can be interpreted and analyzed. Visualization Tool Kit (VTK) rendering was implemented within ParaView 5.7.0. This approach enabled an insightful three-dimensional visualization of the predicted spatial-temporal patterns of NP cell distribution, as well as the accumulation of aggrecan and collagen within the hydrogel matrix over the course of the simulations.

3.8.1 Rendering Technique

The visualization setup in ParaView used ASCII format and structured points for the dataset. This configuration translated discrete data points, cell locations and ECM concentrations, from numerical data into visual form in the hydrogel's three-dimensional space. Volume rendering was employed for visualizing the simulation experiments. This technique used a semi-transparent, three-dimensional display of the hydrogel matrix, with maximum contrast for cells and their secreted components, offering a visual of spatial relationships and behaviors.

A threshold filter was used to distinguish between ECM components, mapping scalar numbers from the simulation data to corresponding color values. Specifically, aggrecan and collagen were represented by red and blue colors with HSV codes 129 and 139, respectively, while activated cells were designated with white (color code 1). For example, applying a threshold filter of scalar number 129 would visualize only aggrecan

elements at this level in green, allowing for differentiation based on concentration. Moreover, the selection of a diverging color map with a gradient of intensities was used to facilitate the tracking of aggrecan and collagen concentration gradients. The gradient mapping was calibrated to enable a direct correlation between color density and quantitative data points. The darker shades correlated with denser component concentrations, allowing for an intuitive visual interpretation of the spatial-temporal evolution of data. This relationship was established within the VTK rendering pipeline via a transfer function, which assigned specific opacity and color values across the data's scalar range.

Chapter 4 Results

4.1 Overview

This chapter presents the results of the IVDH-ABM simulations, detailing the calibration and validation of the regenerative potential of NP cells in alginate hydrogels. The results are organized into four sections: (1) hydrogel elasticity, (2) cell count and ECM production, (3) cytokine production, and (4) in silico experiments. Each section provides a comprehensive analysis of the model's performance, including comparisons with empirical data, statistical evaluations, and visual representations of the simulation outputs.

4.2 Hydrogel Elasticity

The calibration process for hydrogel elasticity involved two key steps: initial parameter estimation using the ordinary least squares (OLS) regression method in Python, followed by optimization using the Nelder-Mead method. This dual approach ensured both accuracy and optimal performance of the model parameters. **Figure 4.1** illustrates the elasticity calibration process, showing the RMSE progression over 300 iterations. The consistent decrease in RMSE indicates that the model's predictions became increasingly accurate with each iteration. Initially, the RMSE was relatively high, reflecting the discrepancies between the model's initial parameter estimates, derived from OLS

regression, and the empirical data. However, as the calibration progressed, the RMSE steadily declined, stabilizing at 0.51 kPa towards the end of the iterations. This stabilization suggests that the calibration process had converged, achieving an optimal set of parameters for predicting hydrogel elasticity.

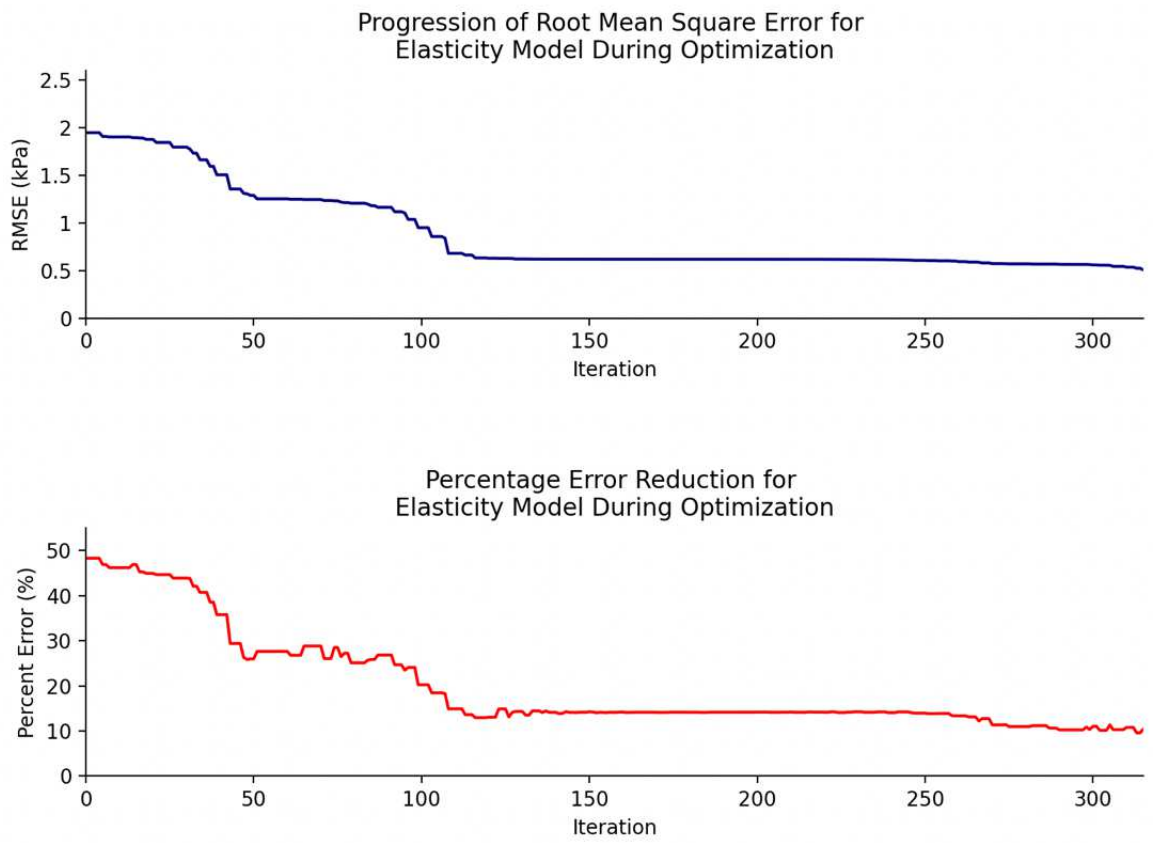

Figure 4.1 Progression of Calibration Metric for Hydrogel Elasticity Predictions. The progression of the RMSE across 300 iterations of the model calibration, illustrating a consistent decrease in RMSE and indicating improved accuracy of the model in predicting hydrogel elasticity as the iterations progress (top). The percentage reduction in error over the same iterations stabilizes, demonstrating the model reaches a point of minimal further improvement, which suggests the convergence of the calibration process.

The calibrated equation for predicting hydrogel elasticity **E** as a function of alginate molecular weight $\mathbf{Alg_{Mw}}$, alginate concentration $\mathbf{Alg_{wv}}$, and calcium crosslinking density $\mathbf{Ca_{XL}}$ is given by Equation 6.

$$\boldsymbol{E} = -125 + 58(\boldsymbol{Alg_{wv}}) - 971(\boldsymbol{Ca_{XL}}) + 1.037(\boldsymbol{Alg_{Mw}}) + 756(\boldsymbol{Alg_{wv}} \times \boldsymbol{Ca_{XL}}) - 0.516(\boldsymbol{Alg_{wv}} \times \boldsymbol{Alg_{Mw}}) - 0.165(\boldsymbol{Ca_{XL}} \times \boldsymbol{Alg_{Mw}}) \quad \text{Equation 6}$$

This equation was derived through regression analysis, incorporating literature data to establish the relationships between the various factors and the resulting elasticity. Each parameter represents the relative impact of the associated material component, providing insights into how changes in the hydrogel composition affect its mechanical properties. The successful calibration of the hydrogel elasticity model is a crucial step in ensuring that the overall model accurately reflects the physical properties of the hydrogel, thereby enabling reliable predictions of NP cell behavior and regenerative potential in subsequent simulations.

To validate the effectiveness of the calibration, the model predictions were compared against empirical data across different calcium concentrations and alginate molecular weights. **Figure 4.2** presents the predicted elasticity values against the measured values from Li et al., (2023) empirical data.[88] The comparison of predicted to empirical elasticities were 2.6 and 2.92 ± 0.33 kPa for 1 kPa-H, 3.03 and 2.89 ± 0.36 kPa for 1 kPa-L, 7.01 and 7.96 ± 1.54 kPa for 3 kPa-H, and 9.11 and 9.19 ± 0.15 kPa for 3 kPa-L hydrogel conditions.

Although the largest percent error between the predicted elastic modulus and empirical value was roughly 12%, all values were within empirical standard deviation. Therefore, the predicted points were aligned, demonstrating a strong correlation between the model predictions and the empirical observations. The close fit indicates that the calibrated model can accurately predict the hydrogel's mechanical properties under varying conditions.

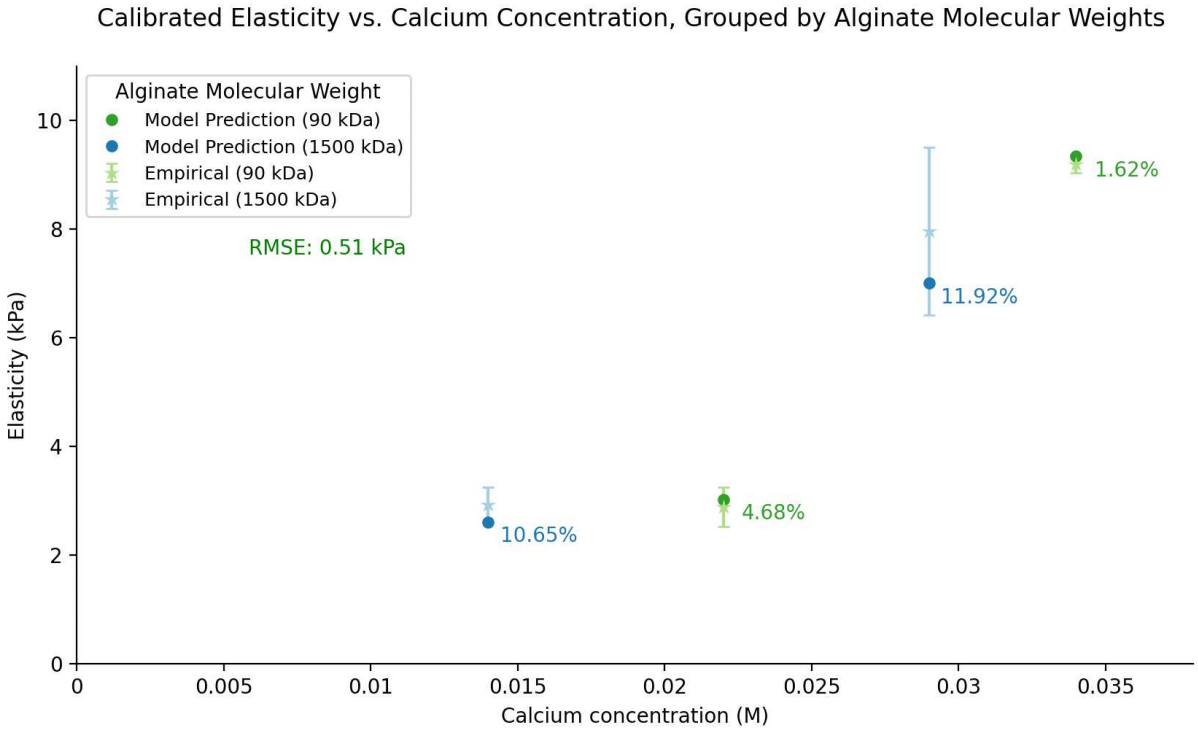

Figure 4.2 Calibration of Hydrogel Elasticity Predictions. Comparison of predicted elasticity values (based on the calibrated model) against empirical data across a range of calcium concentrations and alginate molecular weights. The figure illustrates how closely the model predictions align with laboratory measurements.

4.3 Cell Count and ECM Production

The calibration and validation of cell count and ECM production involved aligning the model's predictions with empirical data on NP cell count, aggrecan, and collagen synthesis over time.

4.3.1 NP Cell Proliferation

Figure 4.3(A) shows the fold changes in NP cell count, normalized to the initial amount over a 21-day period across hydrogels of varying elasticities. Cell counts were normalized to day 0 to remove any initial biases and allow for comparisons across different literature. An initial rapid increase in cell count is observed, rising from 27 000 to 48 772 on day 5, followed by stabilization. A second burst occurs on day 16, reaching 108 257 cells, followed by another stabilization phase. The model demonstrated a strong correlation between predicted and empirical values, consistently falling within the expected range.

In addition, the 3D and 2D visualizations of the 3 kPa - low molecular weight hydrogel condition cell distribution, reveal a progressively increasing cell density over the 21-day period (**Figure 4.3(B)**). Initially, cells are randomly seeded and distributed throughout the hydrogel matrix, but as time progresses, cell proliferation leads to more densely populated areas of the hydrogel. The visualization highlights how cells migrate and proliferate within the matrix, forming clusters that suggest active tissue regeneration.

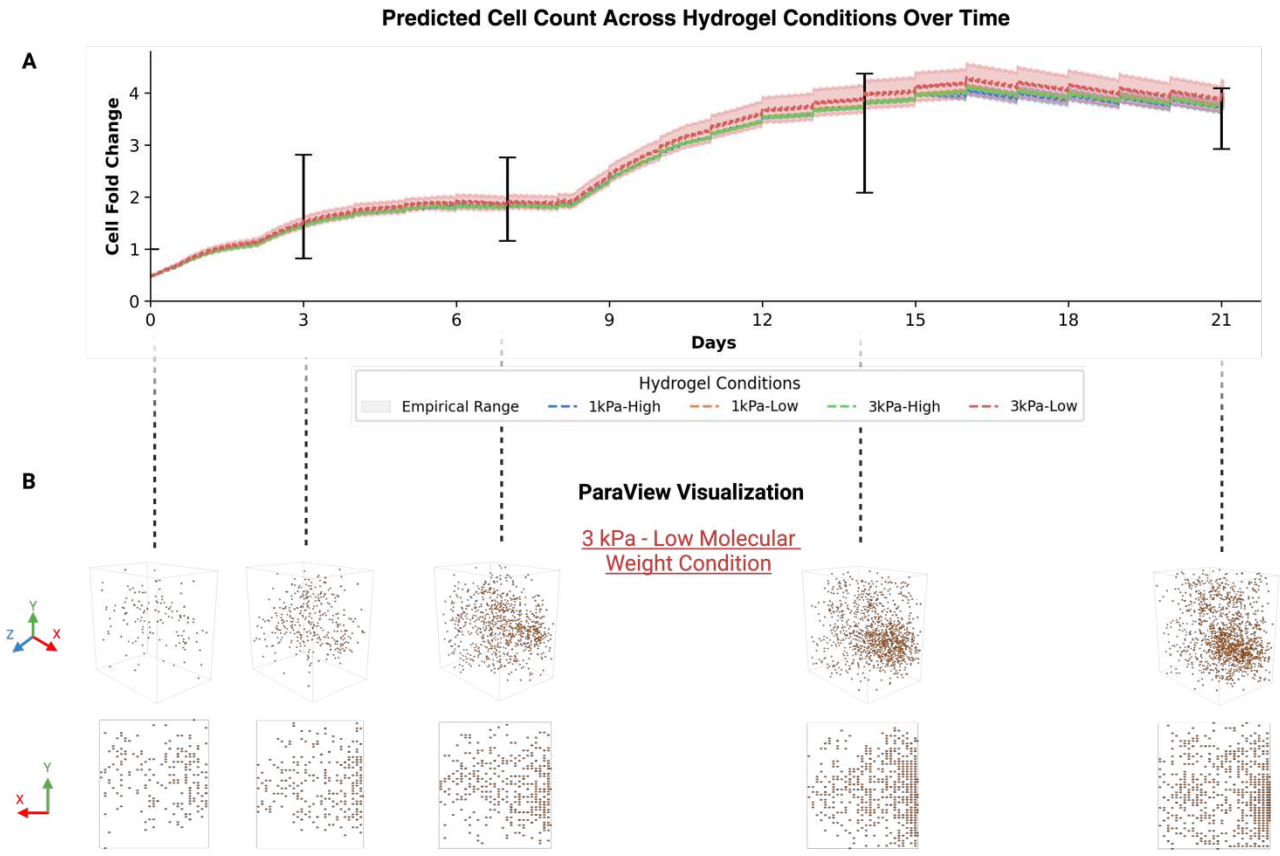

Figure 4.3 Simulation Predictions for Cell Count Over Time. Panel A shows the fold changes in NP cells normalized to the initial amount over a 21-day period across hydrogels of varying stiffness. Black error bars represent the range in empirical values taken from literature on days 3, 5, 14, and 21.[127,159,184] Panel B presents the ParaView 3D and 2D visualizations of NP cell distribution under the 3 kPa – low molecular weight hydrogel condition, illustrating the spatial arrangement and density of cells within the hydrogel matrix over time.

4.3.2 Aggrecan and Collagen Production

Figure 4.4(A) illustrates the predicted aggrecan and collagen profiles over the 21-day period across the different hydrogel conditions. Both components showed steady increases, reflecting sustained ECM production by the NP cells. The model predictions for

aggrecan accumulation remain well within the empirical ranges across the different hydrogel conditions, as indicated by the error bars in Panel A. In addition, the predicted collagen to aggrecan ratio was consistent with empirical ratios varying between 0.18 - 0.42,[23] represented by the shaded grey region. Both ECM components remain well within their respective empirical ranges, indicating that the model effectively captures the temporal patterns of matrix production. Across all simulations, the 3 kPa-low molecular weight hydrogel condition showed the best performance in supporting NP cell proliferation and ECM production. Cell proliferation reached a maximum of 4.11 ± 0.09 folds on day 16, aggrecan levels stabilized at roughly 2764 *ug/mL* after 9 days and increased by 8% by day 21. Conversely, 1 kPa-high hydrogel condition resulted in the worst performance for supporting NP regeneration. Cell count reached a maximum of 4.01 ± 0.21 folds on day 16, aggrecan levels stabilized at roughly 264 *ug/mL* after 9 days and increased by 3.3% by day 21.

Figure 4.4(B) presents a visual comparison of the ECM components, aggrecan (red) and collagen (blue), accumulated within the 3 kPa– low and high hydrogel conditions over the 21- day culture period, revealing distinct spatial distribution patterns. The 3D visualizations on days 1, 2, 3, 6, 9, 15, and 21 enhance the understanding of the interactions and dynamics within the hydrogel environment. In both hydrogel conditions, the ECM components are sparsely distributed throughout the hydrogel on day 1, with no clear clustering. By day 3, aggrecan and collagen begin to centralize, forming a more concentrated distribution at the core. For the 3 kPa- low molecular weight hydrogel

condition, the ParaView renderings depict a higher density of aggrecan and collagen, with the red and blue regions appearing more concentrated and intense. This indicates a more robust ECM deposition in comparison to the 3 kPa- high molecular weight condition, where the distribution of ECM components is less dense, as reflected by the lighter shading and more dispersed arrangement of the red and blue areas. These observations indicate that the spatial distribution of ECM components was not hard-coded but emerged from the collective behavior of the simulated NP cells.

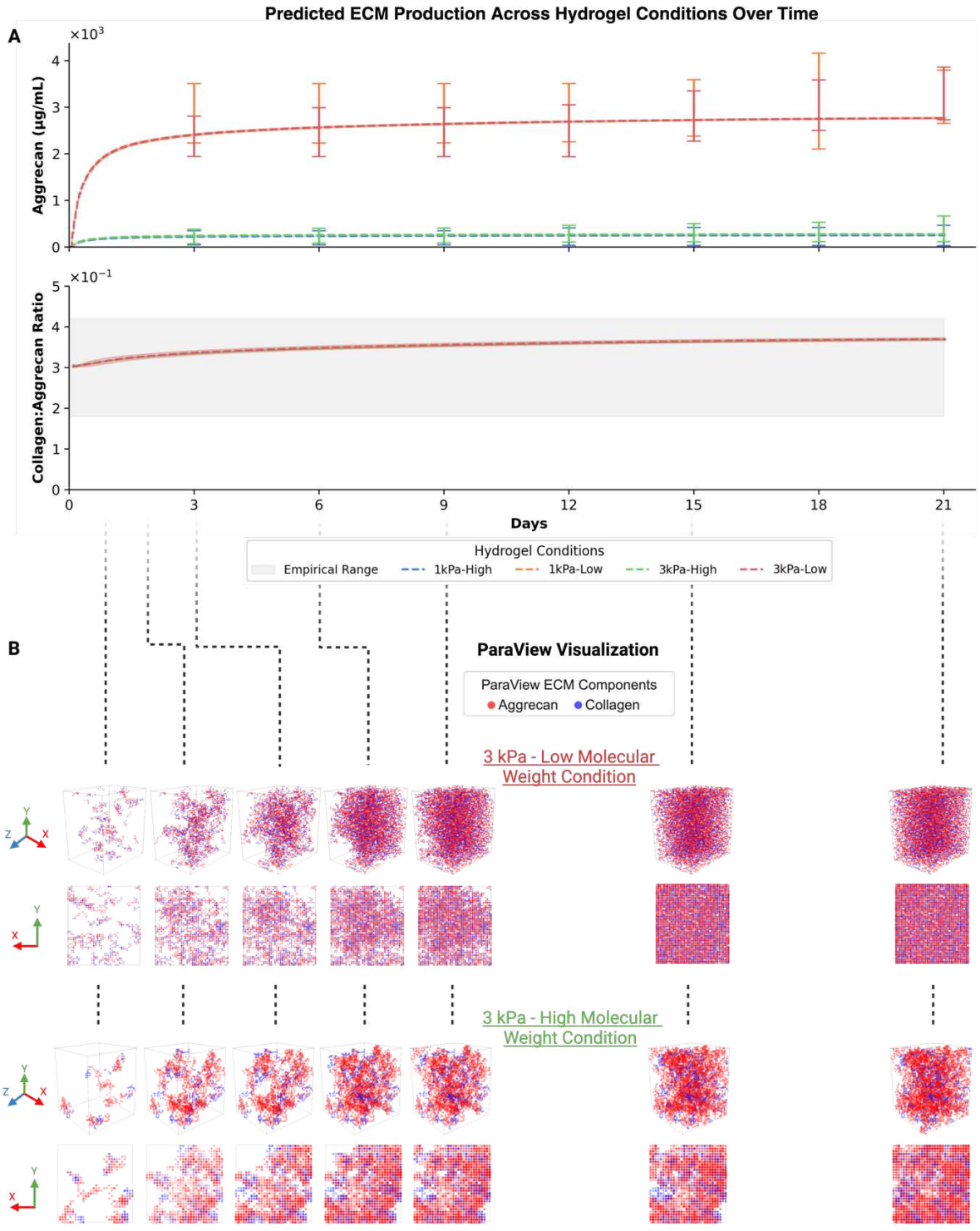

Figure 4.4 Simulation Predictions for ECM Production Over Time. Panel A shows the predicted ECM component profiles compared to the respective empirical values of aggrecan[88] and collagen.[23] In Panel B, the 3D and 2D ParaView visualizations present the density of ECM

components (aggrecan in red, collagen in blue) on days 1, 2, 3, 6, 9, 15, and 21 for the 3 kPa – low and high molecular weight hydrogel conditions. The intensity of the colors reflects the accumulation density of these ECM components, with darker, denser regions indicating higher concentrations of aggrecan and collagen within the hydrogel matrix over time.

4.4 Cytokine Synthesis

The calibration and validation of cytokine synthesis involved predicting the temporal patterns of cytokine production, including TNF-α, IL-1β, and TGF-β, and comparing them with empirical data presented in **Figure 4.5**. The cytokine concentrations were normalized to pg/million cells to enable robust comparisons with empirical data. Overall, the IVDH-ABM reproduced the cytokine patterns as documented in the literature.[161,166,167]

For all hydrogel conditions, the cytokines TGF-β, TNF-α, and IL-1β exhibited a rapid initial increase followed by stabilization within one day. Specifically, TGF-β levels surged to 310 pg/million cells within the first day, demonstrating a sharp rise indicative of the cytokine's role in initiating cell proliferation and ECM production. Following this initial surge, TGF-β levels continued to increase linearly, reaching a peak concentration of 420 ± 30 pg/million cells by day 9. This sustained increase suggests ongoing cellular activity and matrix production, after which TGF-β levels plateaued, indicating a balance between synthesis and utilization in the cellular processes.

Conversely, TNF-α and IL-1β levels rapidly increased to only 140 and 50 pg/million cells, respectively, within the first day. By day 4, TNF-α and IL-1β concentrations peaked

at 190 ± 11 and 90 ± 7.5 pg/million cells, respectively, highlighting their role in the early inflammatory response, followed by stabilization. This trend aligns with TNF-α and IL-1β cytokines' known behavior of mediating early inflammation before subsiding as cell counts surge.[185] These observed trends in cytokine production provide insight into the dynamic interplay of inflammatory and regenerative processes within the hydrogel environment.

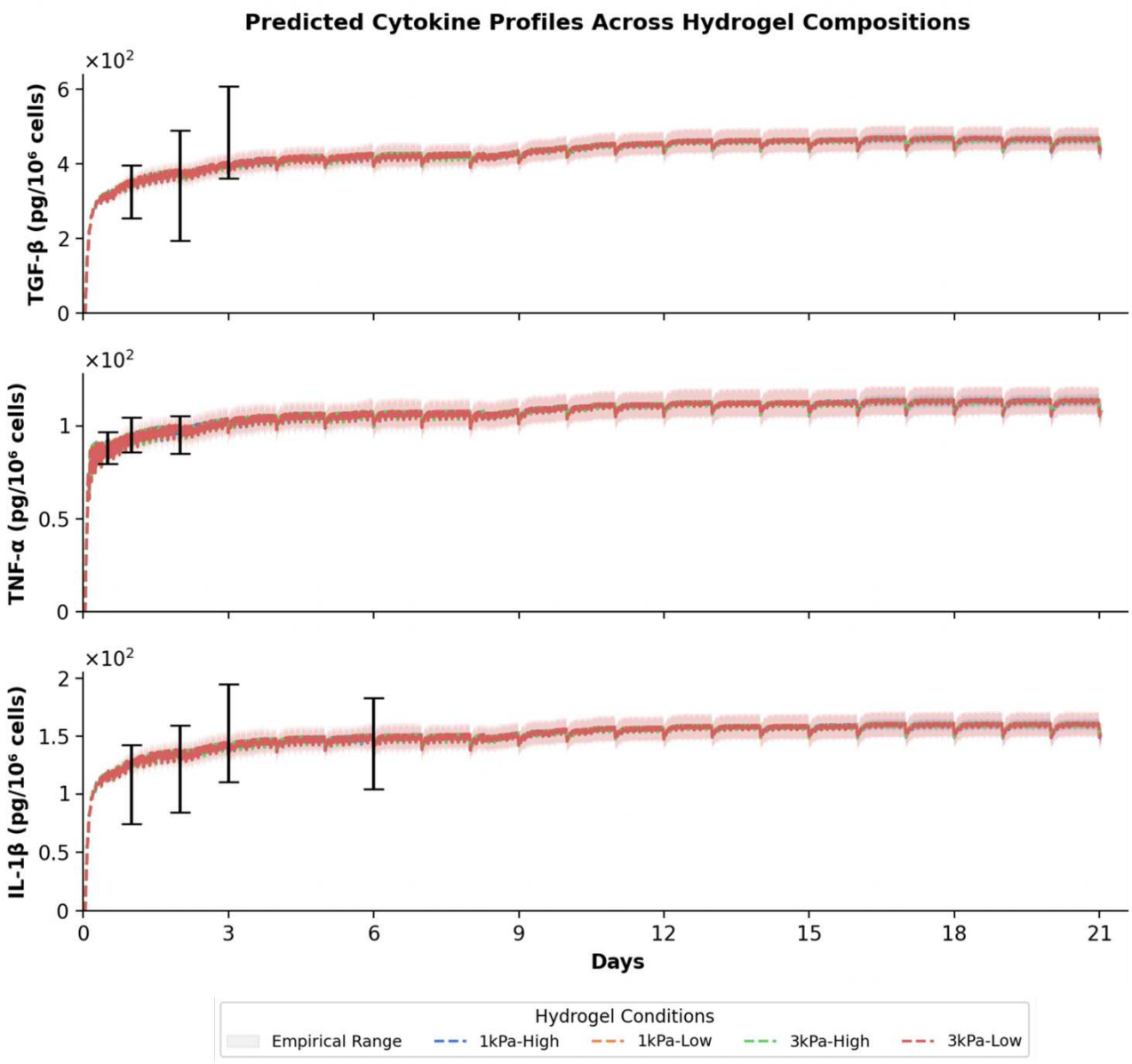

Figure 4.5 Predicted Cytokine Profiles Across All Hydrogel Compositions. Levels of TGF-β, TNF-α and IL-1β per 1 million cells, over 21 days illustrate how cytokine production is affected by the hydrogel's mechanical properties. Black error bars for TGF-β,[161] TNF-α,[166] and IL-1β[167] represent the empirical values taken from corresponding literature.

4.5 In Silico Experiment Results

4.5.1 Identify Optimal Hydrogel Composition for Physiological Elasticity

A 3D plot was generated to visualize the predicted elasticity across a range of possible combinations of alginate concentration, alginate molecular weight, and calcium crosslinking density (**Figure 4.6**). This plot enabled a comprehensive assessment of how different hydrogel compositions affect their mechanical properties. By mapping the elasticity values in three dimensions, it was possible to identify trends and interactions between the variables, providing valuable insights for optimizing hydrogel formulations.

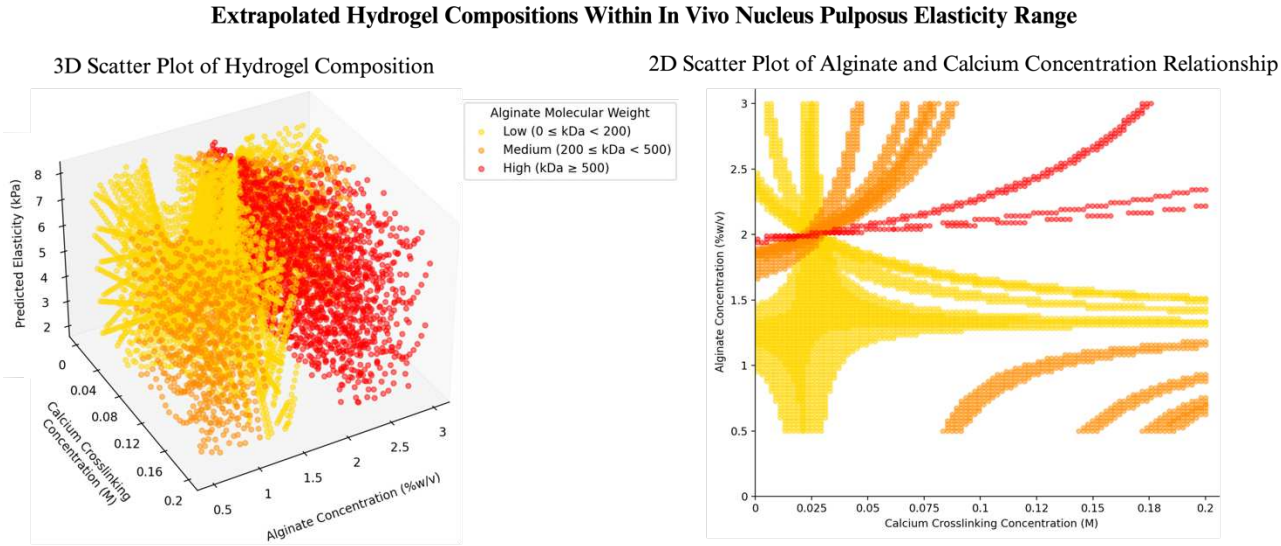

Figure 4.6 Predicted Hydrogel Elasticity for Varying Compositions. A 3D scatter plot showing the distribution of hydrogel composition yielding a predicted elasticity that ranges from 5.39 ± 2.56 kPa (Left). A 2D scatter plot illustrating the relationship between alginate and calcium concentrations (Right). Each point represents a specific combination of alginate molecular weight

and composition, categorized into three groups: low ($0 \leq$ kDa < 200, yellow points), medium ($200 \leq$ kDa < 500, orange points), and high (kDa ≥ 500, red points).

Among the tested combinations, a specific formulation was selected for further experimentation: 200 kDa alginate molecular weight, 1.95% alginate concentration, and 0.02 M calcium crosslinking density (**Figure 4.7**). The selection was supported by the formulation's potential to provide an ideal biomechanical environment for NP cell regeneration, balancing the structural integrity and elasticity needed to simulate real tissue conditions effectively.

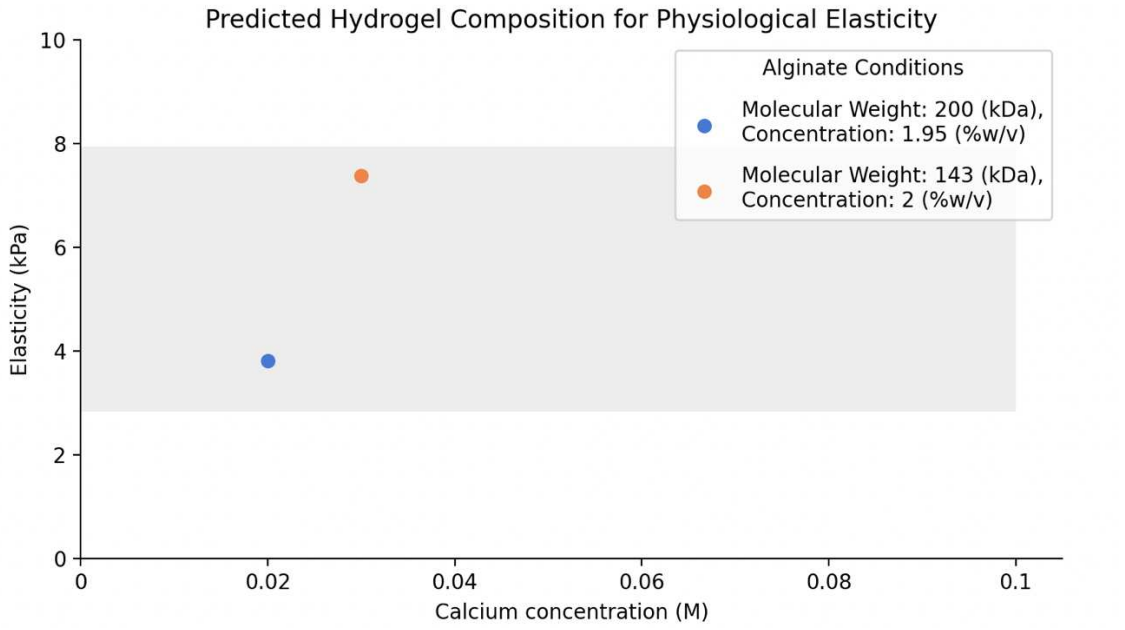

Figure 4.7 Predicted Elasticity of Selected Hydrogel Compositions. A 2D plot displaying the predicted elasticity values for two selected hydrogel compositions. A hydrogel composition with a molecular weight of 200 kDa, alginate concentration of 1.95% w/v, and 0.02 M calcium crosslinker density (blue), was ultimately chosen for further in silico experiments due to its optimal

elasticity. The orange data point represents another composition with a molecular weight of 143 kDa, an alginate concentration of 2% w/v, and a calcium crosslinker density of 0.03 M.

4.5.2 Predicted NP Cell Response to IVDH-ABM-Optimized Hydrogels

Following the selection of the optimal hydrogel composition with a molecular weight of 200 kDa, an alginate concentration of 1.95% w/v, and a calcium crosslinking density of 0.02 M, an *in silico* experiment was conducted to evaluate the regenerative response of NP cells. This composition was specifically chosen for its elasticity closely matching the physiological conditions of human lumbar NP tissue, deemed essential for mimicking the natural environment in which NP cells interact.

The virtual experiment simulated the behavior of NP cells within the hydrogel over a 21-day period, capturing detailed data on key biological processes in tissue engineering and regenerative medicine. These processes included monitoring cell proliferation, cytokine production, and ECM production which are crucial for tissue integrity and repair. The execution of these experiments aimed to confirm the sustainability of the hydrogel composition and provide detailed insights into the mechanisms through which the hydrogel supports NP cell regenerative capacities. The findings were intended to inform further enhancements to biomaterial designs for clinical applications in treating intervertebral disc degeneration.

Figure 4.8(A) presents the NP cell fold change over the 21-day period. Initial proliferation was rapid, driven by high TGF-β levels, which later stabilized due to spatial

constraints. The maximum cell count fold increase of approximately 4.15 reached at day 16. Both aggrecan and collagen levels increased steadily throughout the simulation, reflecting the ongoing ECM production by the NP cells. In addition, the temporal patterns of cytokine production (TNF-α, IL-1β, and TGF-β) were analyzed to understand their role in regulating NP cell behavior and ECM production. The aggrecan levels reached to 2950 *ug/mL* by the end of the 21-day period, whereas collagen reached to approximately 1095 *ug/mL*. **Figure 4.8(C)** shows that TGF-β levels peaked early in the simulation, promoting initial cell proliferation and ECM production. TNF-α and IL-1β levels exhibited more complex dynamics, reflecting their roles in modulating inflammation and cell behavior.

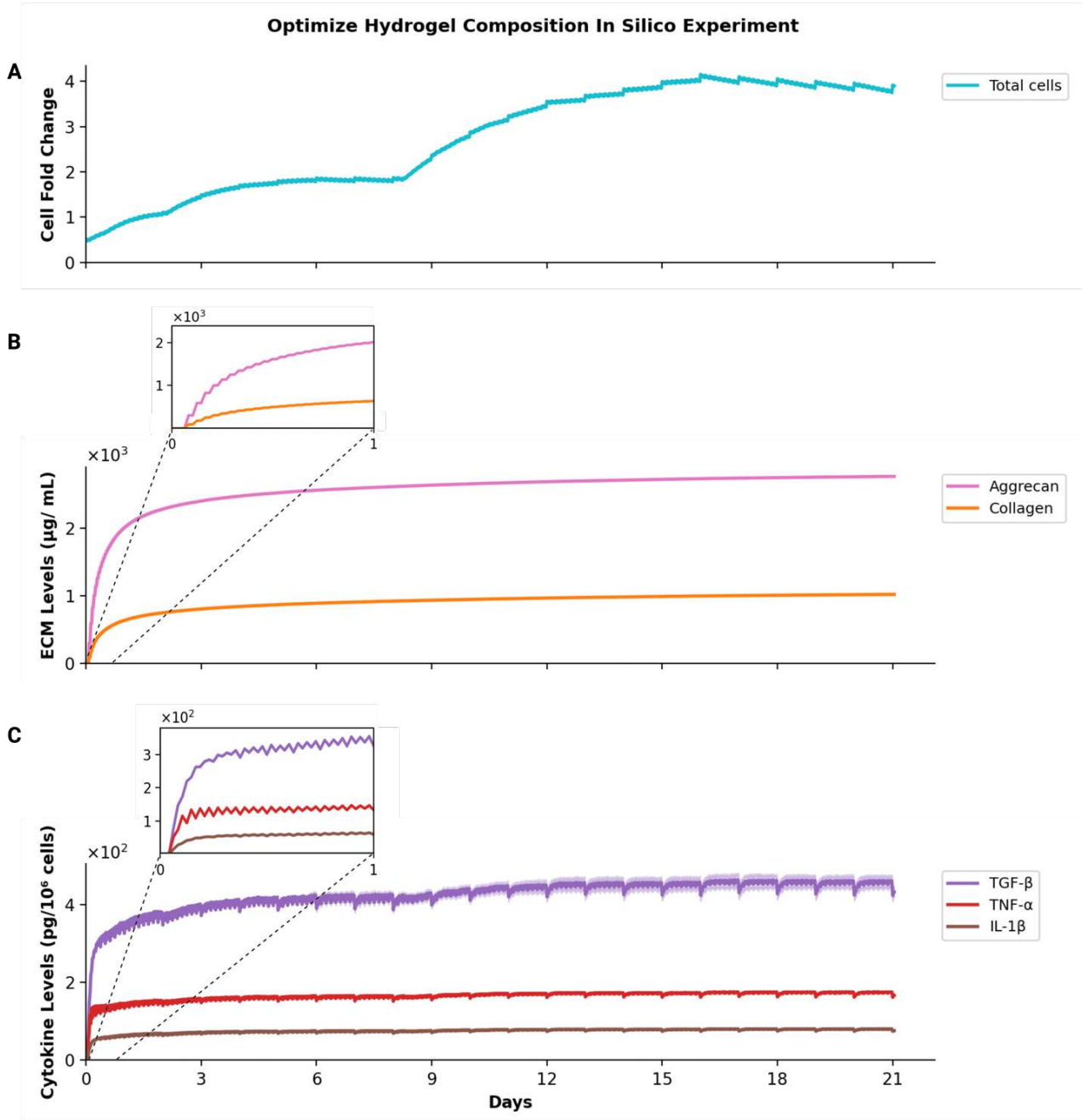

Figure 4.8 Simulation Outputs of Optimized IVDH-ABM Hydrogels. Panel A shows the predicted NP cell fold change. Panel B shows the predicted collagen and aggrecan profiles. Panel C shows the predicted cytokine TGF-β, TNF-α, and IL-1β levels over 21 days for a hydrogel of 200 kDa alginate molecular weight, 1.95% w/v alginate concentration, and 20 mM calcium crosslinking density. The model was run five times, and the average results are shown.

Chapter 5 Discussion and Conclusion

This chapter discusses the results obtained from the IVDH-ABM to simulate NP cell behavior within alginate hydrogels. In this work, the IVDH-ABM was trained and validated with available data found in literature and in-house laboratory data. The IVDH-ABM was also used to identify hydrogel compositions that could be optimal for IVD regeneration.

5.1 IVDH-ABM Reproduces Relation Between Hydrogel Composition and Elasticity.

Empirical data (**Figure 3.4**) was used to develop and train the model. The calibration process involved iterative adjustments of the compositional properties; alginate concentration, calcium crosslinking density, and alginate molecular weight to fit experimental observations. Validation against independent data set from Li et al., (2023) confirmed the model's reliability,[88] ensuring that the predictions were robust and consistent with observed data, as evidenced by the RMSE metric of 0.51 kPa.

Higher alginate molecular weight and concentrations resulted in increased stiffness, aligning with literature that higher polymer concentrations enhance mechanical strength. Secondly, increased calcium crosslinking density led to stiffer hydrogels, as calcium ions form the crosslinks with alginate, create a more rigid network.[186] The model's ability to

predict hydrogel elasticity within narrow error margins validates its utility for simulating various hydrogel compositions.

5.2 Hydrogel Elasticity Influences Cell Proliferation and ECM Production

The IVDH-ABM accurately predicted the NP cell count and ECM synthesis, with results aligning well with empirical observations (**Figure 4.3** and **Figure 4.4**). Cell proliferation was influenced by cytokine concentrations and hydrogel composition. An unexpected and unprogrammed observation was the "bump" in cell fold change, which represented a transient increase in cell proliferation followed by stabilization. This phenomenon can be explained by several factors within the model dynamics.

The initial high levels of TGF-β stimulated a burst in cell proliferation. As TGF-β levels peaked and stabilized on day 8 (**Figure 4.5**), the proliferation rate decreased, leading to a leveling-off of the cell fold change. Additionally, the model incorporated feedback mechanisms, where secreted cytokines and ECM components influenced cell behavior. An initial surge in cell proliferation led to increased ECM production, which in turn affected further cell proliferation rates.[187] Spatial constraints may also explain the double cell count fold stabilizations. As cells proliferated, spatial limitations within the hydrogel matrix became more apparent, resulting in competition for space and resources that slowed down further proliferation.

The model also accurately reflected the temporal dynamics of ECM synthesis. Aggrecan synthesis, driven by TGF-β, showed a consistent increase, while collagen production, although less abundant, also demonstrated a stable and significant synthesis. The ratio of aggrecan to collagen (approximately 3:1) aligned with empirical data and literature, confirming the model's validity in replicating the native ECM composition of NP tissue.[23]

5.3 Dynamics of Cytokines is a Key Driver of Modulating Cell Dynamics

The production of cytokines varied with hydrogel composition and played a crucial role in influencing NP cell behavior and ECM production, through autocrine and paracrine signaling. Normalizing cytokine concentrations to *pg/million cells* provided a robust basis for comparison across different conditions and experimental data. The model's predictions of cytokine concentrations were validated against empirical data, demonstrating its ability to simulate the complex biochemical interactions within the hydrogel environment. TGF-β promoted ECM production, particularly aggrecan and collagen synthesis, whereas both TNF-α and IL-1β inhibited ECM synthesis and induced catabolic activity. These cytokines reflect their known roles in maintaining matrix homeostasis and inducing inflammation and matrix degradation in the NP.[161]

5.4 In Silico Experiment: Optimized Hydrogel Composition Supports NP Cell Regeneration

Results from the *in silico* experiment identified a hydrogel formulation that supports ECM production and cell proliferation for IVD application. For this specific formulation, an alginate molecular weight of 200 kDa, a concentration of 1.95% w/v, and a 20 mM calcium crosslinker density were found to yield an elastic modulus of 3.66 kPa. This modulus falls within the physiological NP disc elasticity range of 5.39 ± 2.56 kPa.[183] The optimized hydrogel composition demonstrated enhanced cell viability, proliferation, and ECM synthesis, effectively supporting NP cell regeneration.

5.4.1 Optimized Hydrogel Composition Supports Continuous ECM Production.

Aggrecan levels of the optimized hydrogel increased by 6.73% when compared to the levels reached in the 3 kPa-low molecular weight condition. Softer hydrogels promoted the production of ECM components essential for cell function, such as collagen-II and aggrecan. This is supported by findings from Kim et al., (2015), which found that chondrocytes subjected to softer hydrogels (4 kPa compared to 7 kPa) produced 28% and 18% more aggrecan and collagen.[188] This phenomenon can be attributed to several molecular mechanisms involving the mechanotransduction pathways that NP cells utilize to sense and respond to their ECM.

Firstly, softer hydrogels mimic the native mechanical environment of the NP tissue more closely than stiffer matrices (3.66 kPa for the optimized hydrogel and 9 kPa for the

3 kPa-low molecular weight condition). This similarity allows for better cell-matrix interactions, which are crucial for maintaining the cellular phenotype and promoting ECM production. In softer environments, integrins, which are transmembrane receptors that facilitate cell-ECM adhesion, can more effectively bind to ECM proteins such as laminin and fibronectin.[189] This binding activates intracellular signaling pathways, such as the RhoA/ROCK and MAPK/ERK pathways, which are critical for cell survival, proliferation, and ECM synthesis.[189] Moreover, the mechanical properties of the hydrogel can influence the distribution and activity of mechanosensitive ion channels in NP cells. The reduced stiffness of the hydrogel alleviates mechanical stress on NP cells. Softer matrices may allow for more optimal functioning of these channels, further supporting cellular health and ECM synthesis.[190]

The increase in both aggrecan and collagen levels over time indicates that the hydrogel composition effectively supports continuous ECM synthesis, which is essential for NP tissue regeneration. A controlled and continuous production of ECM is essential for effective tissue repair. Mimicking native NP tissue, the collagen and aggrecan rich environment provides the necessary structural support and biochemical signals required for proper tissue function and integration with surrounding tissues.[191] Moreover, ongoing matrix synthesis prevents tissue degradation and creates a stable environment conducive to cell-matrix interactions, aiding cell viability and proliferation, thus enhancing tissue regeneration.[189]

5.4.2 Increased NP Cell Count Reveals Superior Regenerative Capabilities in Optimized Hydrogel Conditions.

Cell count fold changes of the optimized hydrogel increased by 1.23% and 3.3% compared to the 1 kPa- high (4.1 cell count fold change) and 3 kPa- low (4.01 cell count fold change) respectively. A study done by Li et al., (2017) found that the proliferation of chondrocytes cultured in highly crosslinked hydrogels was hindered due to the increased stiffness of the hydrogel.[192] The cell performance variations are likely due to the constraints they imposed on cell proliferation and motility. The limited space and resource availability within these stiffer hydrogels may restrict the ability of the cells to proliferate efficiently,[188] thereby impacting the overall regenerative potential.

In addition, hydrogel elasticity plays a crucial role in cell migration. In highly crosslinked hydrogels, increased stiffness can impede cell movement[193], reducing the cells' ability to migrate. Softer hydrogels, on the other hand, facilitate easier cell movement and reach the target sites more efficiently. The optimized hydrogel composition, with its balanced stiffness, supports both cell proliferation and migration. This balance allows for adequate mechanical support while providing the flexibility needed for cells to move and reorganize within the scaffold. The ability of cells to migrate within the hydrogel is influenced by the matrix's physical properties, such elastic modulus, which is affected by the crosslinking density and polymer composition.

These findings underscore the necessity of fine-tuning hydrogel stiffness to balance mechanical support with cellular activity to optimize tissue regeneration. The superior

regenerative capabilities of NP cells when subjected to the optimal hydrogel conditions confirmed the hypothesis that mechanical properties are crucial for NP cell function (**Figure 5.1**).

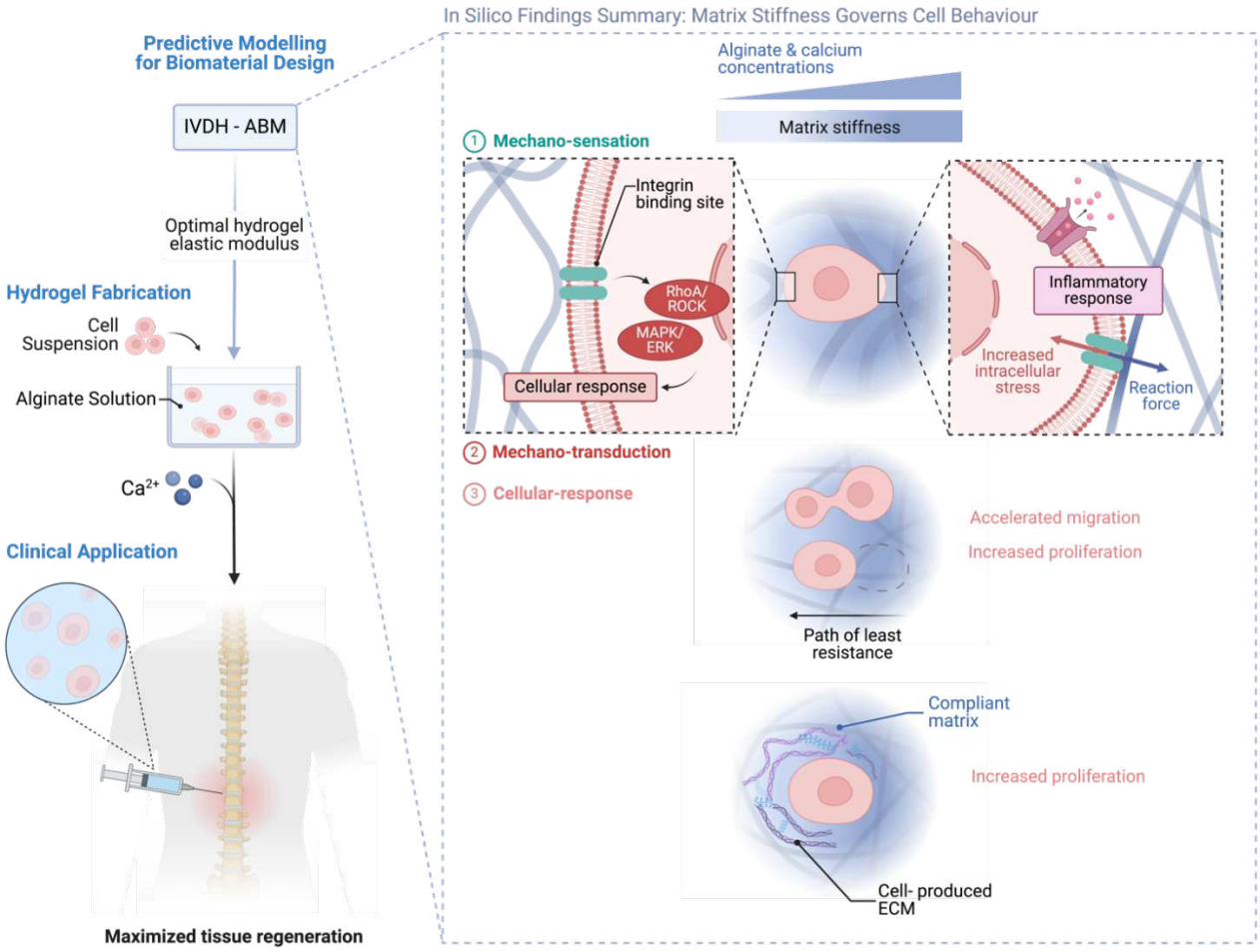

Figure 5.1 In Silico Insights into Biomaterial Design: Impact of Matrix Stiffness on Cell Behavior and Tissue Regeneration. The graphical summary illustrates key findings from the in silico experiment on how matrix stiffness, governed by alginate and calcium concentrations, influences NP cell behavior. Predictive modeling identifies the optimal hydrogel stiffness for maximized tissue regeneration, using the validated IVDH-ABM. For future work, the hydrogel fabrication process involves suspending NP cells within the hydrogel matrix, and clinical

application entails injecting the hydrogel into the degraded NP to promote IVD regeneration. The right panel depicts mechanosensation, where NP cells detect mechanical cues through integrin binding sites, triggering intracellular pathways (RhoA/ROCK, MAPK/ERK) through mechanotransduction; softer matrices result in accelerated cell migration and proliferation due to increased compliancy in a less stressed environment. Created with Biorender.com.

5.5 Model Limitations and Future Directions

Despite the promising findings and significant advancements made through this research, the current computational model has inherent limitations that need to be addressed to enhance its predictive accuracy and applicability. Recognizing these limitations is crucial for guiding future research and improving the model's utility in tissue engineering and regenerative medicine.

Firstly, the IVDH-ABM model assumes a uniform, linear, and static hydrogel elastic modulus. This assumption simplifies the mechanical representation of the hydrogel, allowing for a focus on immediate primary interactions between NP cells and the hydrogel matrix. While this choice was made for computational efficiency, this assumption may not account for the inherent non-linear heterogeneity and viscoelasticity of hydrogels, which exhibit time-dependent mechanical properties. In biological tissues, the elastic modulus can vary spatially and temporally due to dynamic cellular interactions and matrix remodeling. This simplification limits the ability of the model to simulate the actual mechanical environment experienced by cells, potentially affecting the long-term prediction of regenerative outcomes. To consider a time-dependent component of the

hydrogel mechanical properties, nonlinear stress-strain relationships can be incorporated to simulate viscoelastic behavior using finite element analysis (FEA). The FEA can output detailed local spatial and temporal data on stress-strain responses, which can then be used to refine the IVDH-ABM's representation of the mechanical environment. This FEA-ABM coupling would allow for a more realistic simulation of the spatial and temporal variations in hydrogel mechanical properties. Additionally, the model could be enhanced by considering heterogeneous biochemical and mechanical stimuli, such as varying porosity, dynamic degradation rates, and real-time changes in the elastic modulus. This is particularly important in scenarios where mechanical feedback is crucial for cell behavior. For example, NP cells may remodel the hydrogel through the secretion of MMP and TIMP, which will lead to changes in the hydrogel structure and stiffness over time. Incorporating these dynamic feedback mechanisms into the model would enable a more accurate simulation of how cells respond to and influence their surrounding environment, leading to more precise predictions of cell behavior and ECM production.

Secondly, the IVDH-ABM simplifies the complex tissue regeneration process by focusing only on key cellular behaviors, including cell proliferation, apoptosis, migration, ECM synthesis, and cytokine production. This simplification is necessary for computational feasibility, as incorporating more complex biological rules would significantly increase the computational burden. A high-fidelity model may also have many parameters with unknown values that may reduce the accuracy and reliability of model predictions. By focusing on essential behaviors, the model maintains a balance

between fidelity and computational efficiency, allowing for practical simulations within a reasonable timeframe, thus enhancing the model's applicability.

Lastly, future research should focus on transitioning the current model to in vivo conditions for clinical settings. This involves validating the model with real-time, in vivo data from animal studies and, eventually, clinical trials to ensure its efficacy and safety in human applications. Incorporating patient-specific variables, such as genetic information and disc morphology should be prioritized. These advancements aim to bridge the gap between theoretical frameworks and clinical implementation, leading to more personalized and effective healthcare solutions.

5.6 Conclusion

This thesis presented a comprehensive study on the development and application of an IVDH-ABM to simulate NP cell behavior within alginate hydrogels for IVD regeneration. The model was calibrated and validated against experimental data, demonstrating its predictive accuracy and reliability. The model's ability to simulate NP cell activity over a 21-day period provided valuable insights into the dynamics of cell behavior in response to varying hydrogel properties.

The study successfully replicated the relationship between hydrogel composition and its elasticity. It was observed that higher calcium crosslinking density, alginate molecular weight, and concentrations led to increased hydrogel stiffness, aligning with empirical data. The research aimed to optimize hydrogel compositions that promote NP

cell proliferation and ECM production, particularly for scaffolds that mimic the native IVD environment. Key factors included adjusting alginate concentration and calcium crosslinking density to achieve desired mechanical properties. The optimized hydrogel composition, identified as 200 kDa alginate with 1.95% w/v and 20 mM calcium, achieved an elastic modulus of 3.66 kPa. This composition supported ECM production and cell proliferation effectively, indicating superior regenerative capabilities under the specified conditions.

The insights gained from the IVDH-ABM have significant implications for advancing clinical trials in tissue engineering and regenerative medicine. The predictive outcomes can streamline the preclinical testing phase, reducing the time and cost associated with developing new therapies. The tuning of scaffold properties to meet personalized clinical needs paves the way for developing more effective medical treatments.

References

1. Walker BF. The Prevalence of Low Back Pain: A Systematic Review of the Literature from 1966 to 1998. *Journal of Spinal Disorders*. 2000/6// 2000;13(3):205-217. doi:10.1097/00002517-200006000-00003
2. Wu A, March L, Zheng X, et al. Global low back pain prevalence and years lived with disability from 1990 to 2017: estimates from the Global Burden of Disease Study 2017. *Annals of translational medicine*. 2020/3// 2020;8(6):299-299. doi:10.21037/atm.2020.02.175
3. Hoy D, Bain C, Williams G, et al. A systematic review of the global prevalence of low back pain. *Arthritis and rheumatism*. 2012/6// 2012;64(6):2028-2037. doi:10.1002/ART.34347
4. Maniadakis N, Gray A. The economic burden of back pain in the UK. *Pain*. 2000/1// 2000;84(1):95-103. doi:10.1016/S0304-3959(99)00187-6
5. Volz M, Elmasry S, Jackson AR, Travascio F. Computational Modeling Intervertebral Disc Pathophysiology: A Review. Frontiers in Physiology: Frontiers Media S.A.; 2022.
6. Coyte PC, Asche CV, Croxford R, Chan B. The economic cost of musculoskeletal disorders in Canada. *Arthritis care and research : the official journal of the Arthritis Health Professions Association*. 1998;11(5):315-325. doi:10.1002/ART.1790110503
7. Rampersaud YR, Power JD, Perruccio AV, et al. Healthcare utilization and costs for spinal conditions in Ontario, Canada - opportunities for funding high-value care: a retrospective cohort study. *The Spine Journal*. 2020/6// 2020;20(6):874-881. doi:10.1016/J.SPINEE.2020.01.013
8. Rizvi M. Novel treatment strategies for intervertebral disc degeneration. *Saudi Journal for Health Sciences*. 2015;4(1):5-5. doi:10.4103/2278-0521.151403
9. Hartvigsen J, Hancock MJ, Kongsted A, et al. What low back pain is and why we need to pay attention. *The Lancet*. 2018/6// 2018;391(10137):2356-2367. doi:10.1016/S0140-6736(18)30480-X
10. Huang Y-C, Hu Y, Li Z, Luk KDK. Biomaterials for intervertebral disc regeneration: Current status and looming challenges. *Journal of Tissue Engineering and Regenerative Medicine*. 2018/11// 2018;12(11):2188-2202. doi:10.1002/term.2750
11. Post JNL, Sandra; Merks, Roeland M.H.; Carlier, Aurélie. Implementing Computational Modeling in Tissue Engineering: Where Disciplines Meet. Journal. *Tissue Engineering Part A*. 2022;28(11-12):542-554. doi:http://doi.org/10.1089/ten.tea.2021.0215
12. Neubauer P, Glauche F, Cruz-Bournazou MN. Bioprocess Development in the era of digitalization. *Eng Life Sci*. Nov 2017;17(11):1140-1141. doi:10.1002/elsc.201770113
13. Bardini R, Carlo DS. Computational modeling and optimization of biofabrication in Tissue Engineering and Regenerative Medicine. 2023.

14. Macal MC. Everything you need to know about agent-based modelling and simulation. *Journal of Simulation*. 2016;10(2):144-156. doi:https://doi.org/10.1057/jos.2016.7
15. Abar S, Theodoropoulos KG, Lemarinier P, O'Hare MPG. Agent Based Modelling and Simulation tools: A review of the state-of-art software. *Computer Science Review*. 2017;24:13-33. doi:https://doi.org/10.1016/j.cosrev.2017.03.001
16. Baumgartner L, Sadowska A, Tío L, González Ballester MA, Wuertz-Kozak K, Noailly J. Evidence-Based Network Modelling to Simulate Nucleus Pulposus Multicellular Activity in Different Nutritional and Pro-Inflammatory Environments. *Frontiers in bioengineering and biotechnology*. 2021/11// 2021;9doi:10.3389/FBIOE.2021.734258
17. Cortes DH, Elliott DM. The intervertebral disc: Overview of disc mechanics. *The Intervertebral Disc: Molecular and Structural Studies of the Disc in Health and Disease*. 2014/1// 2014:17-31. doi:10.1007/978-3-7091-1535-0_2/FIGURES/00024
18. Moon SM, Yoder JH, Wright AC, Smith LJ, Vresilovic EJ, Elliott DM. Evaluation of intervertebral disc cartilaginous endplate structure using magnetic resonance imaging. *European Spine Journal*. 2013/8// 2013;22(8):1820-1820. doi:10.1007/S00586-013-2798-1
19. Brzuszkiewicz-Kuźmicka G, Szczegielniak J, Bączkowicz D. Age-related changes in shock absorption capacity of the human spinal column. *Clinical interventions in aging*. 2018;13:987-993. doi:10.2147/CIA.S156298
20. Nixon J. Intervertebral Disc Mechanics: A Review. *Journal of the Royal Society of Medicine*. 1986/2// 1986;79(2):100-104. doi:10.1177/014107688607900211
21. Zhang S, Liu W, Chen S, et al. Extracellular matrix in intervertebral disc: basic and translational implications. *Cell and Tissue Research*. 2022/10// 2022;390(1):1-22. doi:10.1007/s00441-022-03662-5
22. Frantz C, Stewart KM, Weaver VM. The extracellular matrix at a glance. *Journal of Cell Science*. 2010/12// 2010;123(24):4195-4200. doi:10.1242/jcs.023820
23. Clouet J, Vinatier C, Merceron C, et al. The intervertebral disc: From pathophysiology to tissue engineering. *Joint Bone Spine*. 2009;76(6):614-618. doi:10.1016/j.jbspin.2009.07.002
24. Yang BL, Yang BB, Erwin M, Ang LC, Finkelstein J, Yee AAJ. Versican G3 domain enhances cellular adhesion and proliferation of bovine intervertebral disc cells cultured in vitro. *Life Sciences*. 2003/11// 2003;73(26):3399-3413. doi:10.1016/j.lfs.2003.06.018
25. Taylor KR, Rudisill JA, Gallo RL. Structural and Sequence Motifs in Dermatan Sulfate for Promoting Fibroblast Growth Factor-2 (FGF-2) and FGF-7 Activity. *Journal of Biological Chemistry*. 2005/2// 2005;280(7):5300-5306. doi:10.1074/jbc.M410412200
26. Hayes AJ, Melrose J. Aggrecan, the Primary Weight-Bearing Cartilage Proteoglycan, Has Context-Dependent, Cell-Directive Properties in Embryonic Development and Neurogenesis: Aggrecan Glycan Side Chain Modifications Convey Interactive

Biodiversity. *Biomolecules*. 2020/8// 2020;10(9):1244-1244. doi:10.3390/biom10091244
27. Wei Q, Zhang X, Zhou C, Ren Q, Zhang Y. Roles of large aggregating proteoglycans in human intervertebral disc degeneration. *Connective Tissue Research*. 2019/5// 2019;60(3):209-218. doi:10.1080/03008207.2018.1499731
28. Alonso F, Hart DJ. Intervertebral Disk. In: Aminoff MJ, Daroff R, eds. *Encyclopedia of the Neurological Sciences*. 2 ed. Elsevier; 2014:724-729.
29. Sivan SS, Wachtel E, Roughley P. Structure, function, aging and turnover of aggrecan in the intervertebral disc. *Biochimica et Biophysica Acta (BBA) - General Subjects*. 2014/10// 2014;1840(10):3181-3189. doi:10.1016/j.bbagen.2014.07.013
30. Sharabi M, Wade K, Haj-Ali R. The Mechanical Role of Collagen Fibers in the Intervertebral Disc. In: Galbusera F, Wilke H-J, eds. *Biomechanics of the Spine*. Academic Press; 2018:105-123.
31. Sivan SS, Wachtel E, Tsitron E, et al. Collagen turnover in normal and degenerate human intervertebral discs as determined by the racemization of aspartic acid. *Journal of Biological Chemistry*. 2008/4// 2008;283(14):8796-8801. doi:10.1074/jbc.M709885200
32. Humphrey JD, Dufresne ER, Schwartz MA. Mechanotransduction and extracellular matrix homeostasis. *Nature Reviews Molecular Cell Biology*. 2014/12// 2014;15(12):802-812. doi:10.1038/nrm3896
33. Heino J. The collagen family members as cell adhesion proteins. *BioEssays*. 2007;29(10):1001-1010. doi:10.1002/bies.20636
34. Liang H, Luo R, Li G, Zhang W, Song Y, Yang C. The Proteolysis of ECM in Intervertebral Disc Degeneration. *International Journal of Molecular Sciences*. 2022/2// 2022;23(3):1715-1715. doi:10.3390/ijms23031715
35. Buschmann MD, Hunziker EB, Kim Y-J, Grodzinsky AJ. Altered aggrecan synthesis correlates with cell and nucleus structure in statically compressed cartilage. *Journal of Cell Science*. 1996;109(2):499-508. doi:10.1242/jcs.109.2.499
36. Lian C, Gao B, Wu Z, et al. Collagen type II is downregulated in the degenerative nucleus pulposus and contributes to the degeneration and apoptosis of human nucleus pulposus cells. *Molecular Medicine Reports*. 2017/10// 2017;16(4):4730-4736. doi:10.3892/mmr.2017.7178
37. Yaltirik KC, Timirci-Kahraman Ö, Gulec-Yilmaz S, Ozdogan S, Atalay B, Isbir T. The Evaluation of Proteoglycan Levels and the Possible Role of ACAN Gene Variant in Patients with Lumbar Disc Degeneration Disease. *In Vivo*. 2019;33(2):413-417. doi:doi: 10.21873/invivo.11488
38. Dou Y, Sun X, Ma X, Zhao X, Yang Q. Intervertebral Disk Degeneration: The Microenvironment and Tissue Engineering Strategies. Review. *Frontiers in Bioengineering and Biotechnology*. 2021;9
39. Frazer A, Bunning R, Thavarajah M, Seid J, Russell R. Studies on type II collagen and aggrecan production in human articular chondrocytes in vitro and effects of

transforming growth factor-β and interleukin-1β. *Osteoarthritis and Cartilage*. 1994/12// 1994;2(4):235-245. doi:10.1016/S1063-4584(05)80075-5
40. Pockert AJ, Richardson SM, Le Maitre CL, et al. Modified expression of the ADAMTS enzymes and tissue inhibitor of metalloproteinases 3 during human intervertebral disc degeneration. *Arthritis & Rheumatism*. 2009/2// 2009;60(2):482-491. doi:10.1002/art.24291
41. Li Y, Zhang T, Tian W, et al. Loss of TIMP3 expression induces inflammation, matrix degradation, and vascular ingrowth in nucleus pulposus: A new mechanism of intervertebral disc degeneration. *The FASEB Journal*. 2020/4// 2020;34(4):5483-5498. doi:10.1096/fj.201902364RR
42. Johannessen W, Elliott DM. Effects of Degeneration on the Biphasic Material Properties of Human Nucleus Pulposus in Confined Compression. *Spine*. 2005/12// 2005;30(24):724-729. doi:10.1097/01.brs.0000192236.92867.15
43. Gruber HE, Hoelscher GL, Ingram JA, Bethea S, Hanley EN. Autophagy in the Degenerating Human Intervertebral Disc. *Spine*. 2015/6// 2015;40(11):773-782. doi:10.1097/BRS.0000000000000865
44. Oh CH, Yoon SH. Whole Spine Disc Degeneration Survey according to the Ages and Sex Using Pfirrmann Disc Degeneration Grades. *Korean Journal of Spine*. 2017/12// 2017;14(4):148-154. doi:10.14245/kjs.2017.14.4.148
45. Bonnans C, Chou J, Werb Z. Remodelling the extracellular matrix in development and disease. *Nature Reviews Molecular Cell Biology*. 2014/12// 2014;15(12):786-801. doi:10.1038/nrm3904
46. Furtwängler T, Chan SCW, Bahrenberg G, Richards PJ, Gantenbein-Ritter B. Assessment of the Matrix Degenerative Effects of MMP-3, ADAMTS-4, and HTRA1, Injected Into a Bovine Intervertebral Disc Organ Culture Model. *Spine*. 2013/10// 2013;38(22):E1377-E1387. doi:10.1097/BRS.0b013e31829ffde8
47. Bondeson J, Wainwright S, Caterson B, Hughes C. *Chapter 263 - ADAMTS5*. 3 ed. vol 1. Academic Press; 2013:1174-1180.
48. Boyd DF, Thomas PG. Towards integrating extracellular matrix and immunological pathways. *Cytokine*. 2017/10// 2017;98:79-86. doi:10.1016/j.cyto.2017.03.004
49. David G, Ciurea AV, Mitrica M, Mohan A. Impact of changes in extracellular matrix in the lumbar degenerative disc. *Journal of medicine and life*. 2011/8// 2011;4(3):269-74.
50. Fearing BVJ, L., , Barcellona MN, Witte SE, et al. Mechanosensitive transcriptional coactivators MRTF-A and YAP/TAZ regulate nucleus pulposus cell phenotype through cell shape. *FASEB journal*. Dec. 2019;33(12):14022-14035. doi:doi: 10.1096/fj.201802725RRR
51. Stokes IA, Iatridis JC. Mechanical conditions that accelerate intervertebral disc degeneration: overload versus immobilization. *Spine*. 2004;29(23):2724–2732. doi:https://doi.org/10.1097/01.brs.0000146049.52152.da

52. O'Connell GD, Tan AR, Cui V, et al. Human chondrocyte migration behaviour to guide the
development of engineered cartilage. *J Tissue Eng Regen Med*. 2017;11(3):9. doi:doi:10.1002/term.1988.
53. Zgheib C, Xu J, Liechty KW. Targeting Inflammatory Cytokines and Extracellular Matrix Composition to Promote Wound Regeneration. *Advances in Wound Care*. 2014/4// 2014;3(4):344-355. doi:10.1089/wound.2013.0456
54. Nagase H, Visse R, Kashiwagi M, Gendron C, Itoh Y. Collagenases and aggrecanases: understanding the role of non-catalytic domains in cartilage matrix breakdown. *Arthritis Research & Therapy*. 2005;7(Suppl 1):S11-S11. doi:10.1186/ar1517
55. Iatridis JC, Setton LA, Weidenbaum M, Mow VC. Alterations in the mechanical behavior of the human lumbar nucleus pulposus with degeneration and aging. *Journal of Orthopaedic Research*. 1997/3// 1997;15(2):318-322. doi:10.1002/jor.1100150224
56. Kadow T, Sowa G, Vo N, Kang JD. Molecular Basis of Intervertebral Disc Degeneration and Herniations: What Are the Important Translational Questions? *Clinical Orthopaedics & Related Research*. 2015/6// 2015;473(6):1903-1912. doi:10.1007/s11999-014-3774-8
57. Tibrewal SB, Pearcy MJ. Lumbar Intervertebral Disc Heights in Normal Subjects and Patients with Disc Herniation. *Spine*. 1985/6// 1985;10(5):452-454. doi:10.1097/00007632-198506000-00009
58. Kepler CK, Ponnappan RK, Tannoury CA, Risbud MV, Anderson DG. The molecular basis of intervertebral disc degeneration. *The Spine Journal*. 2013/3// 2013;13(3):318-330. doi:10.1016/J.SPINEE.2012.12.003
59. Amin RM, Andrade NS, Neuman BJ. Lumbar Disc Herniation. Current Reviews in Musculoskeletal Medicine: Humana Press Inc.; 2017. p. 507-516.
60. Klassen PD, Hsu WK, Martens F, et al. Post-lumbar discectomy reoperations that are associated with poor clinical and socioeconomic outcomes can be reduced through use of a novel annular closure device: results from a 2-year randomized controlled trial. *ClinicoEconomics and Outcomes Research*. 2018/6// 2018;10:349-357. doi:10.2147/CEOR.S164129
61. Atlas SJ, Keller RB, Chang Y, Deyo RA, Singer DE. Surgical and Nonsurgical Management of Sciatica Secondary to a Lumbar Disc Herniation. *Spine*. 2001/5// 2001;26(10):1179-1187. doi:10.1097/00007632-200105150-00017
62. Wang S, Hebert JJ, Abraham E, et al. Postoperative recovery patterns following discectomy surgery in patients with lumbar radiculopathy. *Scientific Reports*. 2022/07/01 2022;12(1):11146. doi:10.1038/s41598-022-15169-8
63. Atlas SJ, Keller RB, Wu YA, Deyo RA, Singer DE. Long-Term Outcomes of Surgical and Nonsurgical Management of Sciatica Secondary to a Lumbar Disc Herniation: 10 Year Results from the Maine Lumbar Spine Study. *Spine*. 2005/4// 2005;30(8):927-935. doi:10.1097/01.brs.0000158954.68522.2a

64. Cao TN, Muthukumaran S, Chen X. Market of tissue engineering in Canada from 2011 to 2020. *Frontiers in Bioengineering and Biotechnology*. 2023;11doi:https://doi.org/10.3389/fbioe.2023.1170423
65. Kim SY, Smoak MM, Melchiorri JA, Mikos GA. An Overview of the Tissue Engineering Market in the United States from 2011 to 2018. *Tissue Engineering Part A*. 2019;25(1-2):1-8. doi:https://doi.org/10.1089/ten.TEA.2018.0138
66. Research P. Tissue Engineering Market - Global Industry Analysis, Size, Share, Growth, Trends, Regional Outlook, and Forecast 2023-2032. https://www.precedenceresearch.com/tissue-engineering-market
67. Mardones R, Jofré CM, Minguell JJ. Cell Therapy and Tissue Engineering Approaches for Cartilage Repair and/or Regeneration. *International Journal of Stem Cells*. 2015;8(1):48-53. doi:10.15283/ijsc.2015.8.1.48
68. Sakai D. Future perspectives of cell-based therapy for intervertebral disc disease. *European Spine Journal*. 2008/12// 2008;17(SUPPL. 4):452-458. doi:10.1007/S00586-008-0743-5/FIGURES/3
69. Hodgkinson T, Shen B, Diwan A, Hoyland JA, Richardson SM. Therapeutic potential of growth differentiation factors in the treatment of degenerative disc diseases. *JOR SPINE*. 2019/3// 2019;2(1)doi:10.1002/jsp2.1045
70. Ren X, Zhao M, Lash B, Martino MM, Julier Z. Growth Factor Engineering Strategies for Regenerative Medicine Applications. *Frontiers in Bioengineering and Biotechnology*. 2020/1// 2020;7doi:10.3389/fbioe.2019.00469
71. Yan X, Chen YR, Song YF, et al. Advances in the Application of Supramolecular Hydrogels for Stem Cell Delivery and Cartilage Tissue Engineering. Frontiers in Bioengineering and Biotechnology: Frontiers Media S.A.; 2020.
72. Williams DF. Challenges With the Development of Biomaterials for Sustainable Tissue Engineering. *Frontiers in Bioengineering and Biotechnology*. 2019/5// 2019;7doi:10.3389/fbioe.2019.00127
73. Chai Q, Jiao Y, Yu X. Hydrogels for Biomedical Applications: Their Characteristics and the Mechanisms behind Them. *Gels*. 2017/1// 2017;3(1):6-6. doi:10.3390/gels3010006
74. Troy E, Tilbury MA, Power AM, Wall JG. Nature-Based Biomaterials and Their Application in Biomedicine. *Polymers (Basel)*. Sep 28 2021;13(19)doi:10.3390/polym13193321
75. Tarun G, Ajay B, Bhawna K, Sunil K, Ravi J. Scaffold: Tissue engineering and regenerative medicine. Review Article. *International Research Journal of Pharmacy*. 2011;2(12):5.
76. Gyles DA, Castro LD, Carrera Silva JO, Ribeiro-Costa RM. A review of the designs and prominent biomedical advances of natural and synthetic hydrogel formulations. *European Polymer Journal*. 2017;88:29. doi:https://doi.org/10.1016/j.eurpolymj.2017.01.027

77. Reddy MSB, Ponnamma D, Choudhary R, Sadasivuni KK. A Comparative Review of Natural and Synthetic Biopolymer Composite Scaffolds. *Polymers (Basel)*. Mar 30 2021;13(7)doi:10.3390/polym13071105
78. Adoungotchodo A, Epure L, Mwale F, Lerouge S. Chitosan-based hydrogels supplemented with gelatine and Link N enhance extracellular matrix deposition by encapsulated cells in a degenerative intervertebral disc environment. *Europea Cells and Materials*. 2021;40:471-484. doi:DOI:10.22203/eCM.v041a30
79. Di Martino A, Sittinger M, Risbud MV. Chitosan: a versatile biopolymer for orthopaedic tissue-engineering. *Biomaterials*. Oct 2005;26(30):5983-90. doi:10.1016/j.biomaterials.2005.03.016
80. Cloyd JM, Malhotra NR, Weng L, Chen W, Mauck RL, Elliott DM. Material properties in unconfined compression of human nucleus pulposus, injectable hyaluronic acid-based hydrogels and tissue engineering scaffolds. Journal. *European Spine Journal*. 2007;6:8. doi:https://doi.org/10.1007/s00586-007-0443-6
81. Jarrah RM, Potes MDA, Vitija X, et al. Alginate hydrogels: A potential tissue engineering intervention for intervertebral disc degeneration. *Journal of Clinical Neuroscience*. 2023/7// 2023;113:32-37. doi:10.1016/j.jocn.2023.05.001
82. Ahmed TA, Dare EV, Hincke M. Fibrin: a versatile scaffold for tissue engineering applications. *Tissue Eng Part B Rev*. Jun 2008;14(2):199-215. doi:10.1089/ten.teb.2007.0435
83. Lust ST, Hoogland D, Norman MDA, et al. Selectively Cross-Linked Tetra-PEG Hydrogels Provide Control over
Mechanical Strength with Minimal Impact on Diffusivity. *ACS Biomaterials and Engineering*. 2021;7:12. doi:DOI: 10.1021/acsbiomaterials.0c01723
84. Wang M, Bai J, Shao K, et al. Poly(vinyl alcohol) Hydrogels: The Old and New Functional Materials. *International Journal of Polymer Science*. 2021;2021:16. 2225426. doi:https://doi.org/10.1155/2021/2225426
85. Basu A, Kunduru KR, Doppalapudi S, Domb AJ, Khan W. Poly(lactic acid) based hydrogels. *Adv Drug Deliv Rev*. Dec 15 2016;107:192-205. doi:10.1016/j.addr.2016.07.004
86. Lee EJ, Kasper FK, Mikos AG. Biomaterials for Tissue Engineering. *Annals of Biomedical Engineering*. 2014/2// 2014;42(2):323-337. doi:10.1007/s10439-013-0859-6
87. Christiani T, Mys K, Dyer K, Kadlowec J, Iftode C, Vernengo AJ. Using embedded alginate microparticles to tune the properties of in situ forming poly(N - isopropylacrylamide) - graft - chondroitin sulfate bioadhesive hydrogels for replacement and repair of the nucleus pulposus of the intervertebral disc. *JOR SPINE*. 2021/9// 2021;4(3)doi:10.1002/jsp2.1161
88. Li X, Liu Y, Li L, et al. Tissue-mimetic hybrid bioadhesives for intervertebral disc repair. *Materials Horizons*. 2023;doi:10.1039/D2MH01242A

89. Leone G, Torricelli P, Chiumiento A, Facchini A, Barbucci R. Amidic alginate hydrogel for nucleus pulposus replacement. *Journal of Biomedical Materials Research Part A*. 2008/2// 2008;84A(2):391-401. doi:10.1002/jbm.a.31334
90. Bron JL, Vonk LA, Smit TH, Koenderink GH. Engineering alginate for intervertebral disc repair. *Journal of the Mechanical Behavior of Biomedical Materials*. 2011/10// 2011;4(7):1196-1205. doi:10.1016/j.jmbbm.2011.04.002
91. Neves MI, Moroni L, Barrias CC. Modulating Alginate Hydrogels for Improved Biological Performance as Cellular 3D Microenvironments. *Frontiers in Bioengineering and Biotechnology*. 2020/6// 2020;8doi:10.3389/fbioe.2020.00665
92. Barbetta A, Barigelli E, Dentini M. Porous Alginate Hydrogels: Synthetic Methods for Tailoring the Porous Texture. *Biomacromolecules*. 2009/8// 2009;10(8):2328-2337. doi:10.1021/bm900517q
93. Malandrino A, Pozo JM, Castro-Mateos I, et al. On the Relative Relevance of Subject-Specific Geometries and Degeneration-Specific Mechanical Properties for the Study of Cell Death in Human Intervertebral Disk Models. *Frontiers in Bioengineering and Biotechnology*. 2015/2// 2015;3doi:10.3389/fbioe.2015.00005
94. Axpe E, Chan D, Offeddu GS, et al. A Multiscale Model for Solute Diffusion in Hydrogels. *American Chemical Society*. 2019;52(18):12. doi:doi: 10.1021/acs.macromol.9b00753
95. Iatridis JC, Nicoll SB, Michalek AJ, Walter BA, Gupta MS. Role of biomechanics in intervertebral disc degeneration and regenerative therapies: what needs repairing in the disc and what are promising biomaterials for its repair? *The Spine Journal*. 2013/3// 2013;13(3):243-262. doi:10.1016/j.spinee.2012.12.002
96. Mariani E, Lisignoli G, Borzì RM, Pulsatelli L. Biomaterials: Foreign Bodies or Tuners for the Immune Response? *International Journal of Molecular Sciences*. 2019/2// 2019;20(3):636-636. doi:10.3390/ijms20030636
97. Galbusera F, Schmidt H, Noailly J, et al. Comparison of four methods to simulate swelling in poroelastic finite element models of intervertebral discs. *Journal of the Mechanical Behavior of Biomedical Materials*. 2011/10// 2011;4(7):1234-1241. doi:10.1016/j.jmbbm.2011.04.008
98. Post JN, Loerakker S, Merks RMH, Carlier A. Implementing Computational Modeling in Tissue Engineering: Where Disciplines Meet. *Tissue Engineering Part A*. 2022/6// 2022;28(11-12):542-554. doi:10.1089/ten.tea.2021.0215
99. Kwon K, Kim H, Lee T, Yoon DS, Kim H-S. Molecular Dynamics Simulation to Investigate Structural Characteristics of Aggrecan in Degenerated Intervertebral Discs. *Biomed Eng Lett*. 2015;5:4. doi:DOI 10.1007/s13534-015-0177-z
100. Hollingsworth SA, Dror RO. Molecular Dynamics Simulation for All. *Neuron*. Sep 19 2018;99(6):1129-1143. doi:10.1016/j.neuron.2018.08.011
101. Ibarz E, Herrera A, Más Y, et al. Development and kinematic verification of a finite element model for the lumbar spine: application to disc degeneration. *Biomed Res Int*. 2013;2013:705185. doi:10.1155/2013/705185

102. Roberts GL, Pallister I. Finite element analysis in trauma & orthopaedics – an introduction to clinically relevant simulation & its limitations. *Orthopaedics and Trauma*. 2012;26(6):6. doi:https://doi.org/10.1016/j.mporth.2012.10.007
103. Sakellarios AI, Potsika VT, Fotiadis DI. *Multiscale Modelling in Biomedical Engineering*. Computational Modeling at Tissue Level. 2023:35.
104. Janssen MA, Alessa L, Barton M, Bergin S, Lee A. Towards a Community Framework for Agent-Based Modelling. *Journal of Artificial Societies and Social Simulation*. 2008;11(2):6.
105. Vodovotz Y, An G. Agent - based models of inflammation in translational systems biology: A decade later. *WIREs Systems Biology and Medicine*. 2019/11// 2019;11(6)doi:10.1002/wsbm.1460
106. Querbes A. Banned from the sharing economy: an agent-based model of a peer-to-peer marketplace for consumer goods and services. *J Evol Econ*. 2018;28(3):633-665. doi:10.1007/s00191-017-0548-y
107. Cavany SM, España G, Lloyd AL, et al. Fusing an agent-based model of mosquito population dynamics with a statistical reconstruction of spatio-temporal abundance patterns. *PLoS Comput Biol*. Apr 2023;19(4):e1010424. doi:10.1371/journal.pcbi.1010424
108. Bayani A, Dunster JL, Crofts JJ, Nelson MR. Spatial considerations in the resolution of inflammation: Elucidating leukocyte interactions via an experimentally-calibrated agent-based model. *PLoS Comput Biol*. Nov 2020;16(11):e1008413. doi:10.1371/journal.pcbi.1008413
109. Norton KA, Popel AS. An agent-based model of cancer stem cell initiated avascular tumour growth and metastasis: the effect of seeding frequency and location. *J R Soc Interface*. Nov 6 2014;11(100):20140640. doi:10.1098/rsif.2014.0640
110. Solovyev A, Mi Q, Tzen YT, Brienza D, Vodovotz Y. Hybrid equation/agent-based model of ischemia-induced hyperemia and pressure ulcer formation predicts greater propensity to ulcerate in subjects with spinal cord injury. *PLoS Comput Biol*. 2013;9(5):e1003070. doi:10.1371/journal.pcbi.1003070
111. Jeanette AIJ, Genevieve LS-OB, Max B, et al. Digitize your Biology! Modeling multicellular systems through interpretable cell behavior. *bioRxiv*. 2023:2023.09.17.557982. doi:10.1101/2023.09.17.557982
112. Ghaffarizadeh A, Heiland R, Friedman SH, Mumenthaler SM, Macklin P. PhysiCell: An open source physics-based cell simulator for 3-D multicellular systems. *PLOS Computational Biology*. 2018/2// 2018;14(2):e1005991-e1005991. doi:10.1371/journal.pcbi.1005991
113. Byrne DP, Lacroix D, Planell JA, Kelly DJ, Prendergast PJ. Simulation of tissue differentiation in a scaffold as a function of porosity, Young's modulus and dissolution rate: Application of mechanobiological models in tissue engineering. *Biomaterials*. 2007/12// 2007;28(36):5544-5554. doi:10.1016/j.biomaterials.2007.09.003

114. Raia RN, Mcgill M, Marcet T, Yucha VES, Kaplan LD. Soft Tissue Engineering. *Biomaterials Science*. 2020:1399-1414. doi:https://doi.org/10.1016/B978-0-12-816137-1.00087-8
115. Vadala G, Ambrosio L, Russo F, Papalia R, Denaro V. Stem Cells and Intervertebral Disc Regeneration Overview—What They Can and Can't Do. *International Journal of Spine Surgery*. 2021/4// 2021;15(s1):40-53. doi:10.14444/8054
116. Wills CR, Malandrino A, van Rijsbergen MM, Lacroix D, Ito K, Noailly J. Simulating the sensitivity of cell nutritive environment to composition changes within the intervertebral disc. *Journal of the Mechanics and Physics of Solids*. 2016/05/01/ 2016;90:108-123. doi:https://doi.org/10.1016/j.jmps.2016.02.003
117. Baumgartner L, Reagh JJ, Gonzalez Ballester MA, Noailly J. Simulating intervertebral disc cell behaviour within 3D multifactorial environments. *Bioinformatics*. 2021/6// 2021;37(9):1246-1253. doi:10.1093/bioinformatics/btaa939
118. Schuh E, Hofmann S, Stok K, Notbohm H, Müller R, Rotter N. Chondrocyte redifferentiation in 3D: The effect of adhesion site density and substrate elasticity. *Journal of Biomedical Materials Research Part A*. 2012/01/01 2012;100A(1):38-47. doi:https://doi.org/10.1002/jbm.a.33226
119. V Thomas L, Vg R, D Nair P. Effect of stiffness of chitosan-hyaluronic acid dialdehyde hydrogels on the viability and growth of encapsulated chondrocytes. *International Journal of Biological Macromolecules*. 2017/11/01/ 2017;104:1925-1935. doi:https://doi.org/10.1016/j.ijbiomac.2017.05.116
120. Pattappa G, Li Z, Peroglio M, Wismer N, Alini M, Grad S. Diversity of intervertebral disc cells: phenotype and function. *J Anat*. Dec 2012;221(6):480-96. doi:10.1111/j.1469-7580.2012.01521.x
121. Tang J, Enderling H, Becker-Weimann S, et al. Phenotypic transition maps of 3D breast acini obtained by imaging-guided agent-based modeling. *Integr Biol (Camb)*. Apr 2011;3(4):408-21. doi:10.1039/c0ib00092b
122. Pleyer J, Fleck C. Agent-based models in cellular systems. *Frontiers Physics*. 2023;10(Biophysics)doi:https://doi.org/10.3389/fphy.2022.968409
123. Crossley RM, Johnson S, Tsingos E, et al. Modeling the extracellular matrix in cell migration and morphogenesis: a guide for the curious biologist. *Front Cell Dev Biol*. 2024;12:1354132. doi:10.3389/fcell.2024.1354132
124. K WKD, D PE, Y D, et al. Life Span of the Chondrocytes from Human Umbilical Cord Derived-Mesenchymal Stem Cell Differentiation. *Biomed Pharmacol J*. 2019;12(1)doi:DOI : https://dx.doi.org/10.13005/bpj/1614
125. Edelstein-keshet L, Spiros A. Exploring the formation of Alzheimer's disease senile plaques in silico. *J Theor Biol*. Jun 7 2002;216(3):301-26. doi:10.1006/jtbi.2002.2540
126. Fu G, Soboyejo WO. Swelling and diffusion characteristics of modified poly (N-isopropylacrylamide) hydrogels. *Materials Science and Engineering: C*. 2010;30(1)(8)doi:https://doi.org/10.1016/j.msec.2009.07.017

127. Chiba K, Andersson GB, Masuda K, Thonar EJ. Metabolism of the extracellular matrix formed by intervertebral disc cells cultured in alginate. *Spine (Phila Pa 1976)*. Dec 15 1997;22(24):2885-93. doi:10.1097/00007632-199712150-00011
128. Kobayashi S, Meir A, Urban J. Effect of cell density on the rate of glycosaminoglycan accumulation by disc and cartilage cells in vitro. *Journal of Orthopaedic Research*. 2008;26(4):493-503. doi:https://doi.org/10.1002/jor.20507
129. Williams RJ, Tryfonidou MA, Snuggs JW, Le Maitre CL. Cell sources proposed for nucleus pulposus regeneration. *JOR Spine*. Dec 2021;4(4):e1175. doi:10.1002/jsp2.1175
130. Barbero A, Grogan S, Sch√ § fer D, Heberer M, Mainil-Varlet P, Martin I. Age related changes in human articular chondrocyte yield, proliferation and post-expansion chondrogenic capacity. *Osteoarthritis and Cartilage*. 2004;12(6):8. doi:https://doi.org/10.1016/j.joca.2004.02.010
131. Schuh E, Kramer J, Rohwedel J, et al. Effect of Matrix Elasticity on the Maintenance of the Chondrogenic Phenotype. *Tissue Engineering Part A*. 2009;16(4):9. doi:10.1089/ten.tea.2009.0614
132. K. Reuther, Rettenmayr M. Perspectives for cellular automata for the simulation of dendritic solidification. *Computational Materials Science*. 2014;95:7. doi:https://doi.org/10.1016/j.commatsci.2014.07.037
133. Phillips KLE, Chiverton N, Michael AL, et al. The cytokine and chemokine expression profile
of nucleus pulposus cells: implications for
degeneration and regeneration of the
intervertebral disc. *Arthritis Research and Therapy*. 2013;15doi:doi:10.1186/ar4408
134. Tsekov R, Lensen MC. Brownian Motion and the Temperament of Living Cells. Journal. *Chinese Physics Letters*. 2013;30(7)doi:10.1088/0256-307x/30/7/070501
135. Shen X, Hu L, Li Z, et al. Extracellular Calcium Ion Concentration Regulates Chondrocyte Elastic Modulus and Adhesion Behavior. *Int J Mol Sci*. Sep 17 2021;22(18)doi:10.3390/ijms221810034
136. Li J, Jung W, Nam S, Chaudhuri O, Kim T, Zhang Y. Roles of Interactions Between Cells and Extracellular Matrices for Cell Migration and Matrix Remodeling. *Multi-scale Extracellular Matrix Mechanics and Mechanobiology*. 2020;23doi:https://doi.org/10.1007/978-3-030-20182-1_8
137. Bolton MC, Dudhia J, Bayliss MT. Quantification of aggrecan and link-protein mRNA in human articular
cartilage of different ages by competitive reverse transcriptase–PCR. *Biochem J*. 1996;319:9.
138. Man E, Easdon C, Mclellan I, Yiu HHP, Hoskins C. Exploration of Nanosilver Calcium Alginate-Based Multifunctional Polymer Wafers for Wound Healing. *Pharmaceutics*. 2023;15(2)doi:10.3390/pharmaceutics15020483

139. Kurowiak J, Kaczmarek-Pawelska A, Mackiewicz AG, Bedzinski R. Analysis of the Degradation Process of Alginate-Based Hydrogels in Artificial Urine for Use as a Bioresorbable Material in the Treatment of Urethral Injuries. *Processes*. 2020;8(3):304.
140. Matyash M, Despang F, Ikonomidou C, Gelinsky M. Swelling and mechanical properties of alginate hydrogels with respect to promotion of neural growth. *Tissue Engineering Part C Methods*. 2014;20(5):10. doi:https://doi.org/10.1089/ten.TEC.2013.0252
141. Gao C, Liu M, Chen J, Zhang X. Preparation and controlled degradation of oxidized sodium alginate hydrogel. *Polymer Degradation and Stability*. 2009;94(9):5. doi:https://doi.org/10.1016/j.polymdegradstab.2009.05.011
142. Wan LQ, Jiang J, Arnold DE, Guo XE, Lu HH, Mow VC. Calcium Concentration Effects on the Mechanical and Biochemical Properties of Chondrocyte-Alginate Constructs. *Cellular and Molecular Bioengineering*. 2008;1(1):9. doi:DOI: 10.1007/s12195-008-0014-x
143. Place ES, Rojo L, Gentleman E, Stevens MM. Strontium- and Zinc-Alginate Hydrogels for Bone Tissue Engineering. *Tissue Engineering Part A*. 2011;17(21):22. doi:DOI: 10.1089/ten.TEA.2011.0059
144. Hwang PY, Chen J, Jing L, Hoffman BD, Setton LA. The role of extracellular matrix elasticity and composition in regulating the nucleus pulposus cell phenotype in the intervertebral disc: a narrative review. *J Biomech Eng*. Feb 2014;136(2):021010. doi:10.1115/1.4026360
145. Seekhao N, Shung C, JaJa J, Mongeau L, Li-Jessen NYK. High-Performance Agent-Based Modeling Applied to Vocal Fold Inflammation and Repair. *Front Physiol*. 2018;9:304. doi:10.3389/fphys.2018.00304
146. Valencia DP, Gonzalez FJ. Understanding the linear correlation between diffusion coefficient and molecular weight. A model to estimate diffusion coefficients in acetonitrile solutions. *Electrochemistry Communications*. 2011;13(2):4. doi:doi:10.1016/j.elecom.2010.11.032
147. Xiang X, Kennnedy R, Madey G. Verification and Validation of Agent-based Scientific Simulation Models. *Agent-Directed Simulation Conference*. 2005;
148. McCulloch J, Ge J, Ward JA, Heppenstall A, Polhill JG, Malleson N. Calibrating Agent-Based Models Using Uncertainty Quantification Methods. *Journal of Artificial Societies and Social Simulation*. 2022;25(2)doi:10.18564/jasss.4791
149. Joseph VR. Optimal ratio for data splitting. *Statistical Analysis and Data Mining: The ASA Data Science Journal*. 2022;15(4):7. doi:10.1002/sam.11583
150. Muraina IO. Ideal dataset splitting ratios in machine learning algorithms: General concerns for data scientists and data analysts. Computer Science Department, School of Science, Adeniran Ogunsanya College of Education.; 2021:9.
151. Jang J, Young-Joon Seol, Hyeon Ji Kim, Joydip Kundu, Sung Won Kim, and Dong-Woo Cho. . Effects of Alginate Hydrogel Cross-Linking Density on Mechanical

and Biological Behaviors for Tissue Engineering. *Journal of the Mechanical Behavior of Biomedical Materials*. 2014;37:8. doi:doi:10.1016/J.JMBBM.2014.05.004.
152. Chippada U, Yurke B, Langrana NA. Simultaneous determination of Young's modulus, shear modulus, and Poisson's ratio of soft hydrogels. *Journal of Materials Research*. 2010;25(3):545-555. doi:10.1557/jmr.2010.0067
153. Kaklamani G, Cheneler D, Grover LM, Adams MJ, Bowen J. Mechanical properties of alginate hydrogels manufactured using external gelation. *Journal of the Mechanical Behavior of Biomedical Materials*. 2014/08/01/ 2014;36:135-142. doi:https://doi.org/10.1016/j.jmbbm.2014.04.013
154. Charbonier F, Indana D, Chaudhuri O. Tuning Viscoelasticity in Alginate Hydrogels for 3D Cell Culture Studies. *Curr Protoc*. May 2021;1(5):e124. doi:10.1002/cpz1.124
155. Kopf A, Claassen M. Latent representation learning in biology and translational medicine. *Patterns (N Y)*. Mar 12 2021;2(3):100198. doi:10.1016/j.patter.2021.100198
156. Saltelli A, Annoni P, D'Hombres B. How to avoid a perfunctory sensitivity analysis. *Procedia - Social and Behavioral Sciences, Sixth International Conference on Sensitivity Analysis of Model Output*. 2010;2(6):2. doi:https://doi.org/10.1016/j.sbspro.2010.05.133
157. Schiavi-Tritz J, Rahouadj R, de Isla N, Huselstein C. Designing a three-dimensional alginate hydrogel by spraying method for cartilage tissue engineering. *Soft Matter*. 2010;6(20):9. doi:DOI: 10.1039/c000790k
158. Abbah SA, Lu WW, Peng SL, et al. Extracellular matrix stability of primary mammalian chondrocytes and intervertebral disc cells cultured in alginate-based microbead hydrogels. *Cell Transplant*. 2008;17(10-11):1181-92. doi:10.3727/096368908787236648
159. Renani HB, Ghorbani M, Beni BH, et al. Determination and comparison of specifics of nucleus pulposus cells of human intervertebral disc in alginate and chitosan-gelatin scaffolds. *Adv Biomed Res*. 2012;1:81. doi:10.4103/2277-9175.102996
160. Wang X-H, Hong X, Zhu L, et al. Tumor necrosis factor alpha promotes the proliferation of human nucleus pulposus cells via nuclear factor-κB, c-Jun N-terminal kinase, and p38 mitogen-activated protein kinase. *Experimental Biology and Medicine*. 2015;240(4):411-417. doi:10.1177/1535370214554533
161. Yang H, AU - Cao C, Wu C, et al. TGF-b Suppresses Inflammation in Cell Therapy for Intervertebral Disc Degeneration. *Scientific Reports*. 2015;5(1)(13254)doi:https://doi.org/10.1038/srep13254
162. Cui L, Wei H, Li ZM, Dong XB, Wang PY. TGF-b aggravates degenerative nucleus pulposus cells inflammation and fibrosis through the upregulation of angiopoietin-like protein 2 expression. *European review for medical and pharmacological sciences*. 2020;24:8. doi:10.26355/eurrev_202012_23991

163. Qu Z, Zhang F, Chen W, Lin T, Sun Y. High-dose TGF-β1 degrades human nucleus pulposus cells via ALK1-Smad1/5/8 activation. *Experimental and Therapeutic Medicine*. 2020;20:7. doi:https://doi.org/10.3892/etm.2020.9088
164. Sutovsky J, Benco M, Sutovska M, et al. Cytokine and chemokine profile changes in patients with lower segment lumbar degenerative spondylolisthesis. *Int J Surg*. Jul 2017;43:163-170. doi:10.1016/j.ijsu.2017.06.024
165. Su X, Liu B, Gong F, et al. Isofraxidin attenuates IL-1β-induced inflammatory response in human nucleus pulposus cells. *Journal of Cellular Biochemistry*. 2019;120(8):7. doi:https://doi.org/10.1002/jcb.28604
166. Li W, Liu T, Wu L, et al. Blocking the Function of Inflammatory Cytokines and Mediators by Using IL-10 and TGF-β: A Potential Biological Immunotherapy for Intervertebral Disc Degeneration in a Beagle Model. *International Journal of Molecular Sciences*. 2014;15:13. doi:https://doi.org/10.3390/ijms151017270
167. Walter BA, Purmessur D, Likhitpanichkul M, et al. Inflammatory Kinetics and Efficacy of Anti-inflammatory Treatments on Human Nucleus Pulposus Cells. *Spine (Phila Pa 1976)*. Jul 1 2015;40(13):955-63. doi:10.1097/brs.0000000000000932
168. Tilwani RK, Bader DL, Chowdhury TT. Biomechanical Conditioning Enhanced Matrix Synthesis in Nucleus Pulposus Cells Cultured in Agarose Constructs with TGFβ. *Journal of Functional Biomaterials*. 2012;3(1):23-36.
169. Harding S, Armstrong J, Faccenda E, et al. The IUPHAR/BPS Guide to PHARMACOLOGY in 2024. *Nucleic Acids Research Database Issue*. 2023;52doi:doi:10.1093/nar/gkad944
170. Hazuda D, Lee J, Young P. The kinetics of interleukin 1 secretion from activated monocytes. Differences between interleukin 1 alpha and interleukin 1 beta. *The Journal of Biological Chemistry*. 1988;263(17):6. doi:DOI: https://doi.org/10.1016/S0021-9258(18)68502-3
171. Ma Y, Zhao S, Shen S, et al. A novel recombinant slow-release TNF-a derived peptide effectively inhibits tumor growth and angiogensis. *Scientific Reports*. 2015;5(1)doi:10.1038/srep13595
172. Jang J, Seol Y-J, Kim HJ, AU - Kundu J, Kim SW, Cho D-W. Effects of alginate hydrogel cross-linking density on mechanical and biological behaviors for tissue engineering. *Journal of the Mechanical Behavior of Biomedical Materials*. 2014;37:8. doi:https://doi.org/10.1016/j.jmbbm.2014.05.004
173. Studer RK, Vo N, Sowa G, Ondeck C, Kang J. Human nucleus pulposus cells react to IL-6: independent actions and amplification of response to IL-1 and TNF-α. *Spine (Phila Pa 1976)*. Apr 15 2011;36(8):593-9. doi:10.1097/BRS.0b013e3181da38d5
174. Garg A, Yuen S, Seekhao N, et al. Towards a Physiological Scale of Vocal Fold Agent-Based Models of Surgical Injury and Repair: Sensitivity Analysis, Calibration and Verification. *Applied Sciences*. 2019;9(15):2974.

175. Houska T, Kraft P, Chamorro-Chavez A, Breuer L. SPOTting Model Parameters Using a Ready-Made Python Package. *PLoS ONE*. 2015;10(12)doi:https://doi.org/10.1371/journal.pone.0145180
176. Bárdossy A, Singh S. Robust estimation of hydrological model parameters. *Hydrology and earth system sciences*. 2008;12(6):1273-1283.
177. Hagizawa H, Koyamatsu S, Okada S, Kaito T, Tsumaki N. Chondrocyte-like cells in nucleus pulposus and articular chondrocytes have similar transcriptomic profiles and are paracrine-regulated by hedgehog from notochordal cells and subchondral bone. Original Research. *Frontiers in Cell and Developmental Biology*. 2023-May-15 2023;11doi:10.3389/fcell.2023.1151947
178. Aota Y, An HS, Imai Y, Thonar EJ, Muehleman C, Masuda K. Comparison of cellular response in bovine intervertebral disc cells and articular chondrocytes: effects of lipopolysaccharide on proteoglycan metabolism. *Cell and Tissue Research*. 2006;326(3):6. doi:https://doi.org/10.1007/s00441-006-0225-1
179. Rajasekaran S, Soundararajan DCR, Nayagam SM, et al. Novel Biomarkers of Health and Degeneration in Human Intervertebral Discs: In-depth Proteomic Analysis of Collagen Framework of Fetal, Healthy, Scoliotic, Degenerate, and Herniated Discs. *Asian Spine J*. Feb 2023;17(1):17-29. doi:10.31616/asj.2021.0535
180. Grandison A. Determining Confidence Intervals, and Convergence, for Parameters in Stochastic Evacuation Models. *Fire Technology*. 2020;56(5):40. doi:10.1007/s10694-020-00968-0
181. Li NYK, Verdolini K, Clermont G, et al. A Patient-Specific in silico Model of Inflammation and Healing Tested in Acute Vocal Fold Injury. *PLoS ONE*. 2008;3(7)doi:https://doi.org/10.1371/journal.pone.0002789
182. Li NY, Vodovotz Y, Hebda PA, Abbott KV. Biosimulation of inflammation and healing in surgically injured vocal folds. *Ann Otol Rhinol Laryngol*. Jun 2010;119(6):412-23. doi:10.1177/000348941011900609
183. Umehara S, Tadano S, Abumi K, Katagiri K, Kaneda K, Ukai T. Effects of degeneration on the elastic modulus distribution in the lumbar intervertebral disc. *Spine (Phila Pa 1976)*. Apr 1 1996;21(7):811-9; discussion 820. doi:10.1097/00007632-199604010-00007
184. Häuselmann HJ, Aydelotte MB, Schumacher BL, Kuettner KE, Gitelis SH, Thonar EJ. Synthesis and turnover of proteoglycans by human and bovine adult articular chondrocytes cultured in alginate beads. *Matrix*. Apr 1992;12(2):116-29. doi:10.1016/s0934-8832(11)80053-3
185. Shnayder NA, Ashhotov AV, Trefilova VV, et al. Cytokine Imbalance as a Biomarker of Intervertebral Disk Degeneration. *International Journal of Molecular Sciences*. 2023;24(3):2360.
186. Luo T, Tan B, Zhu L, Wang Y, Liao J. A Review on the Design of Hydrogels With Different Stiffness and Their Effects on Tissue Repair. Review. *Frontiers in*

Bioengineering and Biotechnology. 2022-January-25 2022;10doi:10.3389/fbioe.2022.817391

187. Chen H, Tan X-N, Hu S, et al. Molecular Mechanisms of Chondrocyte Proliferation and Differentiation. Review. *Frontiers in Cell and Developmental Biology*. 2021-May-28 2021;9doi:10.3389/fcell.2021.664168
188. Kim J-H, Lee G, Won Y, et al. Matrix cross-linking–mediated mechanotransduction promotes posttraumatic osteoarthritis. *Proceedings of the National Academy of Sciences of the United States of America*. 2015;112doi:10.1073/pnas.1505700112
189. Kibble MJ, Domingos M, Hoyland JA, Richardson SM. Importance of Matrix Cues on Intervertebral Disc Development, Degeneration, and Regeneration. *Int J Mol Sci*. Jun 21 2022;23(13)doi:10.3390/ijms23136915
190. Gilchrist CL, Darling EM, Chen J, Setton LA. Extracellular matrix ligand and stiffness modulate immature nucleus pulposus cell-cell interactions. *PLoS One*. 2011;6(11):e27170. doi:10.1371/journal.pone.0027170
191. Desai SU, Srinivasan SS, Kumbar SG, Moss IL. Hydrogel-Based Strategies for Intervertebral Disc Regeneration: Advances, Challenges and Clinical Prospects. *Gels*. Jan 15 2024;10(1)doi:10.3390/gels10010062
192. Li X, Zhang J, Kawazoe N, Chen G. Fabrication of Highly Crosslinked Gelatin Hydrogel and Its Influence on Chondrocyte Proliferation and Phenotype. *Polymers*. 2017;9(8):309.
193. Schwab A, Wesdorp MA, Xu J, et al. Modulating design parameters to drive cell invasion into hydrogels for osteochondral tissue formation. *Journal of Orthopaedic Translation*. 2023;41(42)doi:10.1016/j.jot.2023.07.001